Theoretical and Practical Geological Remote Sensing in an Arid Environment: Landsat MSS Imagery of the Central Zone of the Damara Orogen, Namibia.

Jeffrey Lord

Thesis presented in partial fulfilment of the
Degree of Master of Philosophy, October 1994.

Frontispiece.

The picture shown opposite is one of two Landsat MSS images which have been used in this study to investigate the geology of the Central Zone of the Damara Orogen, Namibia. The study area covers the top half of this image, and the southern half of the adjacent Landsat image to the north. The image was taken during the month of August, 1973, by the Multispectral Scanner on-board the Landsat-1 satellite. It has subsequently been digitally processed using the principal components transformation (see Chapter 5) to emphasise the spectral information contained therein. The southern region is covered by giant longitudinal sand dunes which continue all the way down to the border with South Africa, 800 kilometres away. These are some of the biggest dunes to be found, up to 300 metres high and 3 kilometres wide. To the north, the paths of the Khan and Swakop Rivers are well-defined. These rivers are usually dry, but bright red areas of vegetation pick out their paths well, and suggest the presence of groundwater. Rock exposure is best along the paths of these two rivers, probably due to the removal of sediment from adjacent areas by tributaries. At the top centre of the image, the SJ Dome is well-exposed. This is an area of basement rocks surrounded by an oval ring of bright quartzites of the Etusis Formation. Basement dome features such as these characterise the geology of the Central Zone. In the centre of the image, the Tumas Dome is flanked by a W-shaped outcrop of bright marbles, of the Karibib Formation, which can be traced further to the south. Much of the ground appears streaked by the action of offshore prevailing winds.

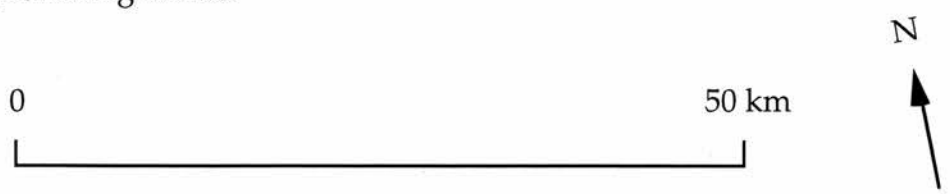

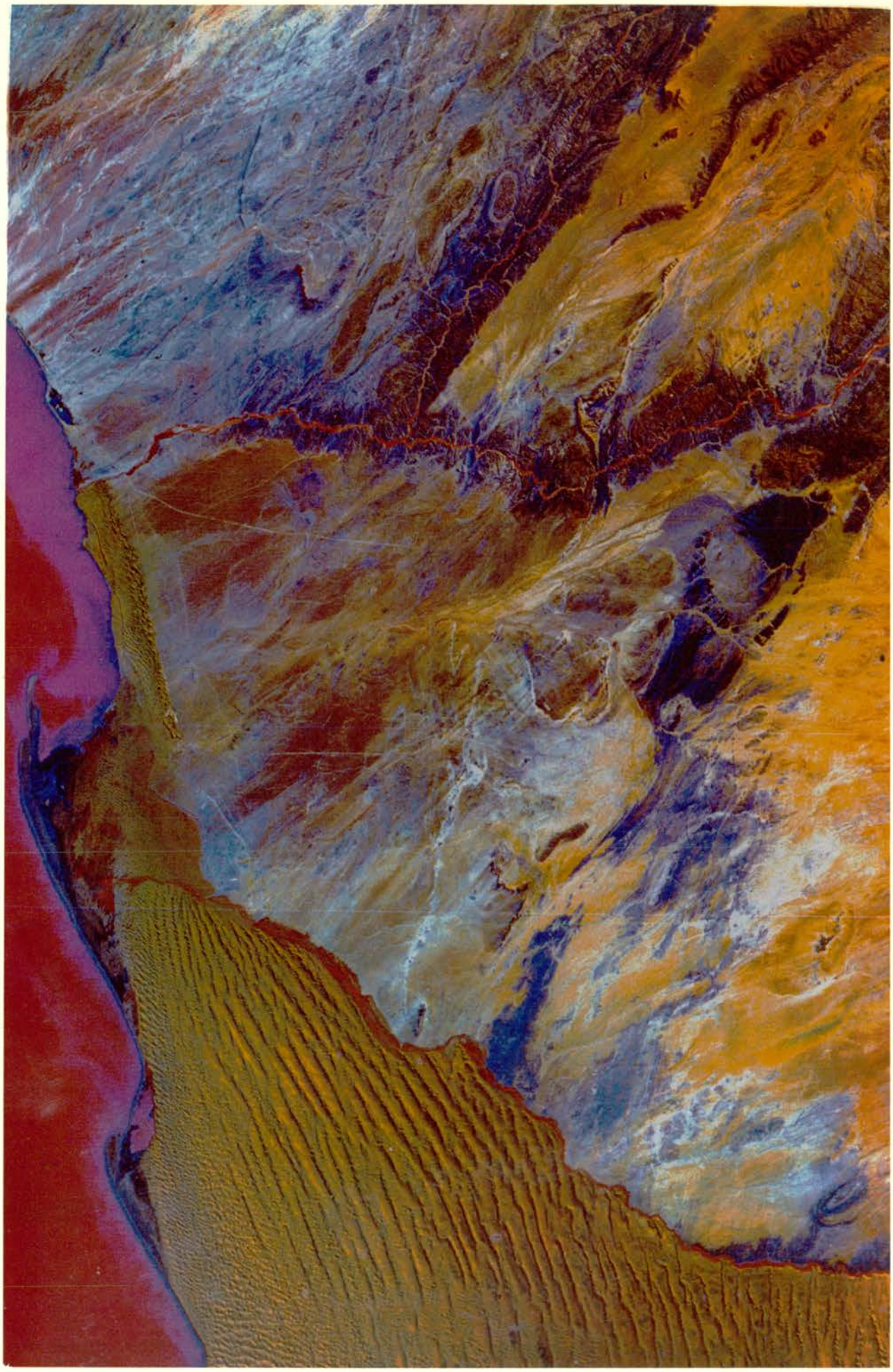

Thesis Declaration.

I, Jeffrey Lord, hereby certify that this thesis has been composed by myself, that it is a record of my own work, and that it has not been accepted in partial or complete fulfilment of any other degree or professional qualification.

Signed..... Date.13/11/94.

I was admitted to the Faculty of Science of the University of St. Andrews under Ordinance General Number 12 on.....1ST OCTOBER, 1993.....

I hereby certify that the candidate has fulfilled the conditions of the Resolutions and Regulations appropriate to the degree of M.Phil.

Signed..... Date.13th Nov 1994

Signed..... Date.13th November 1994.

Abstract.

Two adjacent Landsat Multispectral Scanner (MSS) scenes have been digitally processed and enhanced to maximise the display of geological information contained within imagery covering the western portion of the Central Zone of the Damara Orogen, Namibia.

Structural information has been obtained from the spatial component of image information through the compilation of lineament maps. Linear features have been objectively enhanced through the generation of the first principal component image and by convolution filtering. By means of visual interpretation, linear features have then been mapped, then digitised and subjected to computer analysis to establish any orientation trends. Positive topographic lineaments, which represent the Etendeka regional dolerite dyke swarm (130-120 Ma), show a strong north-northeast trend and are closely associated with the splitting of Gondwana and the formation of the Southern Atlantic Ocean. Negative topographic lineaments are believed to represent sinistral strike-slip faults and show a strong northwest trend. They are believed to have formed under brittle conditions at the end of the Damaran Orogen. Tonal lineaments, caused by linear lithological horizons, either side of parallel fold axes, show a dominant northeast trend, and are believed to have formed during either compressional or extensional conditions during the main Damaran deformation event. A number of regional photolineaments are also recognisable from the Landsat imagery.

A remotely-sensed geology map has also been produced using both the spatial and spectral components of image information. Mappable lithological units have been established in a previously mapped test area, and these units have been extrapolated further afield to produce a regional geology map of the western portion of the Central Zone of the Damara Orogen. Comparison with published geology maps of the same area shows that the procedure proves generally effective and new outcrops of basement rocks have been recognised in the area to the west of the Namibfontein Dome. However, the limited spectral resolution of the imagery is high-lighted by the inability to resolve between the Rossing, Chuos and Karibib Formations.

The study area proves to be well-suited to geological remote sensing using Landsat MSS imagery because of the excellent rock exposure in the region, the lack of vegetation, and the wide variety of lithologies which appear spectrally distinct from one another on digitally-enhanced imagery. The procedure provides a low-cost, effective means of geological reconnaissance which is well-suited to remote and inaccessible areas.

Acknowledgements.

For their help in the production of this thesis, and in ascending order of importance, acknowledgement is given to Mr Graham Sandeman, Mr Jim Allen, Dr Jack Jarvis, Mr Richard Batchelor, Dr John Soulsby, Dr Grahame Oliver and my parents. Many thanks to you all.

Contents.

--o0o--

List of Figures.

List of Plates.

Plate: Title:

Chapter 1

Introduction.

Chapter 1. Introduction.

Landsat Multispectral Scanner (MSS) imagery was obtained for the area covering the western portion of the Central Zone of the Damara Orogen. Using various image processing techniques, the intention was to digitally process the imagery to highlight and extract as much information concerning the geology of the area as possible. Several research aims were established at the beginning of the exercise:

1.1. The Aims of the Project.

The project aims were:

(i) To review the available literature concerning the geological applications of remote sensing using Landsat MSS data, with particular reference to arid and semi-arid environments.

(ii) From this review, to establish a suitable methodology whereby the maximum amount of geological information could be extracted from the Landsat MSS data covering the western portion of the Central Zone of the Damara Orogen.

From the literature review, the following methodology was proposed:

1--Structural information would be obtained through the compilation of lineament maps of various features. Unlike many previous lineament studies, it was considered appropriate to map different features separately. These features included positive topographic lineaments, negative topographic lineaments, tonal lineaments and fold axes.

2--The methodology for lineament mapping would set out to be as objective as possible. To this end, the imagery would be digitally enhanced and filtered to highlight real line segments, and would be analysed uniformly by the visual interpretation of a series of image sub-scenes.

3--Any linear features recognised would then be digitised and subjected to computer analysis to establish whether or not there were any orientation trends. Two histograms of the digitised data would be produced: lineament frequency versus azimuth, and total lineament length versus azimuth.

4--An attempt would be made to reconcile the structural significance of any trends, that were established from the lineament data, with the known geology of the area.

5--For a delimited test area, where actual lithologies were established from previous mapping work (Smith, 1965), various digital image processing and enhancement techniques would be applied to the MSS data to establish mappable lithological units.

6--Lithological contacts would be mapped from the Landsat MSS imagery over the study area, and those units established in the test area would be extrapolated further afield in an attempt to produce a remotely-sensed geological map of the Central Zone of the Damara Orogen.

7--The results of the remotely-sensed map of the geology would be compared with existing geology maps of the same area. Where differences occurred between maps, the imagery would be re-assessed and comment made of the original interpretation.

1.2. Organisation of the Thesis.

Chapter 1 presents the aims of the study and gives details concerning the location of the study area and its geological setting. Chapter 2 then goes on to review the literature relevant to this study. The first section of this chapter looks at lineament analyses, in particular those carried out using Landsat MSS data. The second section is concerned with the use of remote sensing for lithological mapping, with particular emphasis on the use of Landsat data in arid and semi-arid environments. The final section lists conclusions from the review.

Chapter 3 describes the Landsat satellite, how the data is collected, at what wavelengths and also discusses the format of that data. With this knowledge, one is able to make a more informed decision as to which of the image processing techniques available will provide the best enhancements. The geometric correction of imagery is described, as is the image processing system used in this study. The penultimate section describes how different geological information is contained within different components of the imagery, prior to the conclusions of the chapter.

Chapter 4 describes the methodology employed in the lineament analysis, in particular the various image processing techniques that have been used to objectively enhance any linear features that are present. Criteria are given for the linear features mapped, and the digitising methodology and computer analysis of that data are also described. Chapter 5 deals with the theoretical and practical use of remote sensing for lithological mapping, particularly in arid and semi-arid environments. The various digital image processing techniques used to enhance the geology of the area are described, along with the technique of visual interpretation.

The proceeding two chapters discuss the results of the chapters 4 and 5 respectively. Chapter 6 discusses lineament trends and their structural significance, and comment is made on lineament density and the use of lineament maps for water resources and mineralisation. Chapter 7 is a discusses of the remotely-sensed geology map. The effectiveness of lineament mapping using Landsat MSS imagery is assessed by comparing the results of the remotely-sensed geology map with previously published geology maps of the same area. The final section, chapter 8, contains the conclusions from the study as a whole.

1.3. The location and geological setting of the study area.

The Damara Orogen is part of a much larger late-Precambrian Pan-African mobile belt. Miller (1983) has made a comprehensive review of the evolution of the Damara Orogen. The Damara episode was initiated between 900 and 1,000 Ma ago during widespread fluviatile deposition from local sources within and marginal to intracontinental rifts trending north-northwest, northeast and south from a triple junction situated west of Swakopmund (see Figure 1.1). General subsidence that followed in the northeast-trending branch of the orogen is ascribed to a gradual evolution from rifting to spreading (Miller, 1983), and by ~700 Ma, this has developed to full continental rupture with the formation of a Pan-African South Atlantic Ocean.

Following the development of this ocean, there was a reversal of spreading associated with northwestward subduction of the Kalahari Craton below the Congo Craton (Miller, 1983). The collision between these two cratons was responsible for the main period of Damaran deformation and metamorphism (Middle Cambrian to lower-most Ordovician).

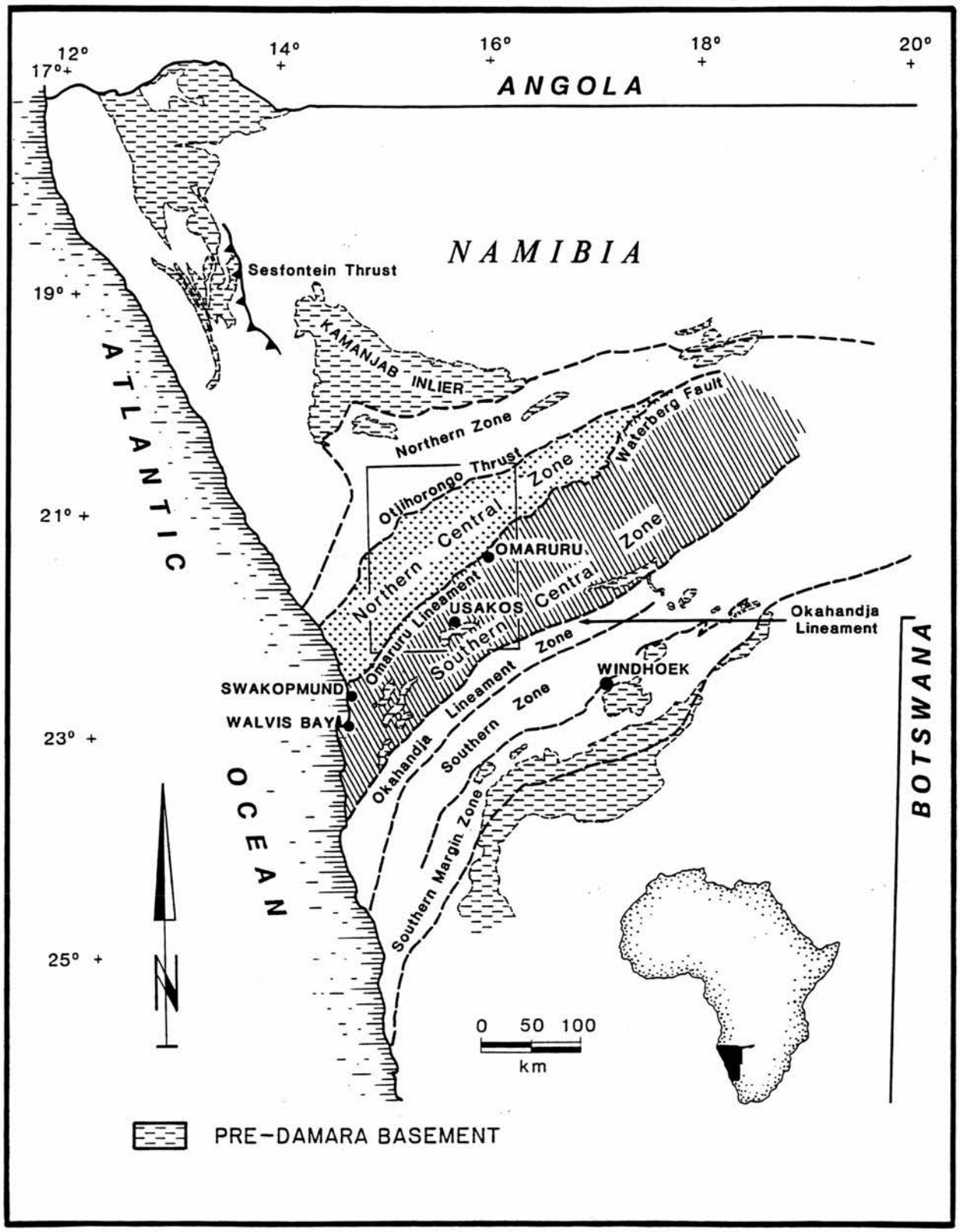

Figure 1.1. Tectonostratigraphic zones of the Damara Orogen (from Steven, 1993).

In Namibia, the Damara belt has been divided into contrasting tectonostratigraphic zones (Miller, 1983). These various zones are shown in Figure 1.1. The location of the study area, which covers the western portion of the Central Zone is also highlighted on this map. The Central Zone is separated into the Northern and Southern Central Zones by the Omaruru Lineament (Corner, 1983). The latter zone is bounded to the southeast by the Okahandja Lineament and the former to the northwest by the Otjihorongo Thrust and Autseib Fault (see section 6.14).

The Central Zone is composed of medium- to high-grade predominantly metasedimentary cover rocks derived from a continental source (the detailed stratigraphy is discussed in section 7.2). These cover rocks are associated with keel-shaped periclinal synclinoria which separate granitic basement gneisses. These basement rocks form flat-topped elongate domes which characterise the regional northeast-trending structure of this part of the Orogen. Smith (1965) mapped the contact between basement and cover rocks as an unconformity, although Oliver (1993) considers this to represent a regional mid-crustal detachment with displacements in the order of many tens of kilometres. Oliver argues that this was caused during the main period of deformation with failure between the basement and the cover, which then flowed and escaped towards the southwest during the collision of the Kalahari and Congo Cratons.

Figure 1.2 shows a map of the study area, showing the course of the Khan and Swakop Rivers. It also shows the location of various physiographical features referred to in the text. Much of the area is mantled by alluvial and eluvial deposits (see frontispiece), but there is also excellent rock outcrop in many p;laces, especially along the courses of the Khan and Swakop Rivers. Vegetation is scarce, and restricted to the channels of these two rivers.

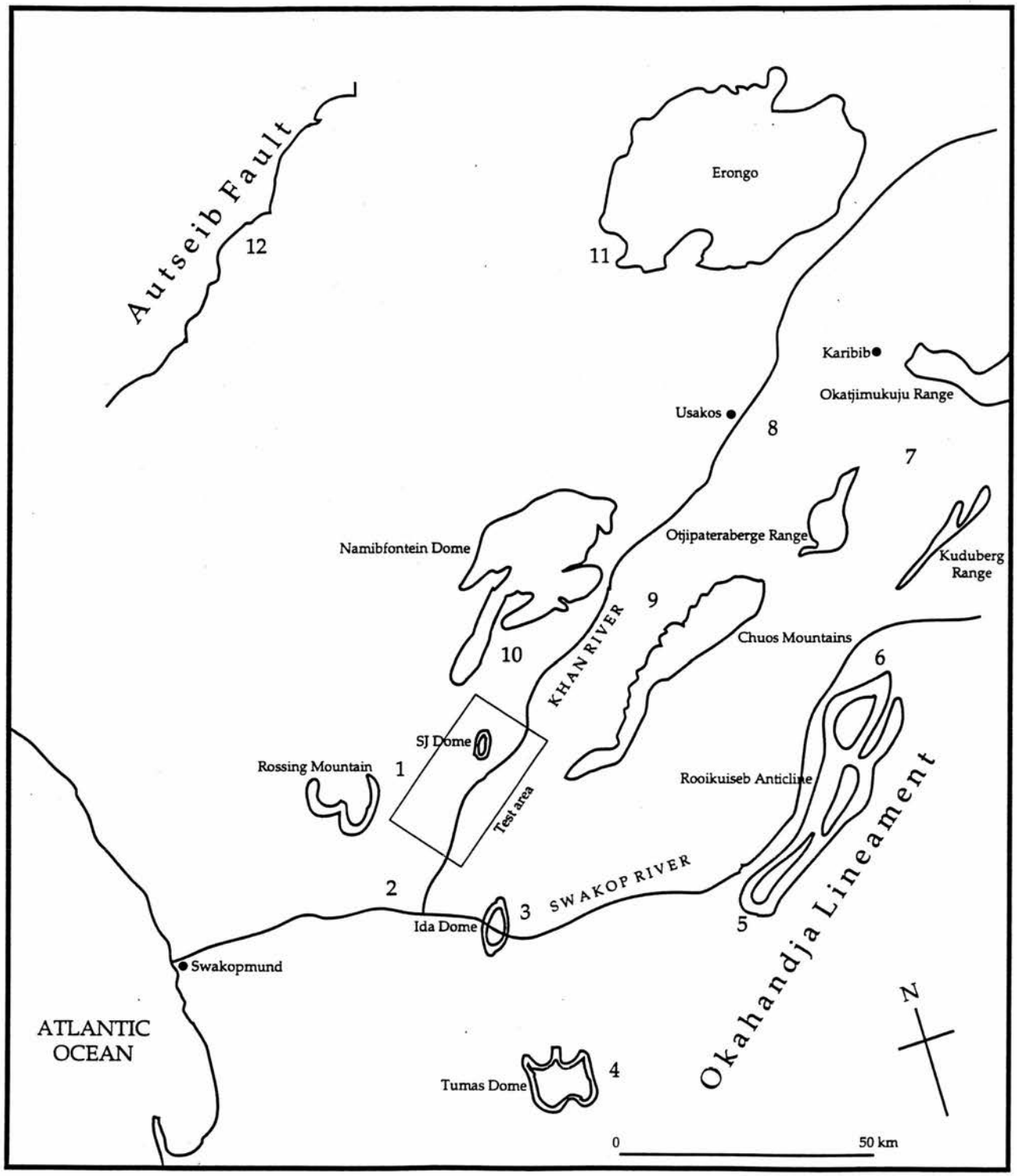

Figure 1.2. Map of the study area.

Chapter 2

Literature Review.

Chapter 2. Literature review.

2.1. Literature review - lineament studies.

2.1.1. Introduction.

Following the launch of Landsat-1 in 1972, and the subsequent widespread availability of satellite imagery for most areas of the world, lineament studies soon began to reappear (Gold *et. al.* , 1973). Much of the work is largely concerned with the practical mapping and interpretation of linear features, but more recent papers have questioned the validity of many of the techniques employed in earlier studies and have sought to adopt a more objective approach (Moore and Waltz, 1983). However, great debate continues to exist both to the subjectivity of lineament mapping and to a suitable methodology.

2.1.2. Review.

The earliest paper to deal with the subjectivity involved in lineament analysis was presented by Huntingdon and Raiche (1978). The study investigated the variations that occurred between lineament interpretations of the same scene by one observer on different occasions, as well as between interpretations of the same scene by several observers, who may have used different methods. By using correlation coefficient data for comparison between different interpretations, the study showed how subjective the interpretation of the same scene by different people could actually be - "these differences can be of the same order as would be expected for one person interpreting two scenes with entirely different geology." The work argued for a "standardisation of interpretation methods" and the results showed that the same interpreter should be used throughout any interpretation.

Most lineament studies try to establish whether or not any directional trends exist in the lineament data. Csillag (1982) interpreted Landsat data in an area of southwest Hungary. Linear features seen in MSS band-7 were recorded and the results displayed in the form of a lineament map, and as histograms of azimuth frequency. An important discovery of the work was that while the frequency-versus-azimuth histogram revealed a predominant structural trend, when the histogram was weighted, using the length of lineaments in each azimuth class, another orthogonal trend also became apparent. It is possible that there may be a few long lineaments in one particular direction, but many short lineaments in another. Both may be important and be the result of different phenomena. The work showed that measuring azimuth and frequency alone did not reveal all of the possible information and that the total lineament length for each azimuth class gave added information.

Moore and Waltz (1983) outlined objective procedures for lineament enhancement and extraction in an attempt to deal with the problem of operator subjectivity involved in lineament analysis. A five-step convolution (filtering) procedure, possible with the digital processing of imagery, was outlined in the work. As a means of producing edge-enhanced imagery, the procedure proved useful, and is one which would be worthwhile in any lineament analysis. However, the computer algorithms used to extract lineaments from the final images produced a 'lineament map' of only small line segments, many of which would probably have been joined together into a single lineament by visual interpretation.

Parsons & Yearley (1986) critically evaluated which MSS band should be used for lineament studies. Comparisons were made between lineament maps compiled from four images obtained at the same time, but in different wavebands, and between two images obtained in the same waveband but during different seasons. All the maps were produced by visual interpretation by a single operator, but any

criticisms made by Moore & Waltz (1983) were countered by stating that 'problems of subjectivity are not insuperable' and that 'there is a real possibility that the failure of machine processing to identify particular lineaments found by visual interpreters may well be due as much to the inadequacy of algorithms as to subjectivity on the part of human operators'. Generally, the work showed poor correlations between the lineament maps produced, although interestingly, all maps identified the same preferred lineament orientation. The study concluded that each MSS band contributes unique lineament information. It also suggested that little value could be placed on lineament density 'as any observed density may have as much to do with selective identification from a total population of lineaments as it has with geologic significance'.

Walsh and Mynar (1986) described the benefits of lineament analyses using Landsat MSS data. They noted that the imagery was well-suited because of its oblique illumination, synoptic view and the regional coverage offered. They noted the importance of lineament detection for the identification of fault and fracture zones which may represent both potential hazards and economically important environments. They suggested a wide variety of digital processing techniques to enhance the imagery, all of which provided some unique lineament information, but discovered that the first principal component image revealed the most lineaments.

A statistical approach to lineament analysis has been adopted by many workers, in particular for the purposes of lineament density analysis. Conradsen *et. al.* (1986) mapped and digitised linear features seen from Landsat MSS band-7 data covering South Greenland. Having statistically delimited ten significant azimuth trends, maps of lineament density for each trend were then constructed, and an attempt made to try to resolve this with geological knowledge of the area. Importantly, the work revealed a bias connected with the solar illumination

direction whereby linear features parallel to the sun's azimuth were under-represented, a feature also noted by Koopmans (1986). It is likely that by only using MSS band-7 the study missed much lineament data contained in other spectral bands (Parsons and Yearley, 1986). By limiting the length of the lineaments mapped, results may also have been biased away from any major structural trends. The concept of lineament density has been questioned by Parsons and Yearley (1983), although the study did seem able to relate areas of high lineament density to known geological phenomena, namely intrusive complexes and associated zones of mineralisation.

Lineament density analysis was also used by Ananaba & Ajakaiye (1987) as evidence for the tectonic control of mineralization in Nigeria. Using Landsat MSS coverage for the whole country, each spectral band was analysed for lineament information, rather than just band-7. Criteria were given for lineaments seen on the imagery, recognising them as linear, geomorphic and tonal features, but the authors went little further than stating that "the causative mechanism is not well understood but there is general agreement that their origin is related to global tectonics." A dominant azimuth trend was found from the data, but only by using large 30 degree azimuth intervals. The contour map produced of lineament density related reasonably well to known areas of mineralization, suggesting that primary mineralization in Nigeria was tectonically controlled.

Reddy (1991) investigated the spatial pattern of lineaments in Southern India observed from a published lineament map compiled using MSS band-5. Using a grid cell approach, maps were produced of the spatial distribution (density) of the number of lineaments in each cell, the number of lineament intersections in each cell, and the number of lineaments present in a particular azimuth trend, recognised from the data. Through this rasterization technique, a numeric value for each cell was obtained and a digital lineament database produced. Reddy

argued that this "would assist in routine real-time, unbiased information generation and interpretation." However, if the lineament database is biased, which was likely since it has been produced using only MSS band-5, then so too would have been any results.

The move towards total automation of lineament extraction and analysis was highlighted by Zlatopolsky (1992). The paper described the experimental results of a computer algorithm used by the (then) U.S.S.R. Ministry of Geology to extrapolate and investigate lineaments from air photos and satellite imagery. The computer program automatically extracted linear features such as lines and edges, analysed their spatial arrangement, and enabled an interactive study of the obtained results. The results showed that the program was successful for edge detection, but rather like the results of Moore and Waltz (1983), long lineaments were not detected, only sections of them.

The use of Landsat lineament data for tectonic analysis has been well-documented by many workers. Stefouli & Angelopoulos (1990) integrated Landsat lineament data with aeromagnetic data to aid their structural analysis of Crete and S.E. Peloponessus. Using this inter-disciplinary approach, they discovered that "the interpretation of the aeromagnetic data gave linear features that have similar trends to those of... Landsat." The fact that the two data sets complement one another shows that lineaments seen on Landsat imagery are indeed related to sub-surface structure. Ferrandini *et. al.* (1993) used Landsat imagery to study the fault system in the basement rocks of the Western High Atlas. A lineament map of the region was produced, and from rose diagrams of this data, the precise direction of major Alpine faults could be deduced.

2.2. Literature review - Multispectral lithological mapping in arid terrains.

2.2.1. Introduction.

The MSS exposed a significant portion of the geological community to the concept of multispectral imaging as well as to digital image processing. The result was a significant turn away from the use of standard photo-interpretative techniques on black-and-white and colour aerial photography to an expanded use of the spectral properties of surface materials for mapping (Goetz *et. al.*, 1983).

2.2.2. Review.

Abrams (1980) discussed lithological mapping using remotely-sensed data. Included were standard photogeology interpretation techniques, including landform and drainage analysis, but particular emphasis was placed on the use of multispectral imagery. The procedure was described as cost-effective and time-saving since 'lithological contacts can be extended over large areas with a minimum of ground control, and identification of rock types can be extrapolated on the basis of spectral and geomorphic information'. With the availability of sufficient ground truth data, the inferred composition of the various lithologies could be confirmed and a true geological map could be prepared.

Abrams suggested that arid and semi-arid regions were well-suited to such geological remote sensing. Where precipitation was scant, the dominant geomorphic process was physical weathering. Mass movement of surface material was minimal and therefore the varying resistance of rock units beneath slopes was often sharply reflected in the topography. Outcrops of bedrock in these areas were further enhanced by the exceptionally slow rate of soil formation and the scarcity, or even lack of vegetation. Owing to the almost total absence of water,

the weathering mantle was not excessively leached, and closely resembled the composition of the underlying bedrock. Abrams argued that these areas would therefore yield the greatest amount of geological information to remote sensing.

The work proposed that the spectral reflectance of earth materials was often the most useful and diagnostic criterion for lithological discrimination. This spectral reflectivity was expressed in images as either photographic tone or colour. Colour was probably the single most useful recognition element in interpreting imagery because the human eye was capable of distinguishing nearly 1000 times as many tints and shades of colour as shades of grey. Colour also provided a means of simultaneously displaying data from more than one wavelength region. Digital processing techniques were proposed to maximise the display of lithological information. These techniques included contrast-enhancement, band-ratio images, canonical analysis, and automatic classification procedures.

Abrams noted that the discrimination and mapping of lithological units could be most readily accomplished when the materials had relatively large spectral differences over the sensed spectral region. 'In general, spectral differences are evidenced as narrow absorption bands and therefore the width of the sensed wavelength region is crucial'. By narrowing the sensed wavelength regions, better separation of materials could be expected. When using narrow wavebands, the optimal wavelength regions for separating different materials needed to be determined.

Goetz *et. al.* (1983) reviewed the use of multispectral remote sensing as a tool for geological exploration. Although the MSS was designed primarily for agricultural purposes, the paper demonstrated that much valuable geological information had been derived from this source. They described work that showed how the spectral properties of differing lithologies could be used for their identification. They

stated that 'because the MSS collects data in four different wavebands, spectral reflectance information can be derived from Landsat MSS images'. The work was critical, however, as to the limitations of the Multispectral Scanner due to the lack of spectral bands beyond 1.1 μm. They stated that 'the major drawbacks of using Landsat MSS images for geologic purposes have resulted from the lack of stereo capability, coarse spectral resolution, and limited spectral coverage (0.5 - 1.1 μm) which does not extend into regions of the spectrum of most use in characterising the spectral properties of geologic surface materials'. They did show, however, that in reasonably well-exposed areas, 'in spite of the lower spatial resolution and limited spectral bands, Landsat MSS images have yielded valuable regional structural and some lithological information' and that 'many lithological units are distinguishable in MSS images on the basis of their spectral properties'. More modern sensors such as the Thematic Mapper carried by later Landsat satellites have seven, narrower bands and therefore possess a much greater spectral resolution, combined with far greater spatial resolution. Digital processing techniques, similar to those used in MSS studies, are used to display such data (Auquiere *et. al.* , 1993), but the higher spectral (and spatial) resolution allows the discrimination of many more lithologies.

Landsat data have been used for a number of years in arid and semi-arid environments to locate areas of iron oxide occurrences which might be associated with hydrothermal alteration zones. Abrams *et. al*. (1983) discussed the use of multispectral Landsat data for the remote sensing of porphyry copper deposits in Southern Arizona. The work described how Landsat data proved useful for delineating areas of iron oxide on the surface, some of which were associated with altered rocks, and some of which were associated with sedimentary red beds, volcanic rocks, and weathered alluvium. It was noted that the limited spatial resolution of the MSS hampered mapping of some critical geological

relationships, but on the other hand, that the synoptic view was well-suited for examining regional tectonic patterns.

Visual analysis of digitally processed Landsat imagery was also described by Bhan and Hegde (1985) and Rakshit and Swaminathan (1985) for the same area in eastern India. Both studies produced geological maps for certain test areas using various digital processing techniques for Landsat MSS imagery. These included contrast-stretching techniques, band-ratio images, and normal and ratio colour composites (see chapters 4 and 5 for a discussion of these techniques). "Such products have helped in clearly identifying geological units up to formation level and, often, individual lithological members and units within these could also be delineated. Major structural elements including folds, faults and other lineaments could also be delineated" (Rakshit & Swaminathan, 1985). Both works noted that the spectral properties of rocks were affected by a number of geological and ground parameters, which sometimes varied widely with terrain condition. These parameters included mineral composition, colour-indices, texture, structure, nature and condition of decomposition, position and orientation of the surface, ruggedness of exposure surface, incident radiation and type and amount of cover.

The use of MSS band-ratio images for lithological discrimination was documented by Knepper and Raines (1985). They discovered that such images often enhanced the discrimination between lithologically dissimilar rock and soil units as compared to single band images or composites of single band images. Also, the topographic effects on measured radiance were greatly subdued on band-ratio images, allowing the distribution of spectrally different rock and soil units to be better determined. Colour composites, made from band-ratio images, were documented for mapping the regional distribution of spectrally distinct lithological units, especially limonitic material.

A practical demonstration of the procedures mentioned above was provided by Qari (1989). Lithologies of part of the Arabian Shield, identified on the ground by traditional geological mapping methods, were extrapolated on Landsat imagery to produce a remotely-sensed lithological map. Information was obtained from a standard false-colour composite image through human visual analysis - the methodology used was akin to photogeological interpretation. Differing lithologies were mapped on the basis of their tonal characteristics and fracturing character. Although the methodology was a simple one, the study showed that the technique had considerable potential in allowing the quick construction of geological and tectonic maps for large areas of well-exposed terrain.

Principal components analysis of Landsat MSS data over a part of the Indian desert was discussed by Dwivedi and Sankar (1992). The work suggested that if qualitative or semi-quantitative visual interpretation techniques were to be used, some means of combining information from a number of image channels into a single image needed to be employed. A technique suggested was that of principal component analysis, which provided a means of reducing the dimensionality of multi-channel image data. This technique also separated non-random variance (information content) from random variance (noise). The work showed that most information could be compressed into the first principal component, and that successive components contained far less information and increasing levels of noise. False-colour composites derived from the first three components allowed the successful detection and delineation of various terrain features in terms of their spectral separability.

2.3. Conclusions.

Lineament mapping:

1--The use of lineament analysis for tectonic interpretation is well-documented (Ferrandini *et. al.* , 1993, etc.).

2--The extraction of lineaments from imagery, by visual interpretation, is a largely subjective procedure (Huntingdon and Raiche, 1978).

3--Computer algorithms provide a more objective approach to lineament enhancement and extraction (Moore and Waltz, 1983) but fail to identify longer lineaments.

4--Similar lineament orientation trends are easily found, even by different interpreters and by using different methods (Parsons and Yearley, 1986).

5--The frequency of lineaments in azimuth classes may show a preferred trend, but it is also important to take into account the total length of lineaments in each class, as other information may be contained in that data (Csillag, 1982).

6--Lineament information from each spectral band may be unique and data from all bands should therefore be used together in any analysis (Parsons and Yearley, 1986).

7--Solar azimuth is an important consideration since lineaments may be over represented perpendicular to that direction (Conradsen *et. al.*, 1986).

8--Little value can be placed on lineament density (Parsons & Yearley, 1986), although some workers have been able to relate results to known geological phenomena (Ananaba and Ajakaiye, 1987).

Multispectral lithological mapping:

1--Multispectral images taken from the vantage point of space have found their place in the modern geologist's tool box. They provide a cost-effective and time-saving means of reconnaissance mapping (Abrams, 1980).

2--Valuable geological information can be derived from the Landsat Multispectral Scanner, because the spectral characteristics of earth materials allows for their discrimination on MSS imagery (Goetz *et. al.*, 1983).

3--Arid regions are well-suited to geological remote sensing (Abrams, 1980). Topography often reflects lithology, the weathering mantle closely resembles the underlying bedrock, soil formation is slow, and vegetation is absent or scarce.

4--The availability of images in digital form allows the use of digital processing techniques to maximise and enhance the display of lithological information. Suitable techniques include false-colour composites (Abrams, 1980), band-ratio images (Knepper and Raines, 1985), and principal components analysis (Dwivedi and Sankar, 1992).

5--Image interpretation, by visual analysis, using the various digital processing techniques described, is a proven and effective methodology for lithological discrimination (Qari, 1989, etc.).

6--The spectral resolution of MSS imagery is rather broad and does not extend into regions of the spectrum most useful in characterising the spectral properties of geological surface materials. The most important effect that Landsat has had on the geological community is to whet its appetite for more powerful tools and techniques (Goetz *et. al.*, 1983).

Chapter 3

Landsat, imagery and the image processing system.

Chapter 3. Landsat, imagery and the image processing system.

3.1. The Landsat - 1 satellite.

The need to map world resources led to the establishment of the Earth Resources Survey Program by N.A.S.A. in 1965. Its objective was the development of a series of resource satellites which would observe the surface of the Earth repeatedly, from the same viewing angle (directly above), with good resolution, using uniform equipment and observation conditions (Sheffield, 1981).

The first of these satellites, known originally as ERTS-1, and later as Landsat-1 (see Figure 3.1) was launched on 23 July, 1972 and continued to function until 1979. It was the first satellite developed to carry imaging sensors that were designed specifically to provide data for those scientists working in the area of terrestrial resources (Mather, 1987). The satellite was relatively simple, about a ton in weight, travelling around the Earth in a circular, near-polar orbit with a revolution time of 103 minutes. The orbit was chosen to be sun-synchronous (see Figure 3.2) so that it would pass over the Earth at the same local time of day, usually 8:50 a.m. (local Sun time), and thus keep the illumination geometry of scenes imaged by Landsat as constant as possible.

Figure 3.3 shows the orbital coverage pattern of the Landsat satellites. Each Landsat satellite flies at a nominal altitude of 913 km in a circular orbit which ensures that the scale of the imagery is kept relatively constant. As the Earth turns beneath the orbiting satellite, successive swaths of the ground are imaged by the sensors on board, rather like string being wound on to a ball. It takes 18 days before the whole globe has been imaged, allowing the repetitive coverage necessary to monitor changing features on the Earth's surface. The nature of the

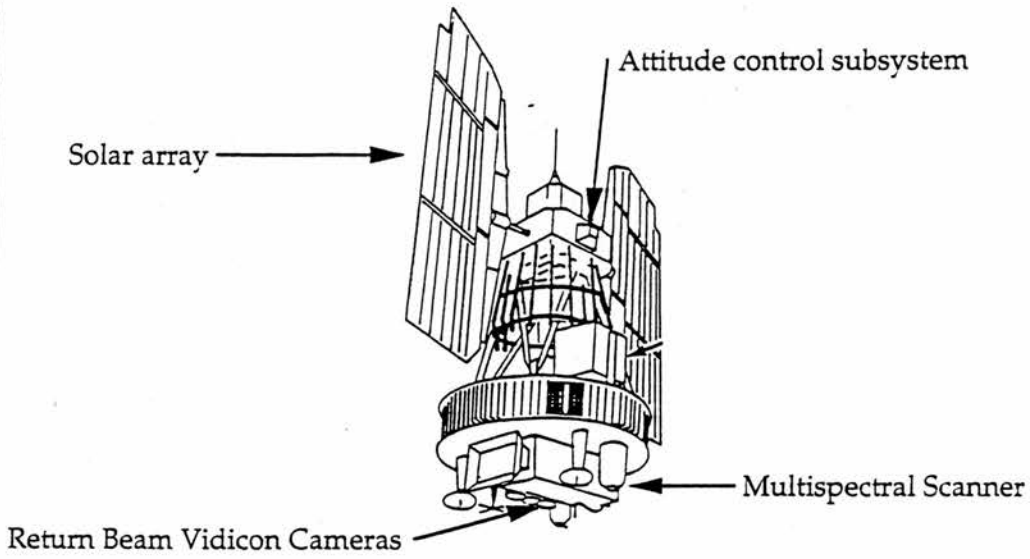

Figure 3.1 - The first generation Landsat satellite (after Harris, 1987)

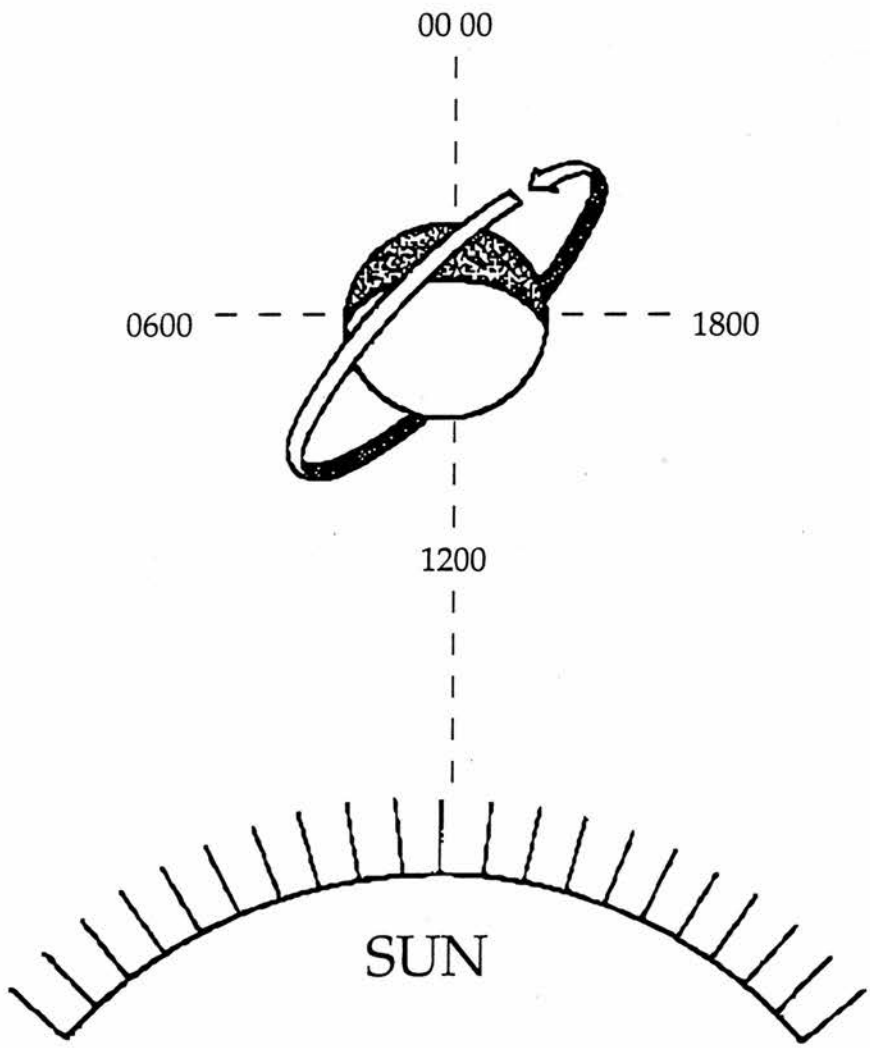

Figure 3.2 - Sun-synchronous orbit (after Mather, 1987)

satellite's orbit means that it never passes the north and south poles and images are thus restricted to regions that lie at latitudes below 81 degrees.

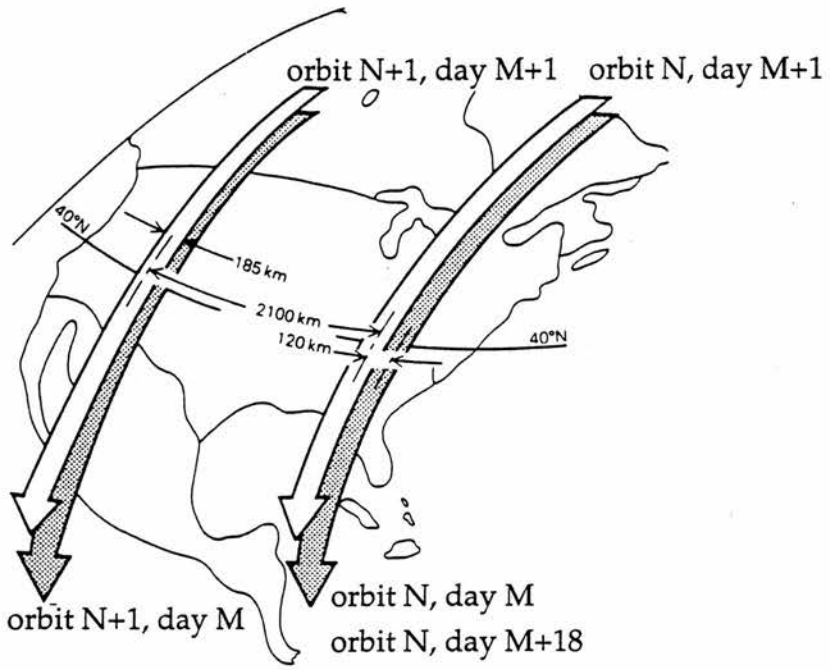

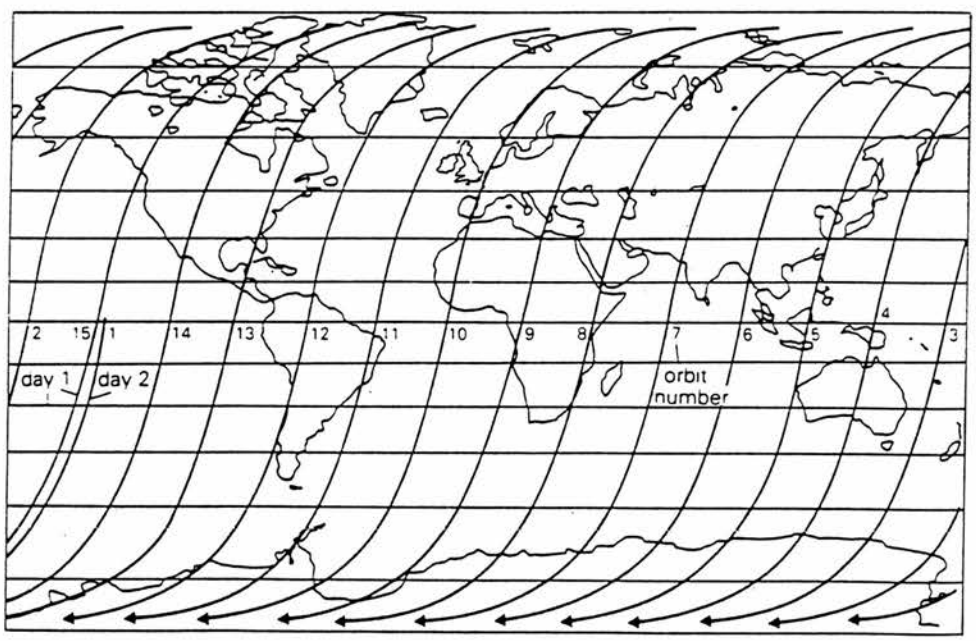

Figure 3.3 Orbital coverage of Landsat (after Drury, 1990)
Top diagram shows successive orbits. Every 103 minutes, the Landsat orbit is shifted 2100 km to the west. On the next day (M+1), the corresponding orbit is shifted 120 km to the west, so that images overlap. The sequence is repeated every 18 days. The orbits appear sinuous because they are sun-synchronous, and are inclined relative to the equator. Only the descending N-to-S orbits are shown, the ascending orbits pass on the night side of the Earth.

3.2. Data collection.

Two instruments were carried aboard the earlier Landsat satellites - The Multi-Spectral Scanner (MSS) and the Return Beam Vidicon (RBV). The latter instrument, essentially 3 video cameras viewing the Earth at separate wavelengths, failed early on in orbit with Landsat-1 and was only used as a standby to the MSS instrument on later satellites (Siegal & Gillespie, 1980). The Multispectral Scanner is a line-scanner which sweeps the ground below the satellite and builds up a picture of the Earth's surface as the satellite's forward motion moves it along (Mather, 1987).

The arrangement of the line scanner consists of an oscillating mirror which collects reflected radiation from an area 92.5 km to either side of the sub-satellite track, (Figure 3.4). Since the satellite velocity is too great to allow the scanning of an image one line at a time, radiation reflected by the mirror is directed towards an array of six sensors for each band, so that essentially six lines are scanned with each sweep of the mirror (Curran, 1985).

Reflected radiation collected by the mirror passes through a diffraction grating which 'filters out' four frequencies which are recorded separately by four sensors, each of which contains a linear array of six detectors, one for each of the six lines being scanned (Figure 3.5). The detectors sense all of the chosen wavebands simultaneously. Because of this arrangement, the response of each detector corresponds exactly to the same portion of terrain as all of the others at precisely the same instant of time. The data for each waveband can then be registered together exactly (Drury, 1987).

The analogue reflectance signals recorded by the sensors are converted to a digital format and transmitted to a ground receiving station. Earlier Landsat satellites

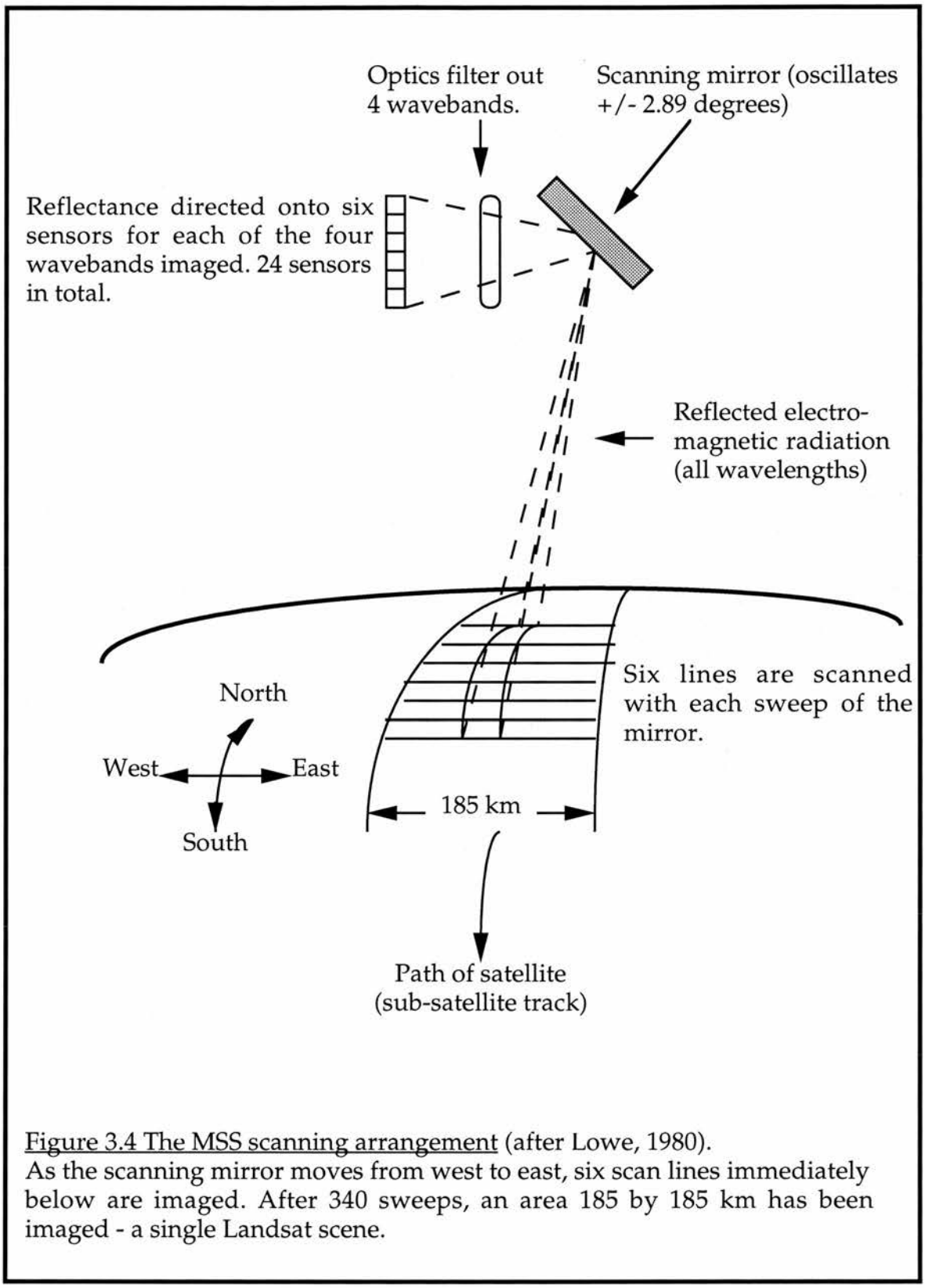

Figure 3.4 The MSS scanning arrangement (after Lowe, 1980).
As the scanning mirror moves from west to east, six scan lines immediately below are imaged. After 340 sweeps, an area 185 by 185 km has been imaged - a single Landsat scene.

carried on-board tape-recorders which were used to store data on areas where the satellite was out of sight of a ground receiving station. Nowadays, image data can be sent immediately to a ground station at White Sands, New Mexico from almost any region of the world by a series of relay satellites.

Two Landsat MSS images have been used in the present study. Their location is shown in Figure 3.6. Image 192/075 was collected on 6th January, 1973, and image 192/076 on 10th August, 1973.

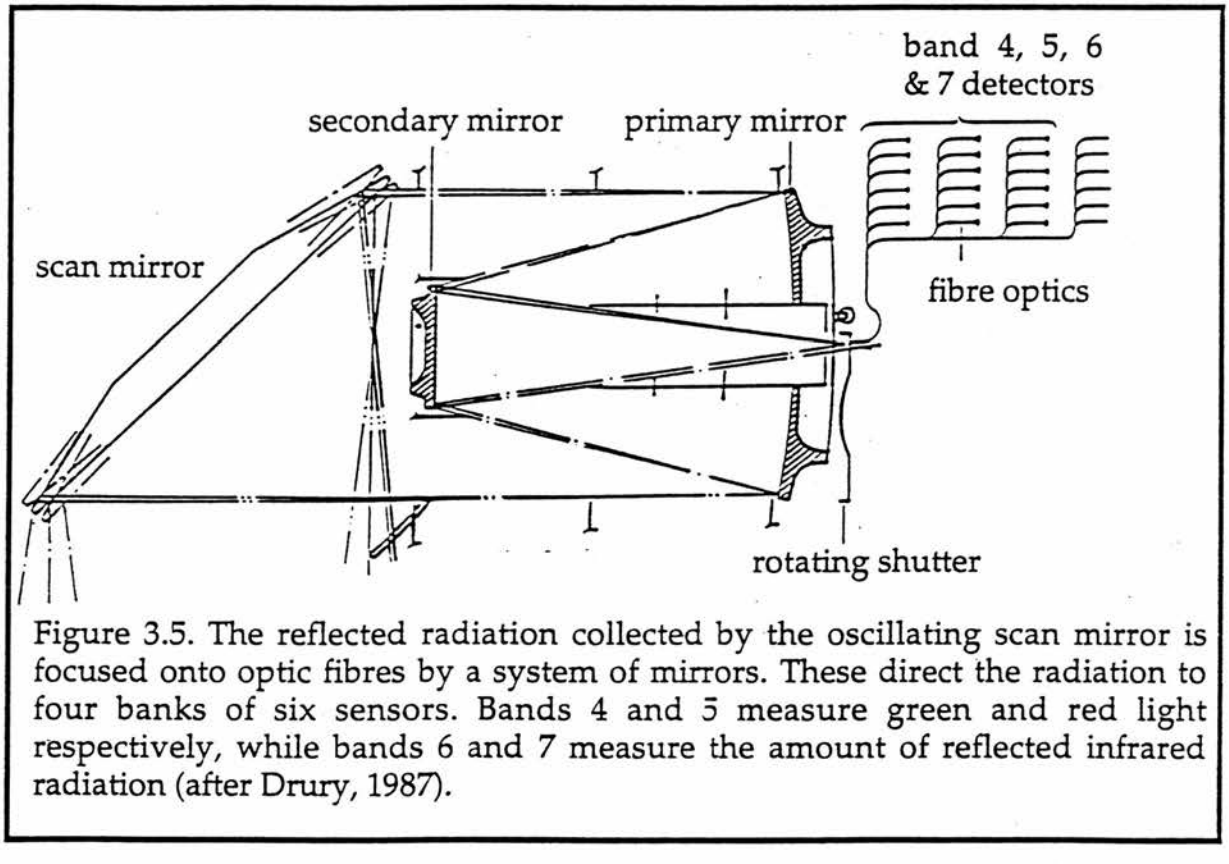

Figure 3.5. The reflected radiation collected by the oscillating scan mirror is focused onto optic fibres by a system of mirrors. These direct the radiation to four banks of six sensors. Bands 4 and 5 measure green and red light respectively, while bands 6 and 7 measure the amount of reflected infrared radiation (after Drury, 1987).

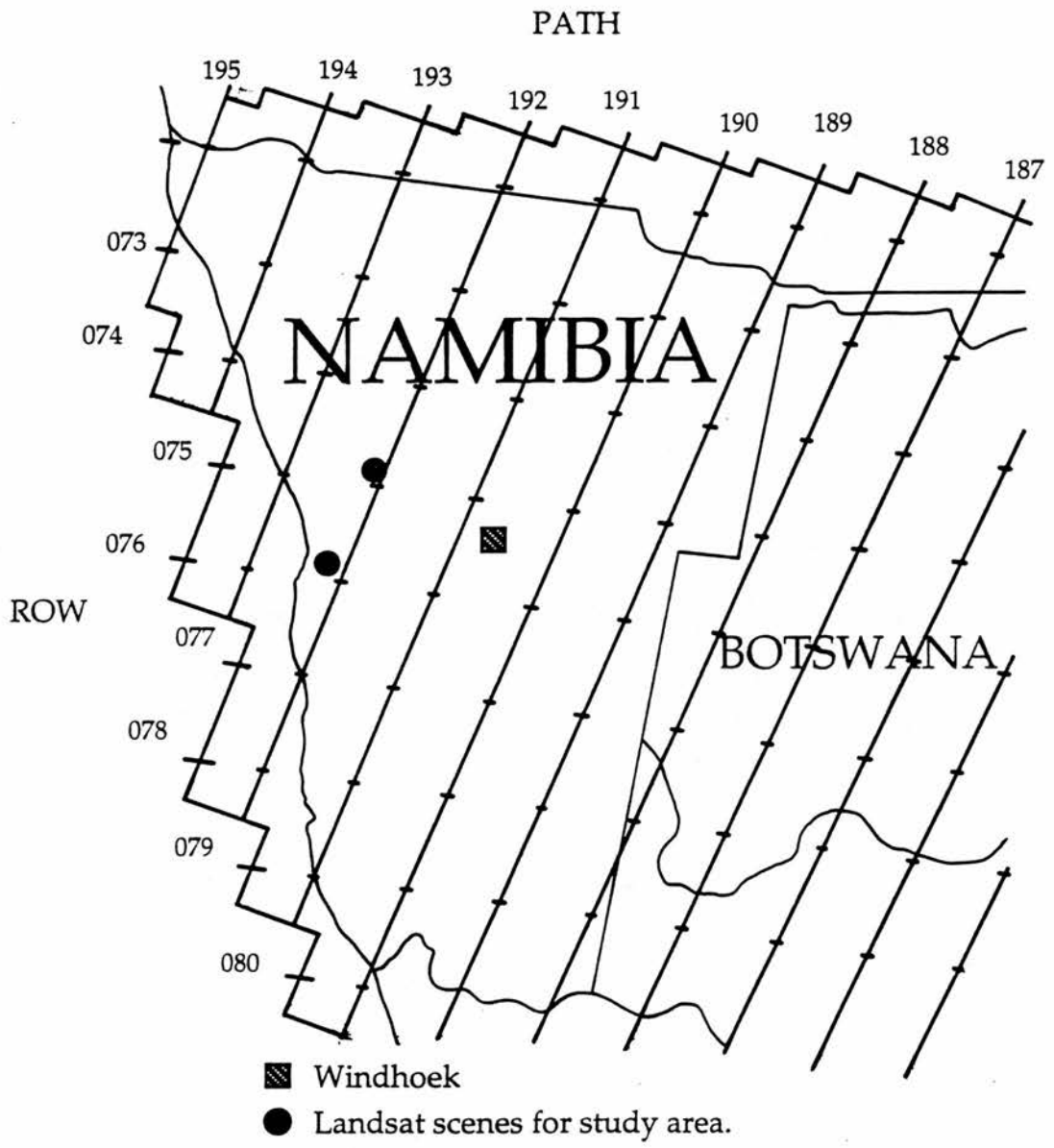

Figure 3.6. Landsat scene co-ordinates.

3.3. Image format.

The Multispectral Scanner simultaneously collects reflected radiation in four relatively broad spectral bands in the visible and near-infrared region of the electromagnetic spectrum, as shown in Figure 3.7. Each Landsat image is therefore made up of four identical images of the same ground area collected in four adjacent, but discrete, regions of the electromagnetic spectrum. Radiance is detected by individual sensors in analogue form, but this is converted to a digital format with a radiometric resolution of 6 bits (64 intensity levels) before being transmitted to a ground station. These data are often decompressed (or re-scaled) to a 0-255 (8-bit) scale by some ground stations for use with digital processing systems.

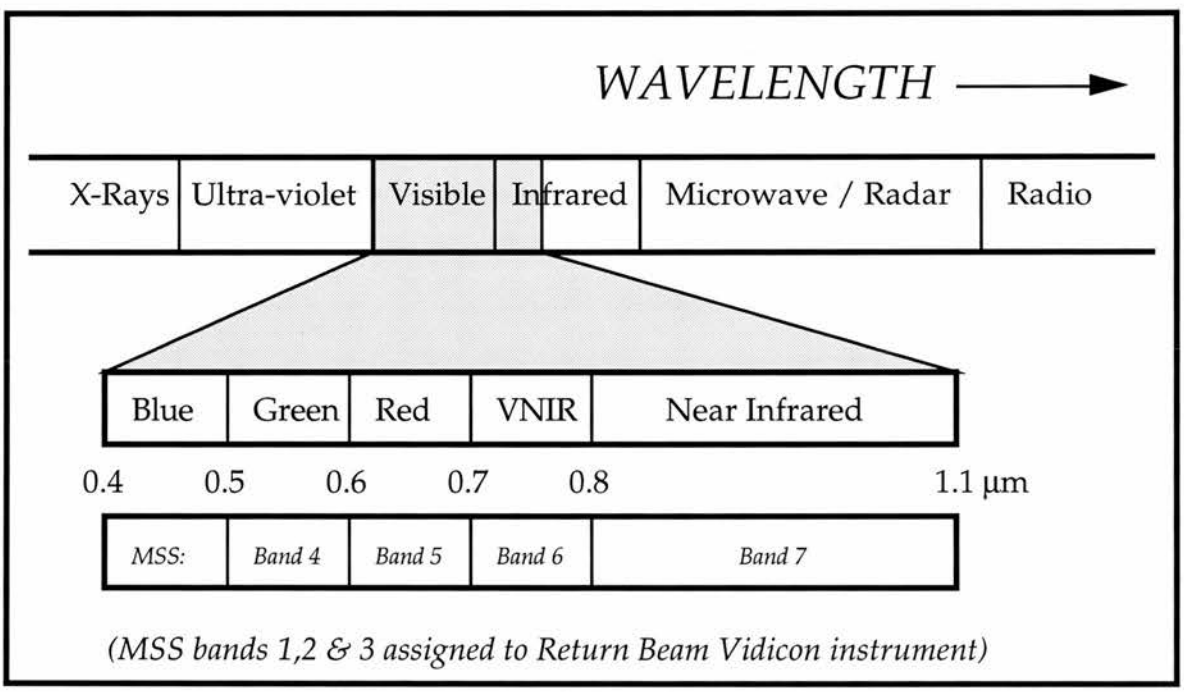

Figure 3.7. The Multispectral Scanner collects reflected radiation in four adjacent regions of the electromagnetic spectrum, between 0.5 and 1.1 µm.

The MSS mirror sweeps an area 474 m across, the detected radiation being directed onto a bank of six sensors for each of the four wavebands. Because six

lines of pixels are produced by each scan, each pixel row is 79 m deep. The analogue signal along each line recorded by the sensors (proportional to the reflected radiation) is sampled every 9.958 μs, corresponding to 56 m on the ground. The individual sampled element therefore relates to an area 79 m in the direction of satellite motion (along the y-axis of the image) and 56 m in the across-track direction (image x-axis). This pixel size (56 X 79 m) is thus less than the nominal instantaneous field of view; the reflectance level is over-sampled by about 40 % in the cross-track direction (Mather, 1987), as shown in Figure 3.8.

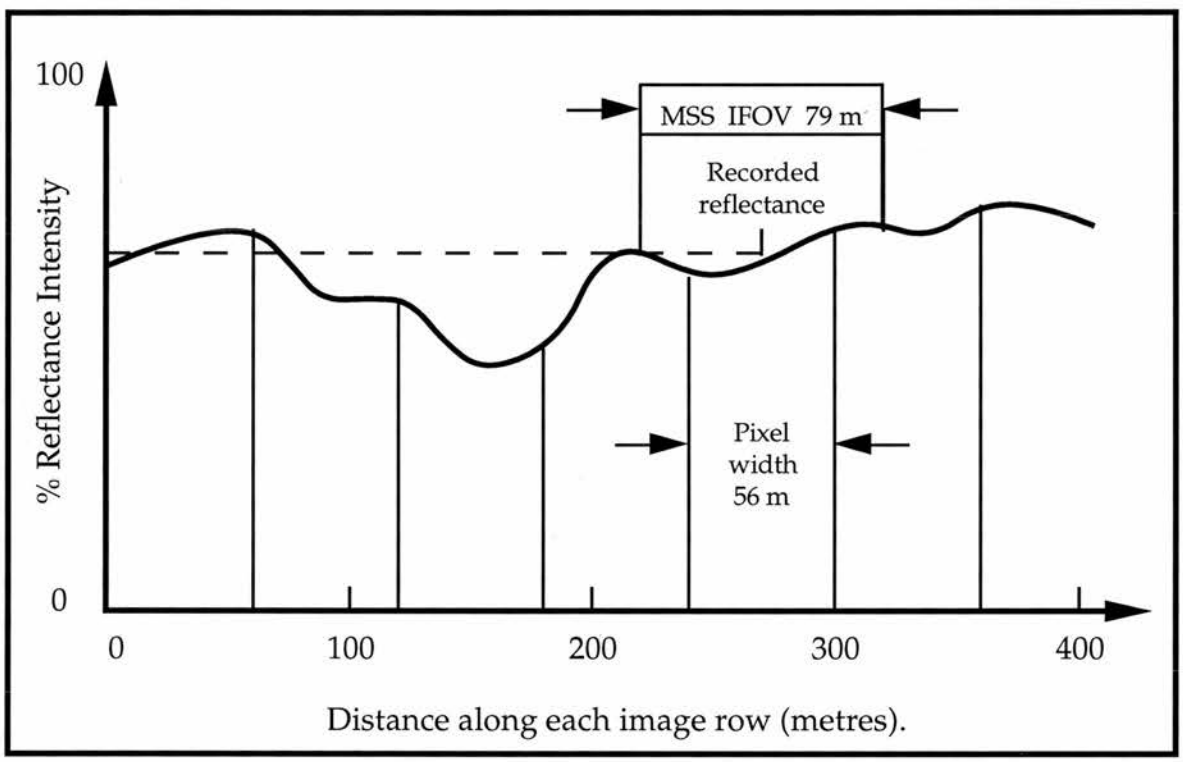

Figure 3.8. The irregular curve represents the variation in reflected energy along a MSS scan line in one waveband. The MSS scanner samples the value every 9.958 μs, which equates to 56 m on the ground, to produce a string of pixels. The scanner's instantaneous field of view (IFOV) is 79 m, so the value assigned to a pixel is the average reflectance over that distance, not that for the pixel itself.

The raw data from the MSS are in the form of a square matrix 2340 lines deep, each containing 3240 pixels (Figure 3.9). This gives a ground cover of 185 by 185

km. This geometrically precise array of pixels is identical in structure for each waveband so that they can be registered exactly. Because the Earth rotates beneath the platform during the 25 seconds taken to produce a whole scene, the square matrix represents a slight parallelogram on the ground.

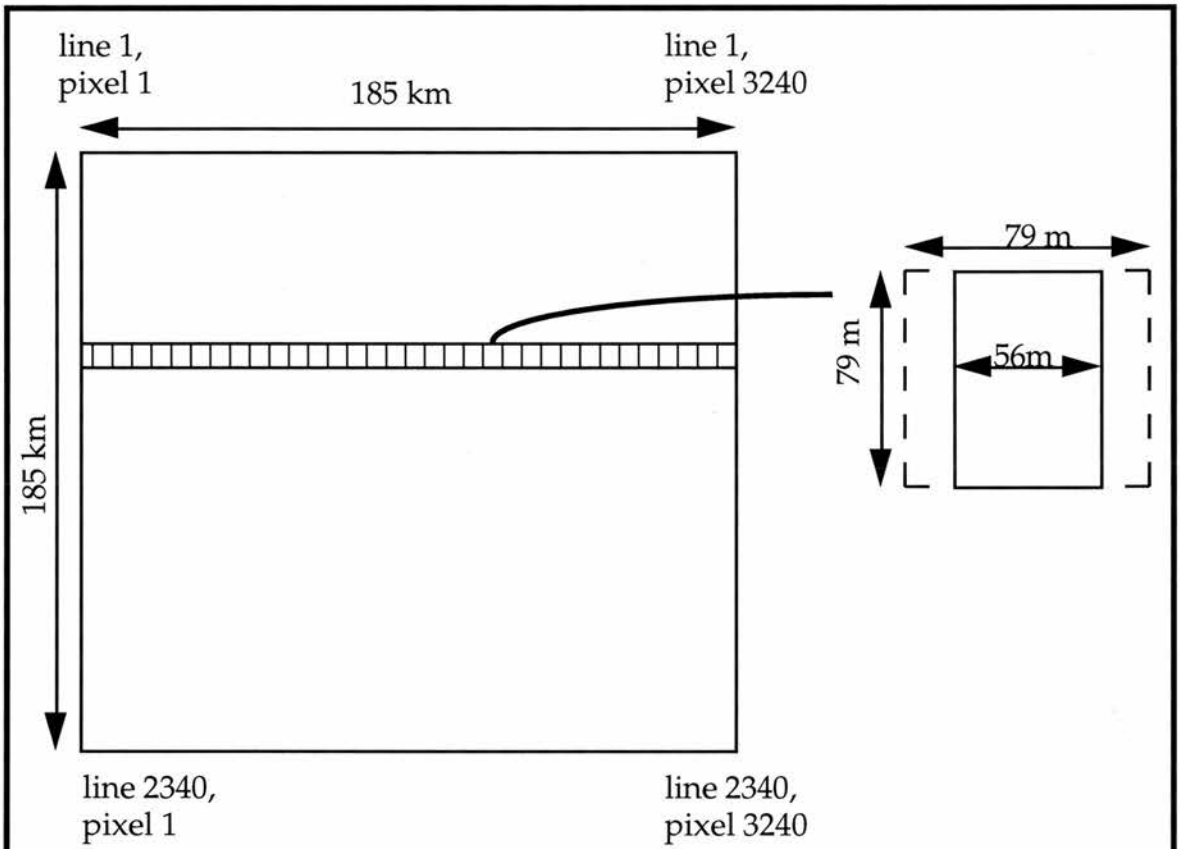

Figure 3.9. The raw data from a single Landsat MSS scene is in the form of a pixel array of 2340 scan lines, each 3240 pixels across. The area that an individual pixel (picture element) represents is shown alongside. Although the IFOV of the MSS is 79 X 79m, the pixel area is 79 X 56m (after Drury, 1990).

3.4. Image sub-sampling for geometric correction.

The Landsat imagery has been digitally processed and interpreted at full resolution for both the lineament analysis and the multispectral lithological mapping. However, the results have been mapped onto a hard-copy that has been resampled to allow for the geometric correction necessary in the horizontal direction of the image. A simple computer program to sub-sample image pixels in rows, but not columns, has been developed and utilised.

The data for a Landsat scene covers a square area 185 by 185 km. However, because reflectance levels are oversampled by about 40 % along the rows of the image, the square image area is represented by a rectangular pixel array (3240 pixels in each row by 2340 pixels in each column, Figure 3.9). When a hard-copy of the image is produced on a printer, individual pixels are printed as square elements, rather than the rectangles which they actually represent. Consequently, the printed image appears 'stretched-out' in the horizontal direction, and the image is not an accurate geometric representation of the imaged area.

To produce a square printout of the image, columns of pixels have been removed at regular intervals from the image at full resolution. A 'batch' program, which uses MS-DOS commands, displays a few columns of pixels, then misses out the next, and so on until the image sampled represents the true ground dimensions. Although real information is removed, it is never more than a single column of pixels at a time, and columns are removed regularly across the image.

Plates 3.1 and 3.2 show an example of the before- and after-effects of the transformation. If anything, the quality of the subsampled image is better,

Plate 3.1. First principal component image of part of the test area, before geometric correction (refer to text on page 34).
Image sub-scene AA (refer to map on page 75).

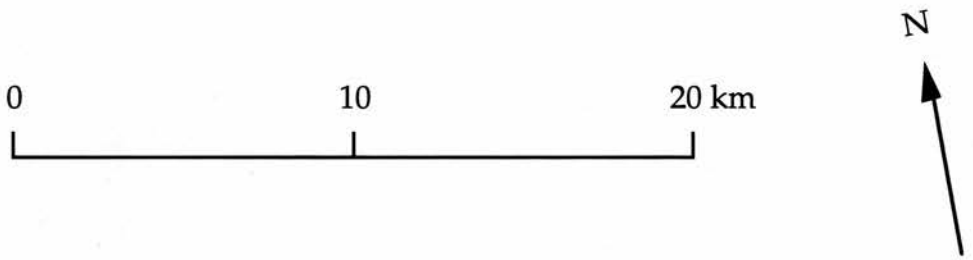

Plate 3.2. First principal component image of the same part of the test area, after geometric correction (refer to text on page 34).

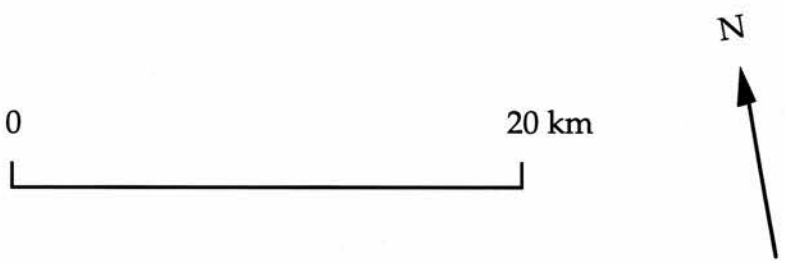

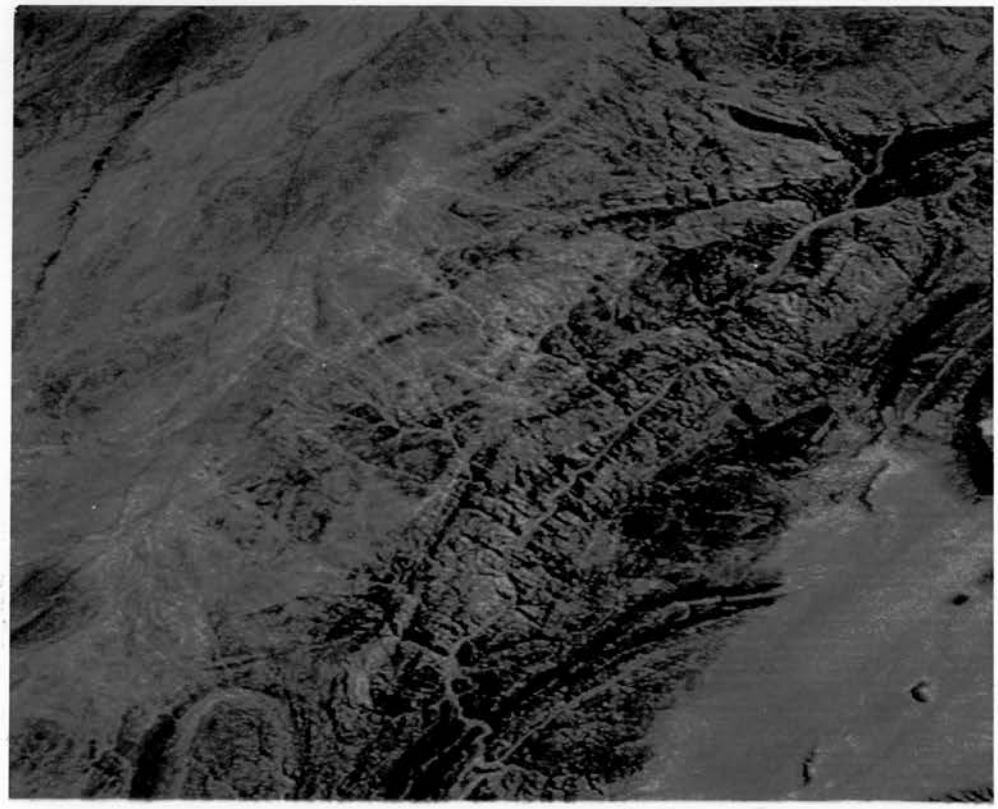

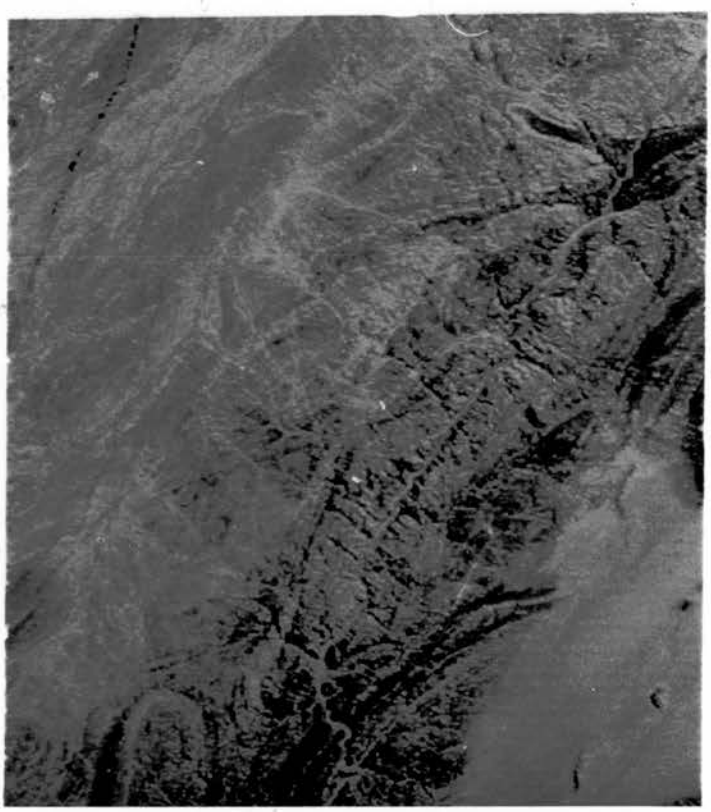

even though information has been lost, because the spatial frequency (see section 4.2.) and contrast across the picture is increased as the image is effectively compressed. In any event, interpretation is taken from full-resolution imagery which retains all the available information, the sub-sampled imagery is only used as a base on which to map results.

3.5. R-Chips image processing system.

The R-Chips image processing package was originally designed as an educational software system to teach the principles of image processing of remotely sensed data. In fulfilling this purpose, several other uses of the software have emerged, namely as a research support system and low-cost workstation system for operational users who had previously been unable to use image processing due to the complexity and cost of other systems. The operating system and processing programs are menu-driven.

Hardware consists of a host computer, a monochrome screen for the display of program menus, and a RGB colour monitor, containing a 512 X 32 (8-bit) graphics card, to display imagery. Digital images with a resolution of 8-bits, i.e. 0-255 intensity levels can be displayed on each of the three colour guns (red, green and blue) so that the intensity of each pixel reflectance level from 0-255 can be assigned a unique brightness intensity, again from 0-255, where 0 equals black, and 255 is the brightest pixel. Images from different spectral bands may be assigned to each of the three colour guns, so that three different bands of the same image may be displayed simultaneously in a colour-composite image. Low-quality hard copies of the screen display are provided by an ink-jet printer. Higher quality hard copies are provided by black-and-white and colour photographs taken from the screen.

The MSS image is 3240 X 2340 pixels in size. However, the colour monitor only allows a portion of the whole MSS image, equal to 512 X 512 pixels, to be displayed at full resolution. This equates to a ground area of approximately 1160 km^2. Processing and interpretation of the image is therefore segmented, although a mosaic of hard copies can be produced. Various image display, image enhancements and image transforms are available in the software; relevant procedures are discussed in the appropriate methodology sections.

3.6. The spatial and spectral components of Landsat imagery.

The information contained within any satellite image or photograph is represented by variance in surface reflection across the image area, either within a single band, or between bands. Where there is no variance and reflection is constant across the area of an image, no real information can be gained from that scene. The information, or variance, contained within imagery can be divided into two different categories - the spatial and spectral components (Lamb and Lawrence, 1993). The component of spatial variance is present in every MSS image band, whereas the component of spectral variance is present between MSS bands.

A multispectral image contains reflection variation (information) from more than one discrete region of the electromagnetic spectrum. It is the variation in reflectance between different spectral bands that allows for the spectral discrimination of different surface features. Information in each spectral band is usually highly correlated, so that features with a strong reflectance in one band, often have a similarly high reflectance in another. Though subtle, reflectance differences between bands are nevertheless sufficient enough to produce a range of colours in a colour-composite image, for example, where

information from three spectral bands are shown respectively as the additive primary colours red, green and blue. These different colours represent the spectral component of the information, which can be enhanced through the use of various digital image processing techniques. Different surface types and features can be identified and mapped on the basis of colour using this spectral information.

All imagery contains a spatial component of information. This includes the variations in tone, differences in surface texture, patterns and boundaries (referred to as 'edges') contained within a single-band or composite image. Just as different surface features could be mapped on the basis of their different colours, from a spectral point of view, those features may be similarly discriminated in colour and black-and-white images from a spatial perspective, in terms of differences in tone and texture (Sali and Wolfson, 1992) across the area of an image. The surface texture of different rock types, for example, may be expressed by different drainage network patterns, by different joint patterns, tonal banding and mottling, etc.

Lineaments are an example of 'edges', a spatial component of imagery. They are represented by lines of sudden tonal change across an image. The rate of change in tone and texture within an image is referred to as the spatial frequency. Rapid changes in tone and texture across an image are referred to as high-frequency changes, gradual ones as low-frequency (see section 4.3.1).

3.7. Conclusions.

1--Launched in 1972, Landsat-1 was the first satellite specifically designed to study terrestrial resources. Its orbit is sun-synchronous, so image scenes have a constant illumination geometry, and repetitive coverage is provided for most areas of the world.

2--Images provided by Landsat-1 are collected by the Multispectral Scanner (MSS) - a line scanning instrument, with a resolution of 79 m, which records reflected radiation from four adjacent regions of the visible and infra-red electromagnetic spectrum.

3--MSS images consist of an array of pixels, 3240 across by 2340 deep, for each of the four bands. Each pixel is described by a digital number (DN) which represents the intensity of reflected radiation for that ground segment. Individual pixels represent an area 79 x 56 m; the ground area that a single scene covers is 185 km^2.

4--Because reflected radiance is recorded every 56 m in the across-track direction, that signal is over-sampled by some 40%. The images have been sub-sampled to allow for the geometric correction necessary.

6--The information present within Landsat imagery is contained within a spatial and spectral component. These components have been enhanced by various digital image processing techniques using the R-Chips image processing package.

Chapter 4

Lineament Analysis.

Chapter 4. Lineament Analysis.

4.1. Introduction.

The analysis of lineaments, as an aid to interpreting regional tectonics, has been widely used (Crain, 1976). By their discrete nature, lineaments are often difficult to map at ground level, and only become visible with the synoptic view afforded by aerial and satellite imagery.

Historically, panchromatic aerial photographs were the only medium available to photogeologists, but even with the availability of multispectral images and the possibility of colour display, lineament studies continue to be based on the interpretation of black-and-white imagery. For the structural and tectonic interpretation of imagery, the eye operates most effectively in black and white (Drury, 1986). Lineaments are an element of the spatial component of imagery (see section 3.6) and are contained within elements of tone, texture and pattern. Whilst this information is included in a colour image, the spatial component becomes somewhat masked by the colour (spectral) information.

Although there is much criticism concerning the subjectivity of lineament mapping by visual analysis, as yet no 'magic algorithms' for the objective identification of lineaments by computer exist (Whittle and Gutmanis, 1993). An experienced interpreter, with geological and geomorphological knowledge, remains an effective and powerful tool.

To be as objective as possible, the Landsat imagery has been digitally enhanced to highlight real line segments. The filter used recognises any 'edges' and is not biased towards a preferred orientation. Inter-operator variance (Huntingdon and Raiche, 1978) is eliminated in this study, as all analyses are

performed by the same interpreter. By dividing the study area into a grid pattern of equally-sized sub-images (Figure 4.2), and examining each sub-scene separately, the whole image is examined uniformly.

Prior to analysis, the images are digitally processed to compress the maximum information from the four spectral bands into a single image, to suppress noise, and to highlight line features.

4.2. Principal Components Analysis.

Landsat MSS data consists of four images taken in four different regions of the electromagnetic spectrum. While these images are highly correlated, they each contain unique lineament information (Parsons and Yearley, 1986). However, many lineament studies are based on the interpretation of single-band MSS images, often biasing results, and different MSS bands are used in different studies. The question arises as to which image band/s are the most appropriate to use for effective lineament mapping? For such purposes it is best to use the most noise-free band from a multispectral image, or to use the first principal component image (Rothery, 1987).

Many workers opt for the use of MSS band-7 images for lineament analysis (Conradsen *et. al.*, 1986; Koopmans, 1986; Csillag, 1982). MSS band-7 has a significantly higher signal-to-noise ratio than other MSS spectral bands (Norwood, 1974) and atmospheric haze penetration is better in the infrared part of the electromagnetic spectrum (Moore and Waltz, 1983). Bare rock, soil and vegetation all appear with a relatively uniform grey tone. Thus, topographic shadows tend to have a fairly uniform contrast with the background. However, Dwivedi and Sankar (1992) find that MSS band-7

images contain the least image variance of the four available spectral bands (only about 20 %) and hence they also contain the least information.

Theoretically, the best approach would be to map lineaments separately from each of the four spectral bands, and combine the results in a final lineament map, e.g. Ananaba and Ajakaiye (1987). When the methodology is by visual interpretation though, this is time-consuming and inefficient, as many lineaments will be replicated in each band. This repetition of information reflects the correlation of image variance, essentially information, between bands and implies a level of 'redundancy' in the data (Mather, 1987).

A well-established process of reducing the redundant information in multispectral imagery is through principal components analysis. The technique is used in chapter 5 as a means of expanding and enhancing the colour (spectral) information in the imagery, but here the technique is used for a very different purpose - as a means of compressing the variance from four images into just one, while retaining most of the significant information. Multispectral datasets generally have a dimensionality that is less than the number of spectral bands. The purpose of the principal components analysis is to define the number of dimensions that are present in a dataset and to fix the coefficients which specify the positions of the set of axes which point in the directions of greatest variability in the data (Mather, 1987).

Figure 4.1 shows a plot of reflectance intensity (represented by a digital number from 0 - 255) for two MSS bands of the same image (plate 5.1). If exactly correlated, the data would plot as a straight line, and although this is not so, there is still a dominant direction of variability. Although the number of variables is two, the dimensionality of the dataset is one. The first principal component is the axis which represents this direction of maximum variance

(information). The information contained within the two axes could be represented in a one-dimensional plot using the line AB - the first principal component.

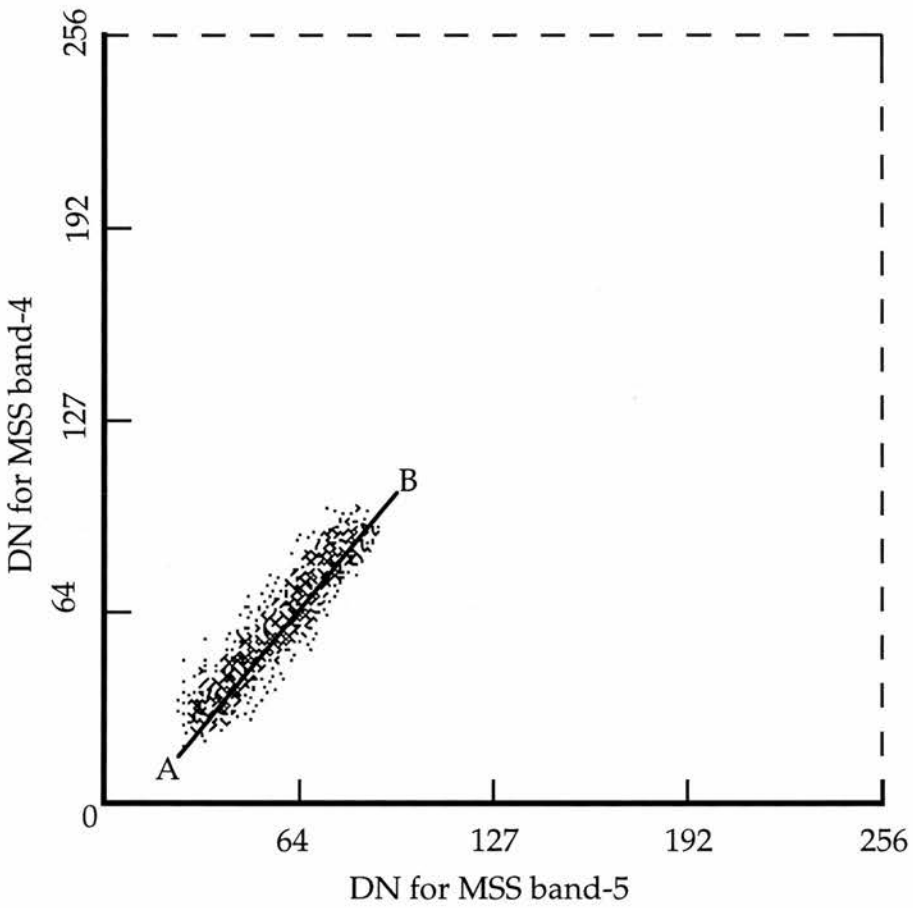

Figure 4.1. The DN values (digital number representing reflection intensity) for two bands of an MSS scene are plotted against one another. The data occupies only a small amount of the feature space available to it due to the high correlation of reflection intensity between image bands and the dynamic range that the sensor needs to work between.

With reference to the above, the first principal component image has been chosen to extract lineament information from, rather than the MSS band-7 image, as is more common. The improvement in quality over band-7 is shown in plates 4.1 and 4.2. Not only does the first principal component image contain most of the information from the four spectral bands (in excess of 90 % of the image variance can be compressed into the first principal component)

but random variance (noise in the imagery such as banding) is also removed. This improvement occurs because random variance/noise is assigned to the higher-order component images, as shown in plate 4.3 (Singh and Harrison, 1985).

Because of the size of the two MSS images, and the amount of data involved, and because of display limitations, the Landsat images have been divided into an arbitrary grid pattern (as shown in Figure 4.2) and the first principal component images derived for each cell area. These images have then been further enhanced through spatial frequency filtering and contrast-stretching techniques, which are discussed in the proceeding sections.

Plate 4.1. Band-7 greyscale image of the test area (refer to text on page 43).
Image sub-scene AA (refer to map on page 75).

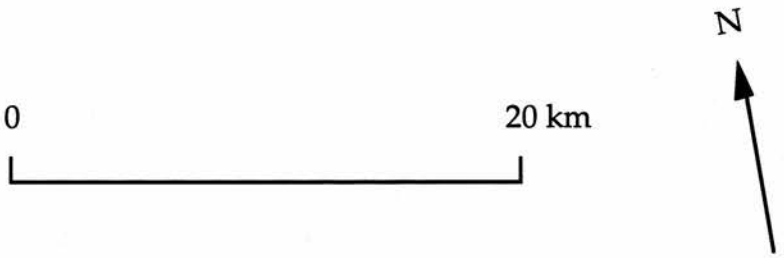

Plate 4.2. First principal component greyscale of the test area (refer to text on page 43).
Image sub-scene AA (refer to map on page 75).

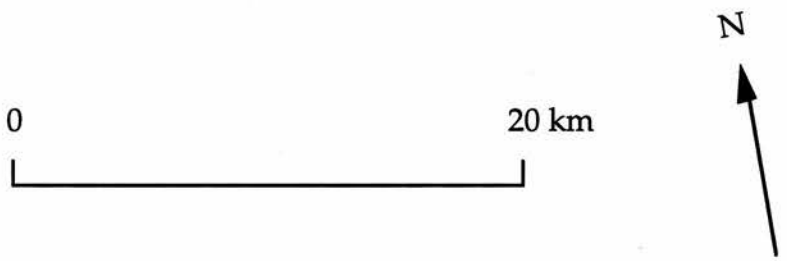

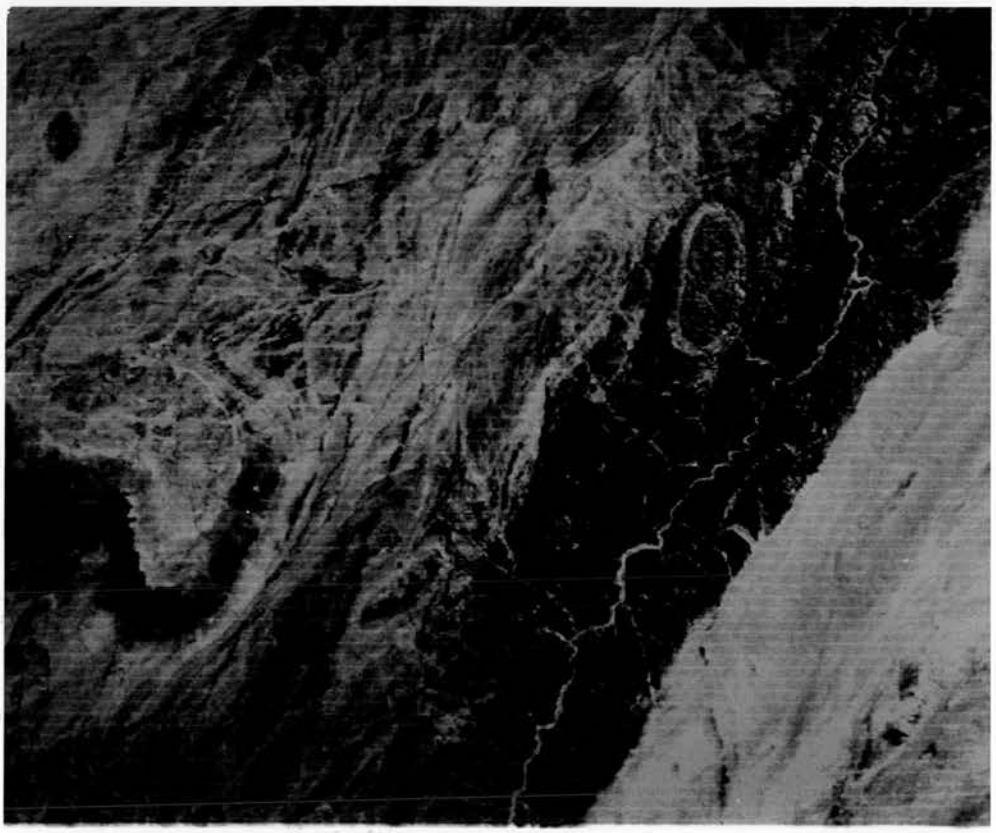

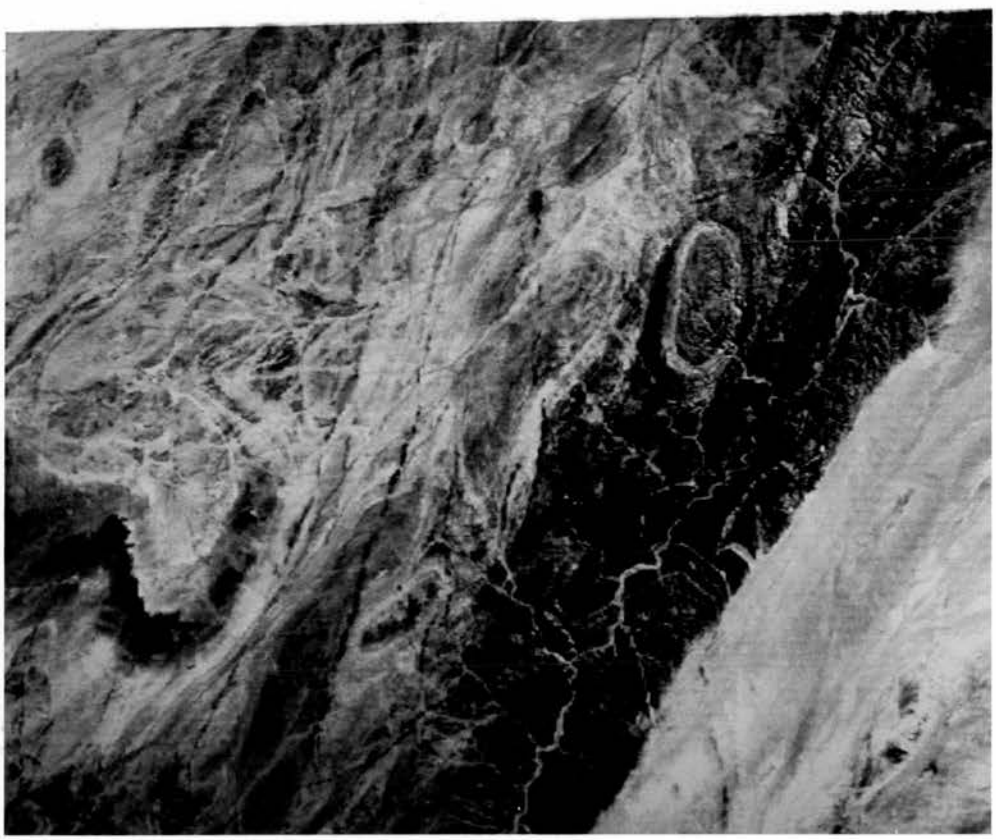

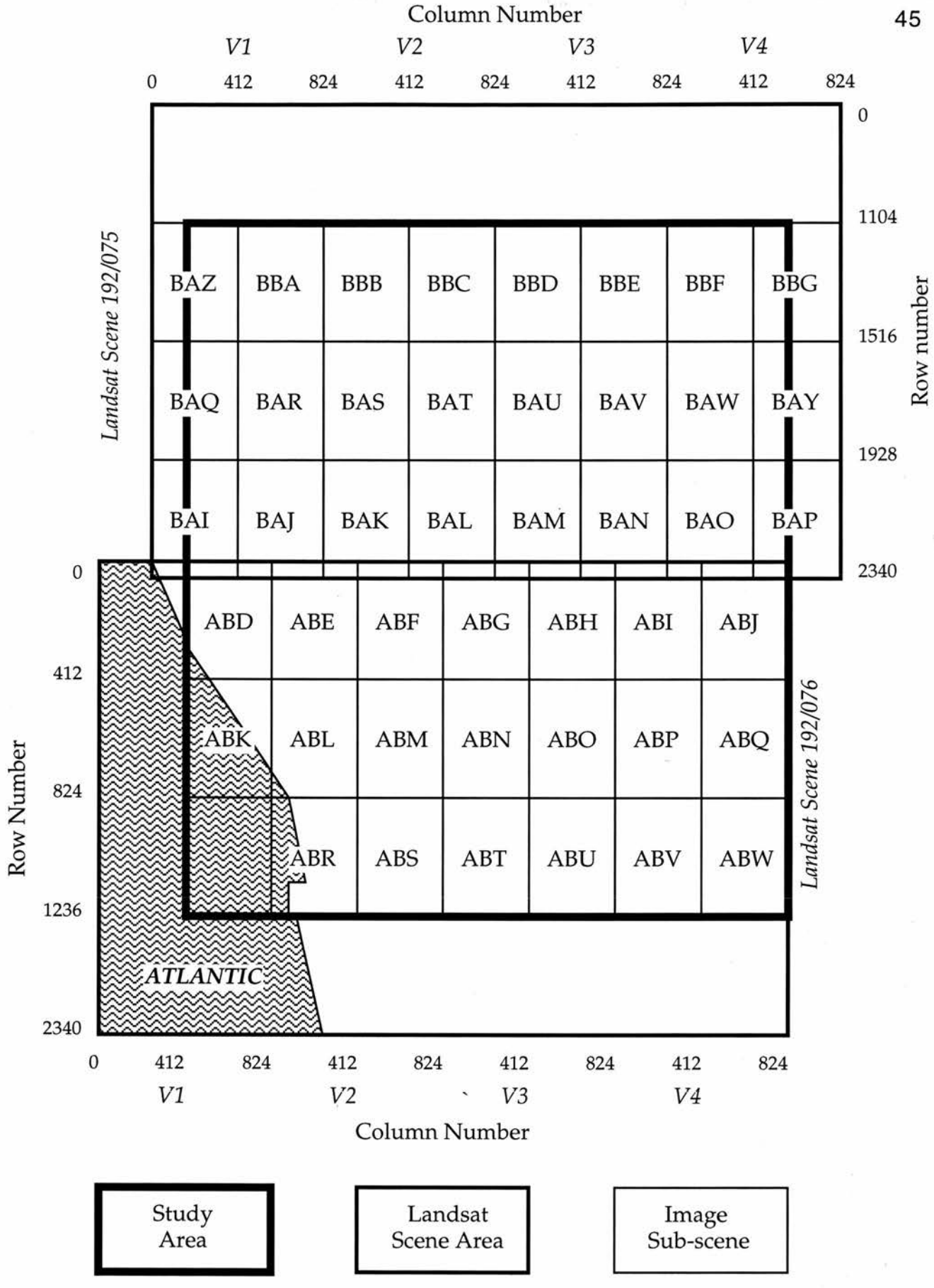

Figure 4.2. Layout of Landsat MSS image sub-scenes covering the study area.

4.3. Image Filtering.

The images derived from the first principal component of the MSS data have subsequently been digitally enhanced to highlight so-called 'edges' (Drury, 1987). Convolution filtering produces an image of 'edges' - a texture image, which has then been added to the original principal component image to produce an edge-enhanced version.

4.3.1. The Concept of Spatial Frequency.

Lineaments appear as 'edges', a spatial component of imagery (see section 3.6). An edge is a discontinuity or sharp change in the intensity value at a particular pixel point and it may have some interpretation in terms of geological structure (Mather, 1987). The rate of change in tone and texture within an image is referred to as the spatial frequency. Rapid changes in tone and texture across an image are referred to as high-frequency changes, gradual ones as low-frequency.

An illustration of the rate of change of tone, or spatial frequency of brightness, is shown by a graph of brightness against distance across an image (curve f in Figure 4.3). This irregular curve reveals rapid and gradual alterations in brightness, referred to respectively as high- and low-frequency changes. The contrast gradients and the spatial resolution of the system control how much information about geological structure can be extracted from an image (Drury, 1987). Although the brightness variation curve is a complex one, it can be broken down into a series of more simple sinusoidal curves, which themselves represent changes in brightness at different frequencies.

Curve f, which represents a theoretical brightness variation curve, can be reconstructed by superimposing a number of more simple, sinusoidal curves, of varying frequencies and amplitudes. The exact value along curve f is replicated by adding together the values of each of the sinusoidal curves below. The example is a rather simple one, but does demonstrate how the observed scene brightness may be composed of different frequency phenomena. Filtering is basically the removal of some of these simple sine waves to leave the ones that represent features of particular interest (Drury, 1990).

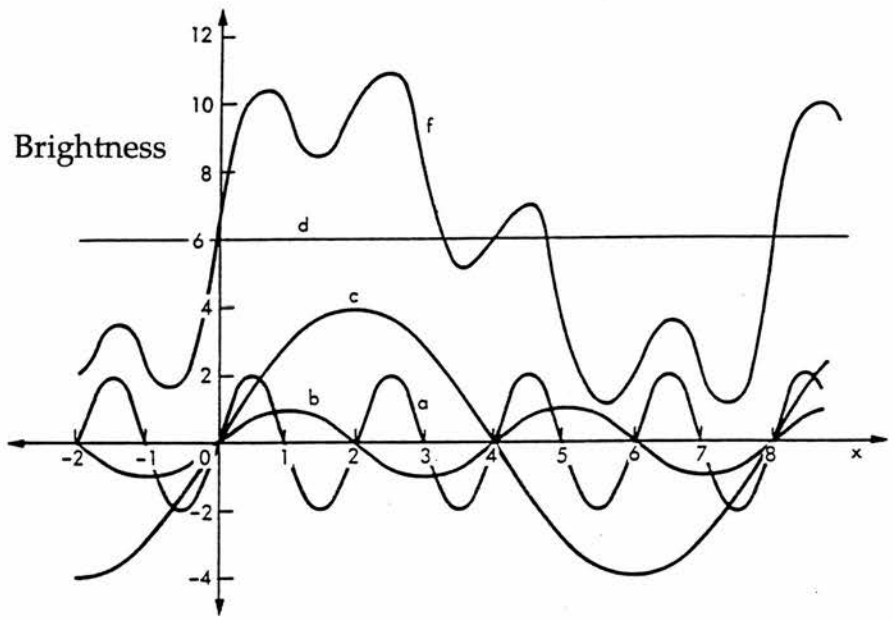

Figure 4.3. An apparently irregular brightness variation curve, illustrated as curve f, is the result of the combination of different frequency phenomena. Filtering emphasises or removes some of these frequencies to highlight features of particular interest (after Gillespie, 1980).

An image scene may contain a complete range from high- through to low-frequency features. For geological purposes, the most important boundaries are often 'edges'. These are high-frequency, high-amplitude features that have steep gradients, i.e. scene brightness alters rapidly over a short distance. Many

geological and geomorphological features such as faults, major joints, dykes and river networks form edges of this kind, often because they have a highlighted topographic expression with adjacent darkened shadowing. Lithological boundaries produce tonal edges between rocks with different reflective properties. Similarly, tonal edges may also be produced by soils derived from different rock types, or vegetation boundaries that have an underlying geological control. Edges may occur in isolation, as in the case of faults or other boundaries separating large, uniform masses of different rock types. They may also be closely spaced, especially when they represent compositional banding or joints.

Whereas edges may represent small-scale geological features, medium- and low-frequency spatial features often show the gross geological features of an area. Many folds repeat stratigraphic sequences on the scale of kilometres. They define medium-frequency spatial features. Phenomena such as batholiths, major fault blocks, sedimentary basins and orogenic belts control low frequency features with dimensions in tens or hundreds of kilometres. The lower the frequency of a feature on an image is, the more subtle it tends to be and the more difficult it is to perceive, depending on the associated contrast.

Scale and resolution of the imagery are important criteria in determining what features are discernible and what specific-frequency features actually represent. The effective resolution element is a measure of the spatial resolution of the imaging system (Wilson, 1988). The highest frequency features seen on MSS images will represent larger-scale features than those observed on Landsat Thematic Mapper images (Townsend, 1987). When mapping high-frequency linear features it is important to quantify what is being mapped, with relevance to the imagery being used - all too few

lineament maps specify the nature of the expression mapped or its quality (Gold, 1980). Where visual interpretation is used, the scale of the displayed imagery is also important. This is due to the resolving power of the eye, and its ability to discriminate between different brightness levels. The eye may not be able to distinguish two objects if they are very close on the image, but can do so if the image is simply enlarged (Drury, 1987). The scale of the imagery displayed must be great enough to allow the visual identification of narrow, high-frequency features, which is how lineaments generally appear.

4.3.2. Spatial Frequency Filtering.

The process whereby the spatial distribution of data in a digital image is enhanced is known as spatial-frequency filtering. This consists of selectively enhancing high-, medium- and low-frequency variations of DN (the 'digital number' from 0-255 assigned to each pixel and proportional to reflection intensity) to highlight particular features. By simply manipulating the contrast of an image, certain features contained therein become more or less apparent. Reducing the contrast leaves visible only the low and medium-frequency features, whereas increasing it accentuates the sharp contrasts associated with edges. However, there is a limit to which either of these transformations can be taken, before the visual quality of the image begins to break down and interpretability begins to degrade. A more powerful technique is to use various mathematical transforms to selectively extract the high-, medium- and low-frequency variations.

Convolution filters can be modified to enhance or suppress low and high-frequency features. Those which emphasise high-frequency ones are referred to as high-pass filters (Drury, 1987). Lineaments appear on imagery as single or

composite high-frequency 'edges' whose parts are aligned in a rectilinear relationship. A high-pass convolution filter has been used as an objective means of edge detection in this study, and should therefore enhance any linear features which are made up of these edges.

Convolution is the movement (pixel by pixel, and line by line) of a filter window through an image. Successive pixels of the original image are multiplied by values within the window, and the products are summed to form the resulting filtered image (Moore and Waltz, 1983). The size of the filter window is proportional to the wavelengths allowed through it (Mather, 1987) so that with high-pass filters, the smaller the window used, the higher the frequency of features which will show up (Drury, 1987). The smallest possible filter window (3 X 3) has been used in this study and its configuration is shown below. Various different edge-detection algorithms were experimented with, the one shown below yielded the best results.

0	-1	0
-1	4	-1
0	-1	0

X 1/2

Figure 4.4. Convolution matrix (filter window) used for edge-detection (high-pass filter).

The filter window is overlain on the first principal component image with its central cell on the top left pixel, and the other cells lying on top of the immediately surrounding pixels. The DN for each pixel overlain by the convolution matrix is multiplied by the corresponding weighting factor, and

the products are summed. It is the sum of the weightings which is used to compute the value to be used in place of the DN of the pixel beneath the centre of the convolution matrix. An output image is produced by the convolution matrix being moved over every pixel in the image (Drury, 1987).

The resulting output image is termed a 'texture image' and an example derived from the first principal component image (plate 4.2) is shown in plate 4.4. It is really an image of the high-frequency features present in the original image. When it is added back to the principal component image, an 'edge-enhanced' image (plate 4.5) is produced which appears 'sharper' than the original. Subsequent enhancement through the digital processing technique of contrast-stretching further improves the appearance and interpretability of the images, prior to visual analysis.

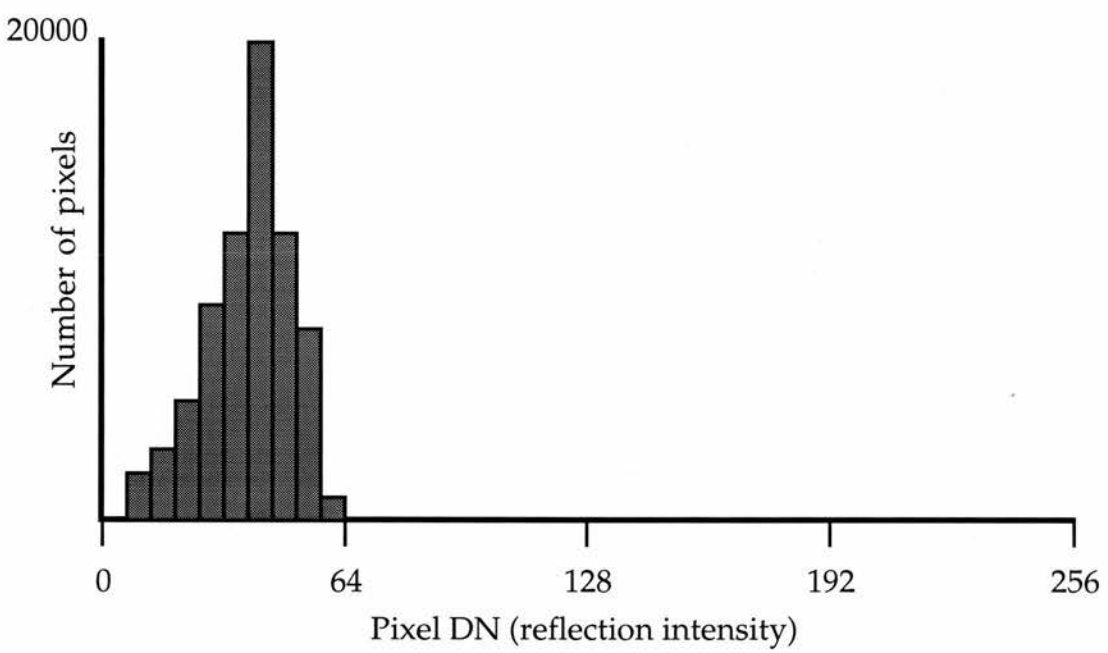

Figure 4.5. Frequency histogram of DN for the pixels that make up plate 4.2

Plate 4.3. Fourth principal component greyscale image of the test area (refer to text on page 44).
Image sub-scene AA (refer to map on page 75).

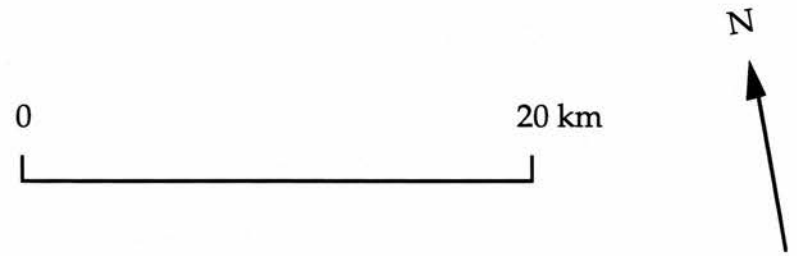

Plate 4.4. Texture image of the test area produced by convolution filtering (refer to text on page 51).
Image sub-scene AA (refer to map on page 75).

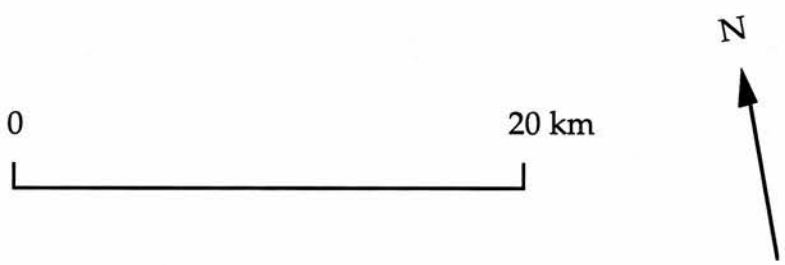

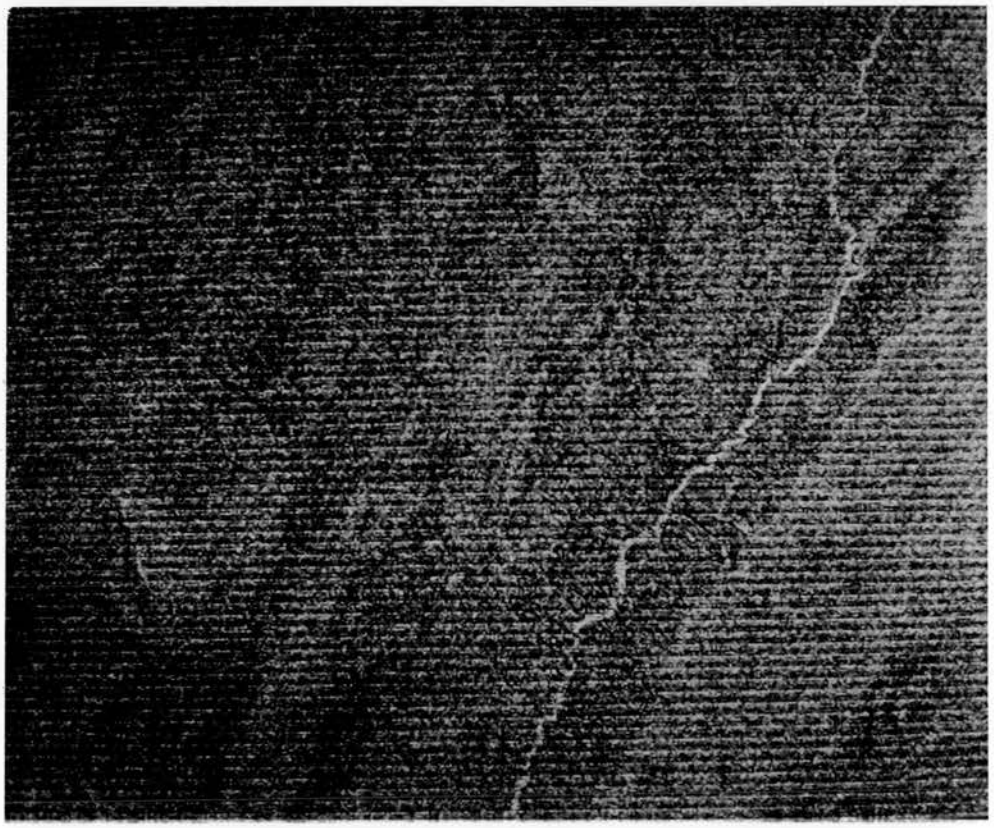

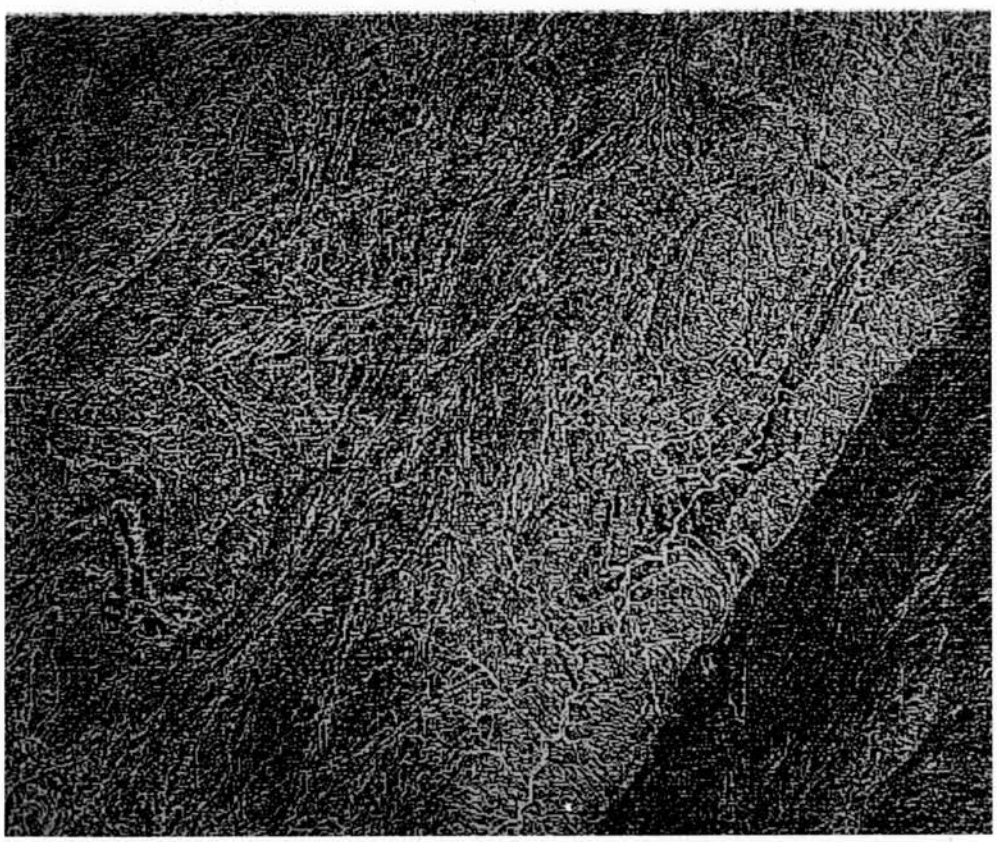

Plate 4.5. Edge-enhanced imaged of the test area (refer to text on page 51).
Image sub-scene AA (refer to map on page 75).

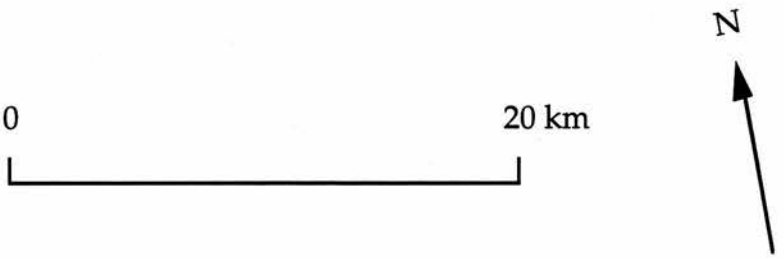

Plate 4.6. Unstretched greyscale image of the test area (refer to text on page 53).
Image sub-scene AA (refer to map on page 75).

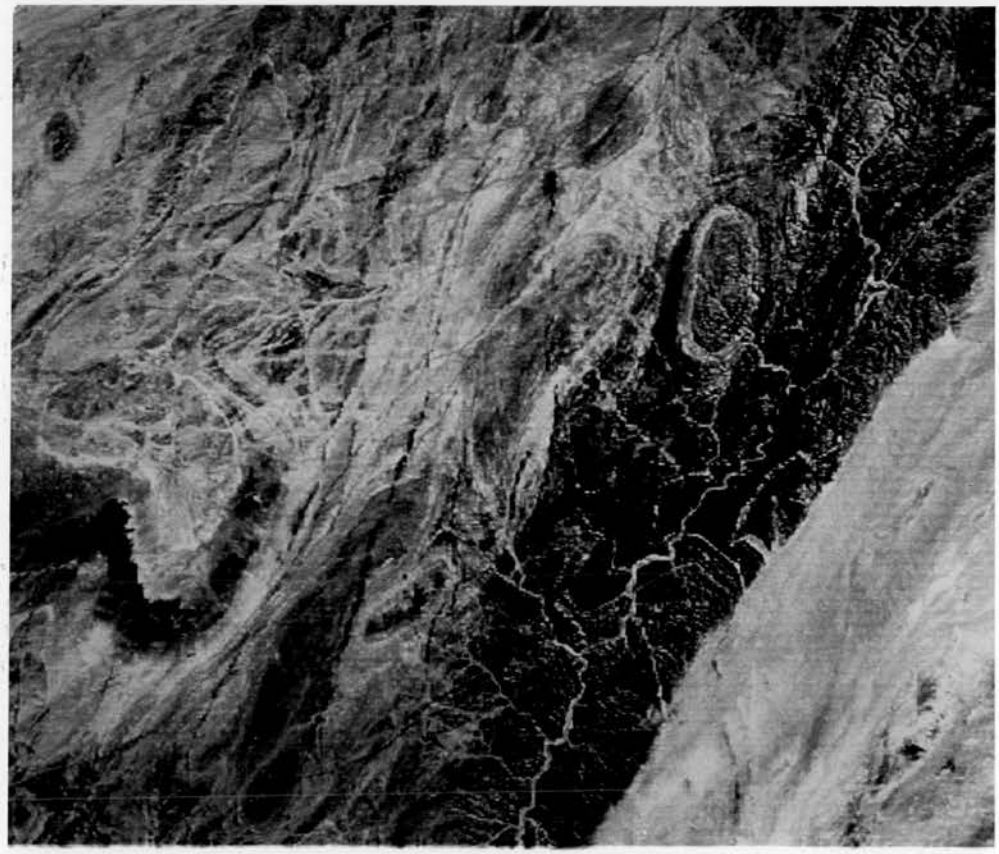

4.4. Contrast Stretching.

The MSS sensors onboard the Landsat satellite record reflected radiation on a 6-bit scale, i.e. over 64 intensity levels. The optical sensors have to be able to record reflected radiation over a wide range of surface conditions, from low radiance levels over water to high levels over snow-covered ground. For a particular scene being imaged, it is unlikely that the whole dynamic range of the sensor will be used (Mather, 1987).

Figure 4.5 shows a frequency histogram plot of DN (digital number) for plate 4.1. Like most images, the histogram is compressed into a relatively small part of the 0-255 range (the 0-63 range of the raw data has merely been rescaled) and therefore the image has low contrast. In photographic terms, the image could be described as being underexposed. Limitations due to the eye's resolving power means that the interpretation of the image by visual analysis is difficult and not much detail can be seen.

By altering the range of grey levels, to fit the full length of the black-to-white DN axis, while maintaining their relative distribution, the contrast between the light and dark areas of the image can be improved. The simplest means of achieving this is through a linear contrast stretch. This involves the mapping of the pixel values in the raw data from DN_{min} to DN_{max} to the full range of the display device, i.e. 0-255 (Mather, 1987).

When this transformation is initiated with R-Chips, the computer sets up a 'look-up table' (LUT) as shown in Figure 4.6. The LUT converts an input DN (x) to an output DN (y) in a linear fashion from $DN_{2.5\%}$ to $DN_{97.5\%}$. The DN less than the 2.5 percentile and above the 97.5 percentile are not included as these data usually represent the effects of atmospheric scattering (discussed

below) and detector noise respectively.

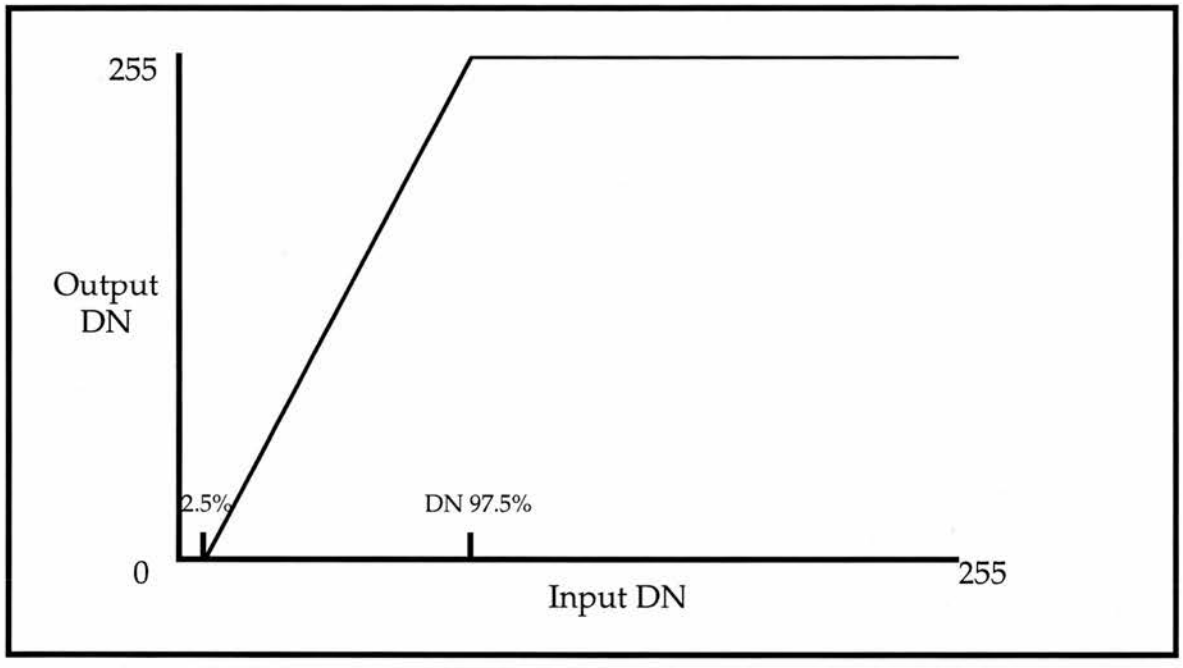

Figure 4.6. A linear contrast stretch is achieved by a simple straight line Look-Up Table which sets the 2.5 percentile DN value to 0 and the 97.5 percentile to 255.

The image histogram (Figure 4.5) shows that no pixels have a DN of zero, yet the image contains areas of shadow which should theoretically receive and reflect no radiation. These areas are affected by atmospheric scattering - the shadows are lit by randomly scattered radiation from the sky (Drury, 1990). The LUT assigns the 2.5 percentile DN to zero. By assigning the actual DN which represent shadows to 0, they appear dark and not hazy. This is important since lineaments are often shown on imagery by a topographic expression with associated shadowing. The improvement in image contrast and quality, brought about by the contrast stretching technique, is shown in plates 4.6 and 4.7.

4.5. Lineament Mapping by Visual Analysis.

4.5.1. Lineament Criteria.

Before lineaments can be mapped from the imagery, it is necessary to define their appearance and mapping criteria. The term 'lineament' was introduced by Hobbs (1904) and it now covers a wide variety of features. Appropriate qualifying adjectives should be used to indicate their mode of expression, for example photo lineaments, topographic lineaments, magnetic lineaments (Gold, 1980). Numerous definitions are available, some of which are given below:

-Lineaments characterize such relationships as crests of ridges or boundaries of elevated areas, drainage lines, coastlines, and boundary lines of formations, petrographic rock types, or lines of rock outcrops (Hobbs, 1904).

-Tectonic lineaments are straight or gently curved, lengthy features of the Earth's surface, frequently expressed topographically as depressions or lines of depressions; these are prominent on relief models, high-altitude air photographs, and radar imagery. Their meaning has been much debated; some certainly express valid structural features, such as faults, aligned volcanoes, and zones of intense jointing with little displacement, but the meaning of others is obscure, and their origins may be diverse, or purely accidental (Gary *et. al.* 1974).

-Lineaments are defined as mappable, simple or composite linear features of a surface, whose parts are aligned in a rectilinear or slightly curvilinear relationship and which differ from the patterns of adjacent features and presumably reflect a subsurface phenomenon (O'Leary *et. al.*, 1976).

-A lineament is any line on an aerial photograph that is structurally controlled; it includes, for photogeological purposes, any alignment of separate photographic images such as stream beds, trees or bushes that are so controlled. Thus the word has very wide applications; it can be used to refer to lines representing beds, lithologic horizons, mineral bandings, veins, faults, joints, unconformities and rock boundaries (Allum, 1978).

-The term lineament is correctly applied to long, often subtle, linear arrangements of various topographic, tonal and geological features (Drury, 1987).

Lineaments are defined in this study as 'mappable, natural linear features which are visible on the imagery as topographic expressions or depressions (as determined by shadowing), and as aligned tonal and/or textural boundaries, and presumed to have some geological significance'. Knowing the sun's azimuth, distinction can be made between positive and negative relief features - positive features have shadowing behind a brighter area, negative features have shadowing in front. Features less than 2 km have not been mapped because over such a short distance any alignment may be due as much to chance as to a structural control. On the basis of the definitions above, four separate lineament maps have been compiled:

1 - Positive topographic lineaments. These are generally caused by more resistant rock units, mostly the dykes that criss-cross the region (see plate 4.8).

2 - Negative topographic lineaments. These express lines of weakness, usually picked out and utilised by linear drainage segments. They often represent faults and major joints (see plate 4.9).

Plate 4.7. Contrast-stretched greyscale image of the test area (refer to text on page 53).
Image sub-scene AA (refer to map on page 75).

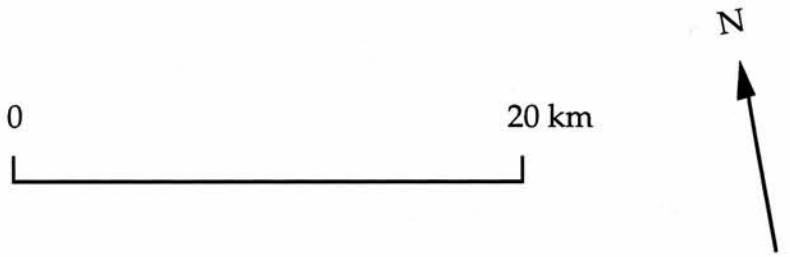

Plate 4.8. In the western portion of this image, north-trending Etendeka dolerite dykes form identifiable positive topographic linements (refer to text on page 56).
Image sub-scene BAR (refer to map on page 45).

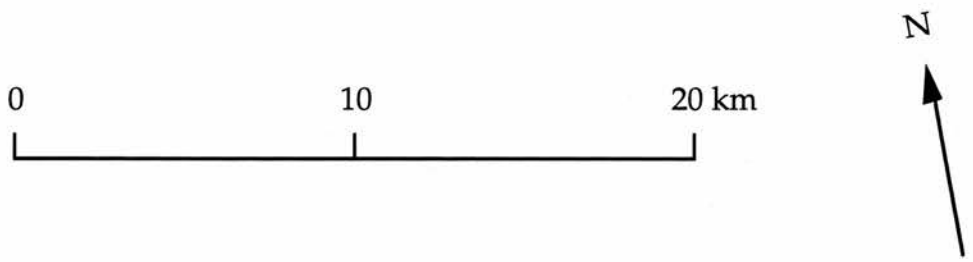

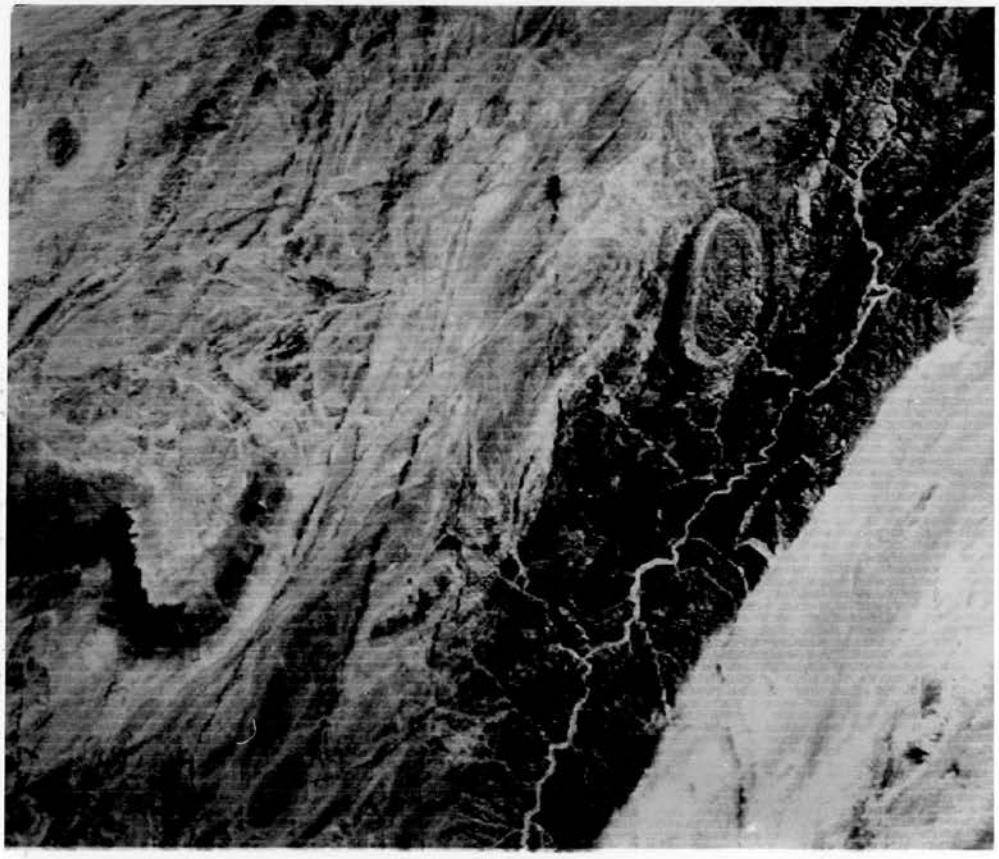

Plate 4.9. Negative topographic lineaments are generally expressed by linear drainage segments, for example the two linear tributaries flowing into the Swakop River, shown in the top left portion of this greyscale image (refer to text on page 56).
Image sub-scene ABP (refer to map on page 45).

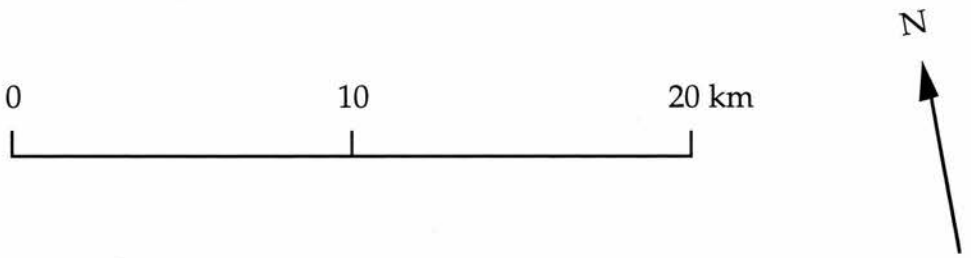

Plate 4.10. Tonal lineaments are generally expressed as linear lithological contacts, for example the lithological horizons picked out on the southeastern slopes of the Chuos Mountains, shown opposite (refer to text on page 56).
Image sub-scene ABH (refer to map on page 45).

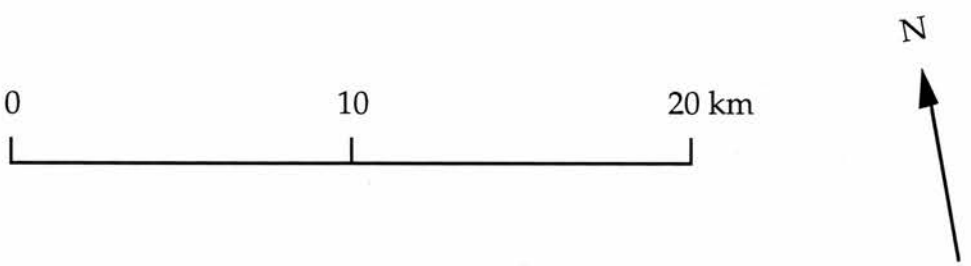

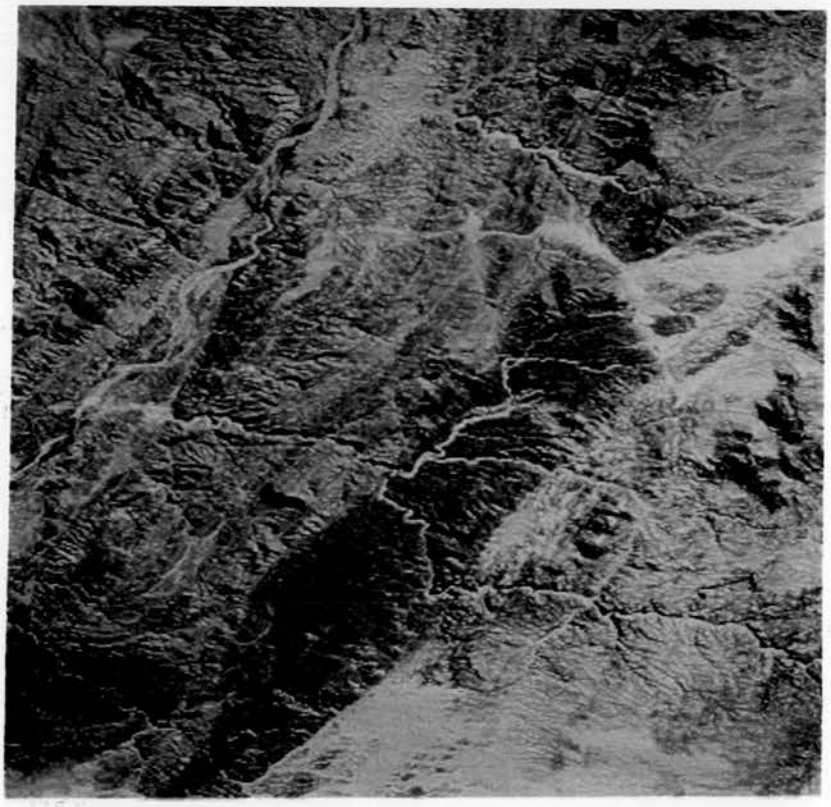

Plate 4.11. Dome features characterise the Central Zone of the Damara Orogen. Their long axes are interpreted to be fold axes (refer to text on page 56).
Image sub-scene BAU (refer to map on page 45).

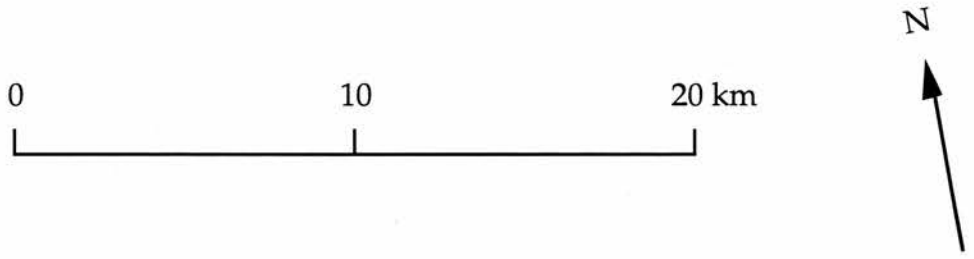

Plate 5.10. The first principal component greyscale image of the test area (refer to text on page 81).
Image sub-scene AA (refer to map on page 75).

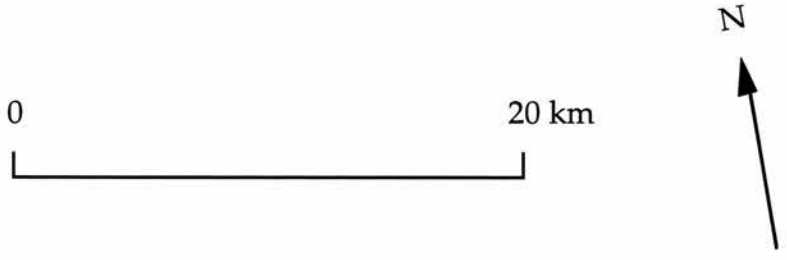

3 - Tonal / textural lineaments. These mark linear boundaries between different ground units. They generally represent lithological boundaries (see plate 4.10), often on the limbs of folds. Fold axes have also been marked on the tonal lineament map, examples of which are shown in plate 4.11.

4 - Combined lineament data. This map combines the lineament data from the three previous maps.

4.5.2. Lineament Mapping.

Based on the categories given in the preceding section, lineament maps have been compiled by visual analysis of the enhanced Landsat imagery. Due to processing and display limitations, the Landsat scene is divided into an arbitrary grid pattern of sub-images. Each of these sub-scenes has been analysed equally and separately so that the entire area is investigated in a near-uniform fashion. Adjacent images have also been analysed together to reveal those lineaments which continue across sub-image boundaries, and the study area as a whole has been viewed to pin-point any major lineaments.

Minor lineaments less than 2 km on the ground have not been included. This distance relates to ~25 pixels on the imagery - such a short general alignment may be due as much to chance as to any geological control. The identification of short lineaments is highly subjective, and by their exclusion there is an increase in the level of confidence that the lineaments actually mapped are real and not a result of some chance alignment of ground features. Only straight lineaments have been mapped, a restriction of the digitising procedure. 'Curvilinears' (O'Leary *et. al.*, 1976) are not included, because of the limitations of the digitising procedure. In any event, they probably only account for a few percent of the total lineament population.

The identification of lineaments has been achieved by the analysis of a mosaic of full-resolution sub-image photographs. Individual sub-scenes have also been viewed on the display monitor of the image processing system, although only one sub-scene can be displayed at any one time. The photo mosaic proves more useful for delineating major lineaments, as they are visible within the context of the whole scene. Any lineaments identified have been drawn onto an overlay placed over resampled imagery. This imagery accounts for the geometric distortion caused by signal over-sampling along each row of the image (see section 3.4).

4.5.3. Digitising Procedure and Computer Analysis.

Following the compilation of the lineament maps, the results have been subsequently digitised to allow a computer analysis of the lineament data and establish whether any azimuth trends exist. Each lineament map is placed on the digitising table and three arbitrary ground control point co-ordinates established, so that all subsequent lineament data digitised can be assigned grid co-ordinates. The lineament maps are all produced at the same scale, using the same ground reference points, so that results from maps **1**, **2** and **3** can be combined for map **4** - Combined Lineament Data.

The digitising procedure involves the allocation of a six figure reference point to the two ends of any line section mapped. Four-figure co-ordinates could be used, but problems arise with the azimuth accuracy of short lineaments, which can range from +/- 10° of their true orientation - over twice the size of the azimuth classes actually used. By using a six-figure co-ordinate system, computing time is increased, but the increased accuracy is more than commensurate so that the measured lineament azimuth can be assigned a degree of accuracy of +/- 2°.

The digitising process is accomplished using the Summagraphics LCL package. The result, for each map, is a data file of pairs of six-figure co-ordinates which represent the end points of each lineament. Following slight editing, these data files are analysed by a FORTRAN program that calculates lineament length (km) between the two end co-ordinates and lineament azimuth (radians). The output file is then analysed by the 'SPSS' statistical package which produces two different azimuth frequency histograms.

The first of these shows the frequency of lineaments for each azimuth class. If the lineaments occur by chance, in the absence of any structural control, the data should be uniformly distributed between each class, so that there are no histogram peaks. Where there is a preferred orientation, this will be revealed by a peak in the data histogram, or peaks should there be more than one set of controls. The degree of kurtosis on any histogram peak will give a qualitative indication of the importance of that control.

The second histogram plots the total length of lineaments (km) for each azimuth class. If there is a single preferred orientation, the modal peak for the lineament frequency and the lineament length histograms should be the same. However, there may be many short lineaments in one particular azimuth class, and a few very long lineaments in another. Both may be important and the result of a different structural control. The high-frequency trend should be revealed in the frequency / azimuth histogram, whereas the long-lineament trend should be revealed in the total distance / azimuth histogram. Csillag (1982) shows the importance of including lineament length in any analysis, frequency alone may not reveal the entire picture.

4.6. Conclusions.

A sumary of the lineament analysis methodology that has been carried out is given below:

1--Information from the four spectral bands was compressed into a single band through the generation of the first principal component image. The transformation also suppressed image noise.

2--Lineaments are contained within the high-frequency information of an image. A convolution filter was passed over the principal component imagery to highlight high-frequency edges. The texture image derived was added back to the component image to produce an edge-enhanced image.

3--Further digital improvements of the imagery were achieved by stretching the narrow spread of DN to fit the whole range of the display device (contrast-stretching).

4--The processed imagery was visually analysed to extract lineament sections longer than 2 km. Four maps were compiled - **positive topographic features, negative topographic features, tonal lineaments** and **combined lineament data**.

5--The resulting maps have been digitised. The data was analysed by computer to establish azimuth trends. Two histograms were produced for each map - lineament frequency for each azimuth class and total length of lineaments for each azimuth class.

Chapter 5

Multispectral Lithological Mapping.

Chapter 5. Multispectral Lithological Mapping.

5.1. Introduction.

Remotely sensed data do not directly represent the age or petrology of rocks but remote sensing is nevertheless being used for geological mapping (Drury *et. al.*, 1993). This is due to the fact that in many arid and semi-arid areas of the world, rocks are sufficiently well-exposed to allow their spectral response to be used as a means of identification on remotely sensed images.

To understand how rocks can be spectrally differentiated on Landsat MSS imagery requires an understanding of the way in which electromagnetic radiation interacts with earth surface materials in the region of the spectrum covered by the sensor (0.5 - 1.1 μm). This is discussed in section 5.2. Unfortunately, this is only a narrow part of the spectrum and the sensor's range does not extend into that part which is most useful in characterising the spectral properties of geological surface materials (Goetz *et. al.*, 1983). Nevertheless, different lithologies do appear to be spectrally distinct on the Landsat MSS imagery covering the study area, even more so when digital processing techniques are employed to enhance those spectral differences.

The spectral characteristics of different rocks result in reflectance variations between the image bands sensed. This information - the spectral component of imagery (see section 3.6) is displayed as different colours in a colour-composite image. Given that the spatial content of imagery is important too, the best image enhancements for lithological discrimination are those which capitalize as fully as possible on spectral information but which leave the eye and brain free to interpret texture and context (Rothery, 1987). These are discussed in section 5.4.

5.2. Spectral signatures of rocks and minerals.

Although the Sun emits electromagnetic radiation (EMR) over a wide range of wavelengths, the maximum radiant emittance of energy occurs at visible wavelengths and so the Sun provides the main source of energy used for passive remote sensing in the visible and near-infrared portions of the electromagnetic spectrum. The path of this radiation, from source to the detector, is shown in Figure 5.1. In terrestrial remote sensing, the transmission properties of the Earth's atmosphere are extremely important (Hunt, 1980) because they impose severe restrictions on those regions of the electromagnetic spectrum that can be sensed. Certain EMR wavelengths are absorbed and scattered by various atmospheric constituents and this limits remote sensing to so-called 'atmospheric windows' (see Figure 5.2). Much like the human eye, Landsat sensors are tuned to the window that occurs in the visible and very-near-infrared, although blue light (0.4-0.5μm) is not sensed by the Landsat MSS because the effects of atmospheric scattering mask true reflectance levels at this wavelength.

Any EMR that is recorded by the sensors onboard Landsat has passed down through the Earth's atmosphere, interacted in some way with the ground material upon which it has been incident, and has then been reflected back up through the atmosphere to the satellite's sensors. Different interactions occur between EMR and different surface lithologies and these produce 'spectral signatures' which are characteristic of those rocks and minerals. A spectral signature is a distinct reflectance curve over the imaged wavelength range, examples are shown in Figure 5.3. At specific wavelengths there are often characteristic absorption features which occur as a result of electronic and vibrational transitions caused when constituent ions and atoms are excited by just the right frequency of radiation.

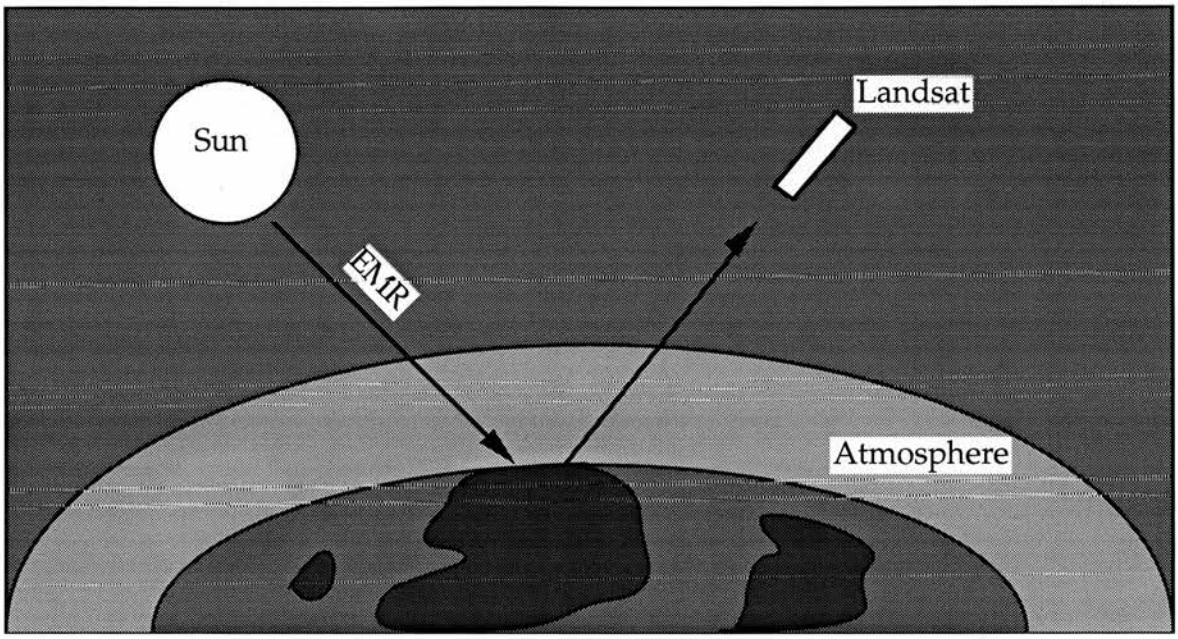

Figure 5.1. Electromagnetic radiation from the Sun passes down through the atmosphere and interacts in various ways with the surface material upon which it is incident. That portion of radiation that is reflected, passes back up through the atmosphere and is sensed by the Multispectral Scanner aboard Landsat.

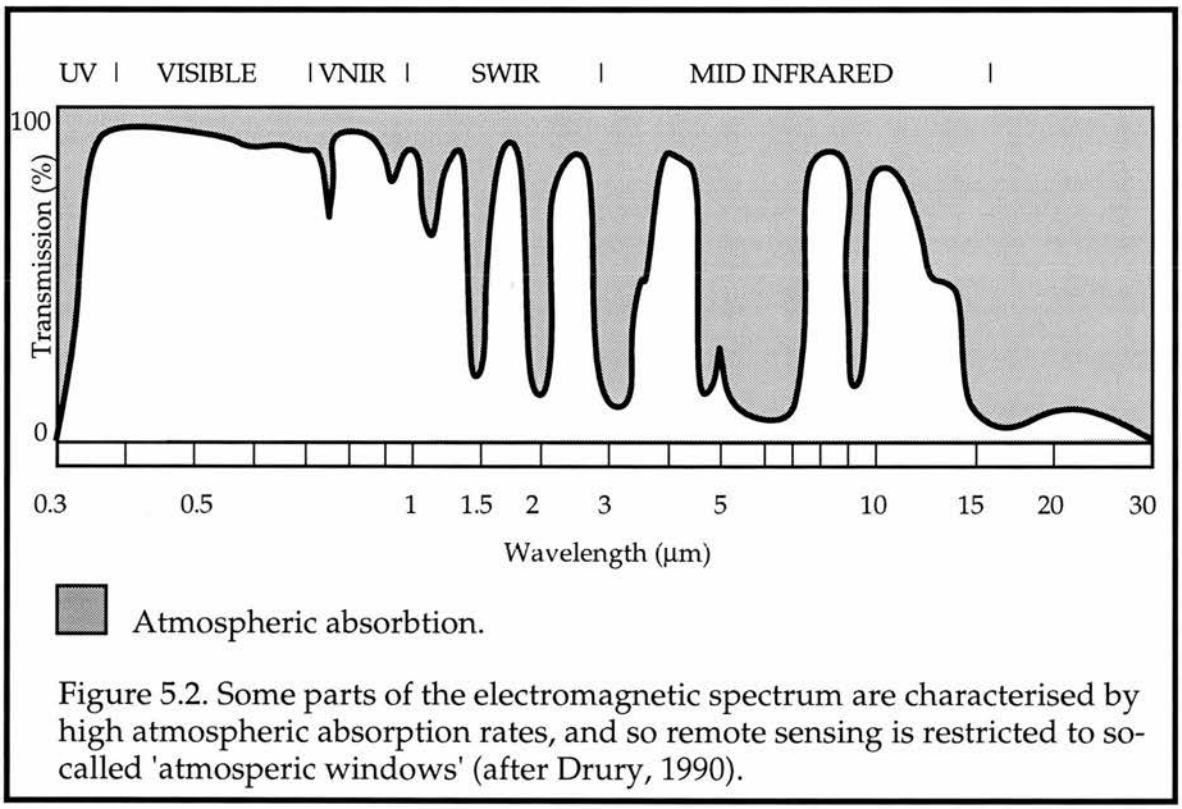

Figure 5.2. Some parts of the electromagnetic spectrum are characterised by high atmospheric absorption rates, and so remote sensing is restricted to so-called 'atmosperic windows' (after Drury, 1990).

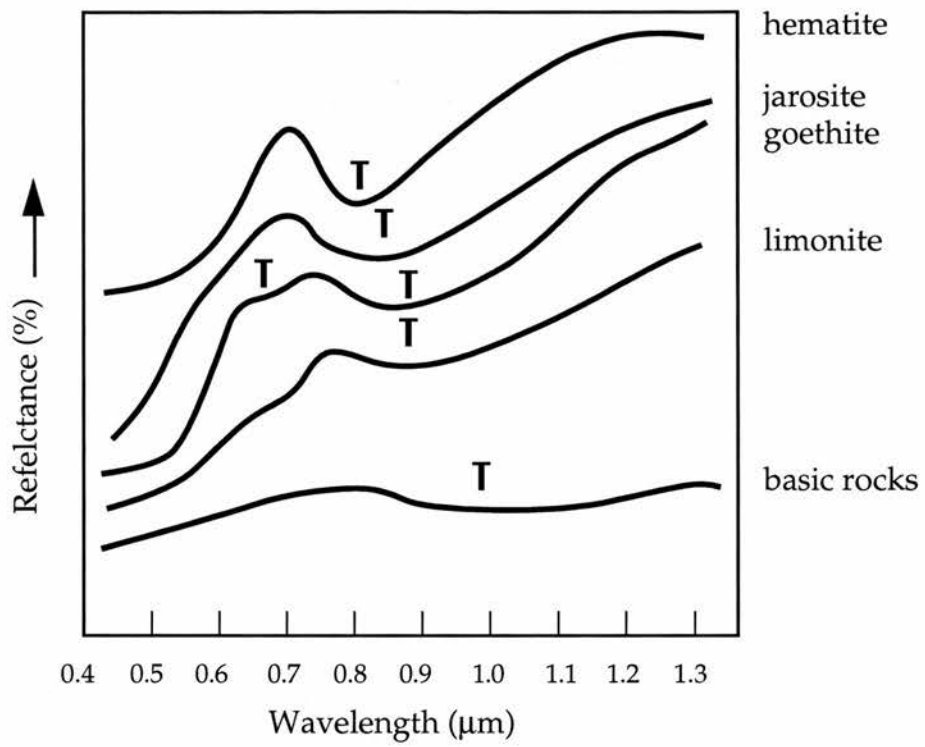

Figure 5.3. The **T** symbols show absorption features in iron oxides and hydroxides. These features occur because energy at specific wavelengths is absorbed by atoms bonded within the minerals' molecular structure. The spectra are vertically offset for clarity (from Drury, 1990).

Electronic transitions occur when ions jump from one electron shell to another, vibrational transitions occur by very small displacements of a molecule's atoms from their equilibrium positions. Both features serve to either subtract from or add to the intensity of the original radiation at specific wavelengths (Hunt, 1980). Electronic transitions require more energy than vibrational ones, so the former characterise the short-wavelength, visible range, whereas the latter dominate the longer wavelength infrared. However, there is some overlap between the ranges of these two processes (Drury, 1987).

The most common constituents of rocks and minerals are the elements oxygen, silicon, and aluminium. However, these have electron shells whose

energy levels are such that transitions between them have little or no effect on the visible to near-infrared range. In this region of the electromagnetic spectrum, the spectra of minerals are dominated by the effects of less-common ions and the molecular structures in which they are bonded. The inclusion of transition metals, most commonly iron, in a rock's mineralogy, plays a large part on the spectra of those minerals in the visible and near-infrared. Absorption features due to electronic transitions in ferrous (Fe^{2+}) ions are shown in the reflectance spectra of several iron-bearing minerals in Figure 5.4.

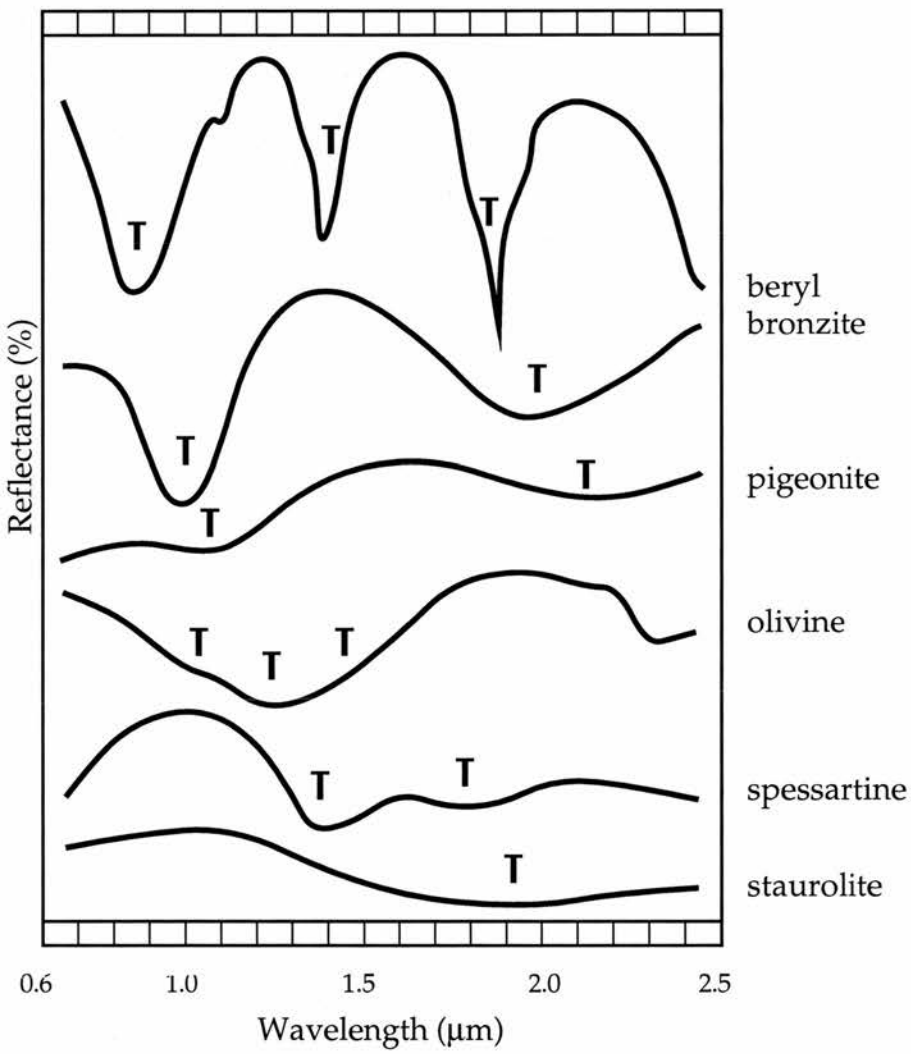

Figure 5.4. The co-ordination of Fe2+ ions, in the molecular structures of the minerals concerned, determines the number and position of absorption features due to electronic transitions (**T**). The spectra are vertically offset for clarity (after Drury, 1987).

The different wavelengths of the features relate to the symmetry, degree of lattice distortion and co-ordination of ferrous ions in the different minerals. Absorption features occur as troughs because energy is absorbed over a small range of wavelengths. Another common electronic transition occurs due to the migration of electrons from iron to oxygen when induced by energy in narrow wavebands of EMR, especially less than 0.55 μm. This is responsible for a steep decline in reflectance towards the blue end of the spectrum, most notably with iron oxides (see Figure 5.3), this being the reason why these minerals and rocks containing them are yellow, orange or red in colour (Drury, 1987). The most important vibrational transitions in minerals, in the visible to near-infrared part of the spectrum, are those associated with the presence of hydroxyl ions (OH^-) or water molecules, either bound in the structure or present as fluid inclusions. This results in a characteristic absorption feature at 1.9, 1.4 and 0.94 μm, as demonstrated in Figure 5.5.

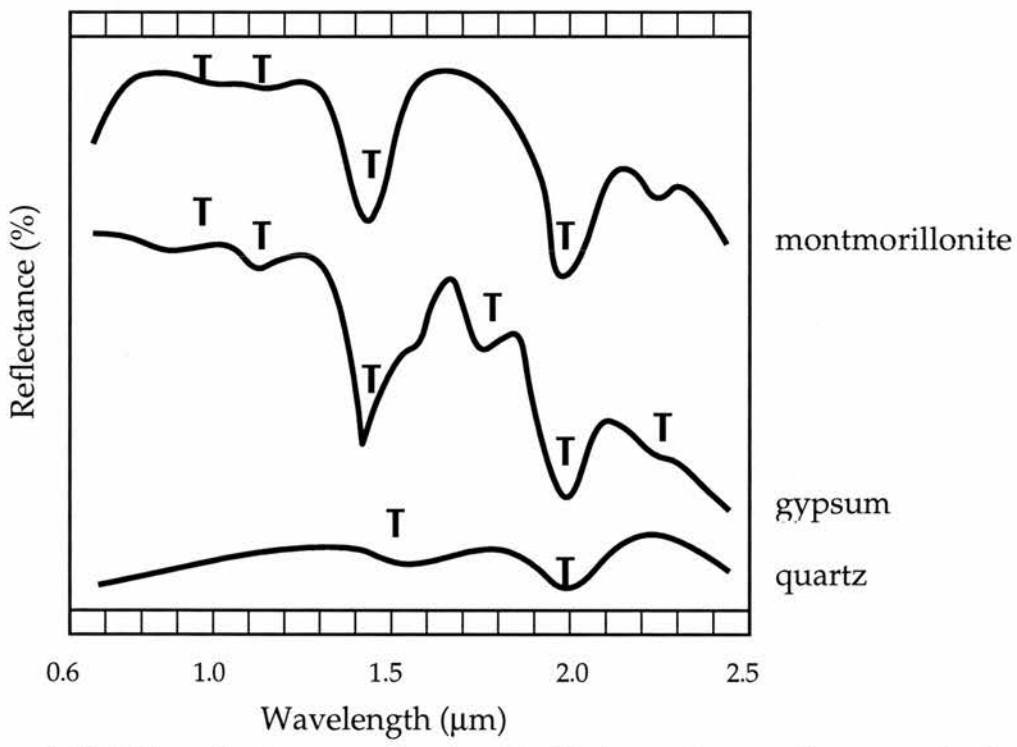

Figure 5.5. Minerals that contain chemically-bound water have particularly distinct absorbtion features (**T**) caused by vibrational transitions. The spectra are vertically offset for clarity (after Drury, 1987).

Not only are the spectra of rocks and minerals affected by their chemistry, but physical and environmental factors also play a part. Macroscopic effects such as reflection, scattering, refraction and so forth, which take place at boundaries, are largely a function of the size and shape of the object and may contribute to the amount of EMR reflected. Furthermore, the presence of vegetation , water, organic compounds and man-made objects contribute to the observed spectral response due to limits imposed by the spatial resolution of the imaging system (Abrams, 1980). All of these chemical and physical parameters serve to modify the wavelength-intensity relationship of the radiation sensed by Landsat, and by the human eye. This explains why, in the visible range of EMR, we see some rocks as dark (energy absorbed), some rocks as light (more energy reflected), and why some rocks appear coloured (more energy absorbed/reflected at certain wavelengths).

5.3. Test Area - Methodology.

In studies such as land-use mapping and vegetation monitoring, a remotely sensed image is often turned into a 'thematic map' Having established reflection thresholds for different known ground cover types, the image as a whole is 'classified' (Mather, 1987), on the basis of spectral properties, and pixels are automatically assigned to represent one of a number of 'themes' or land-cover types. However, geological boundaries drawn on the basis of spectral properties alone are usually quite arbitrary (and misleading) because real lithological contacts are often gradational, and even quite distinct rock types may have very similar spectral responses (Rothery, 1987). This is especially so with Landsat MSS imagery, which is said to have a low spectral resolution (Goetz *et. al.*, 1983) since its spectral bands are relatively broad and only cover a limited portion of the electromagnetic spectrum. Spatial information (see section 3.6), in terms of tone, texture and pattern, are of great importance in helping to discriminate rock types, but this information is completely lost in most types of thematic map.

Because of these factors, a supervised classification technique generally proves unsuitable for geological mapping. A far better procedure is to produce a spectrally-enhanced image, which retains the spatial information component, from which an interpreter with geological knowledge can make an informed interpretation. This methodology employs traditional photogeological interpretation techniques to examine the spatial component of the imagery, combined with digital image processing techniques to highlight the spectral component. Together, these provide a proven and effective mapping technique (Qari, 1989), one used by exploration companies for reconnaissance mapping over large and remote areas (Lamb and Lawrence, 1993), and similarly employed in this study.

When processed, the imagery covering the study area provides a colourful representation of the ground. In this region, precipitation is scant so soils do not develop and vegetation is almost completely absent, and so one might argue that the remotely sensed image is a direct representation of the geology of the area. Because EMR, over the wavelengths imaged by Landsat, cannot penetrate more than a few micrometres into the surface (Drury, 1990), the reflected radiation might only represent a weathered surface layer. However, owing to the almost total absence of water, the weathering mantle is not excessively leached, and so probably closely resembles the composition of the underlying bedrock (Abrams, 1980).

Where an image is thought to represent the geology of an area, that image can be divided into distinct spatial/spectral units, on the basis of colour, texture, etc., without having an *a priori* knowledge of specific lithologies. Image units may not necessarily correspond however to geological units which might be mapped in the field. An established mapping procedure is to first interpret and divide the image into recognisable spatial/spectral units and then, by visiting typical localities in the field, establish what the mapped units actually represent. However, because fieldwork was not an option in this study, the methodology has had to differ accordingly.

From the Landsat MSS imagery covering the study area, different geological units can be easily mapped. However, without the facility to check what these units actually represent in the field, the stratigraphy could not be established, and lithological units could not be named. The procedure as a whole becomes somewhat academic - a demonstration of half the technique. Fortunately, the availability of earlier mapping work, covering part of the area covered by the imagery, gives rise to an alternative methodology.

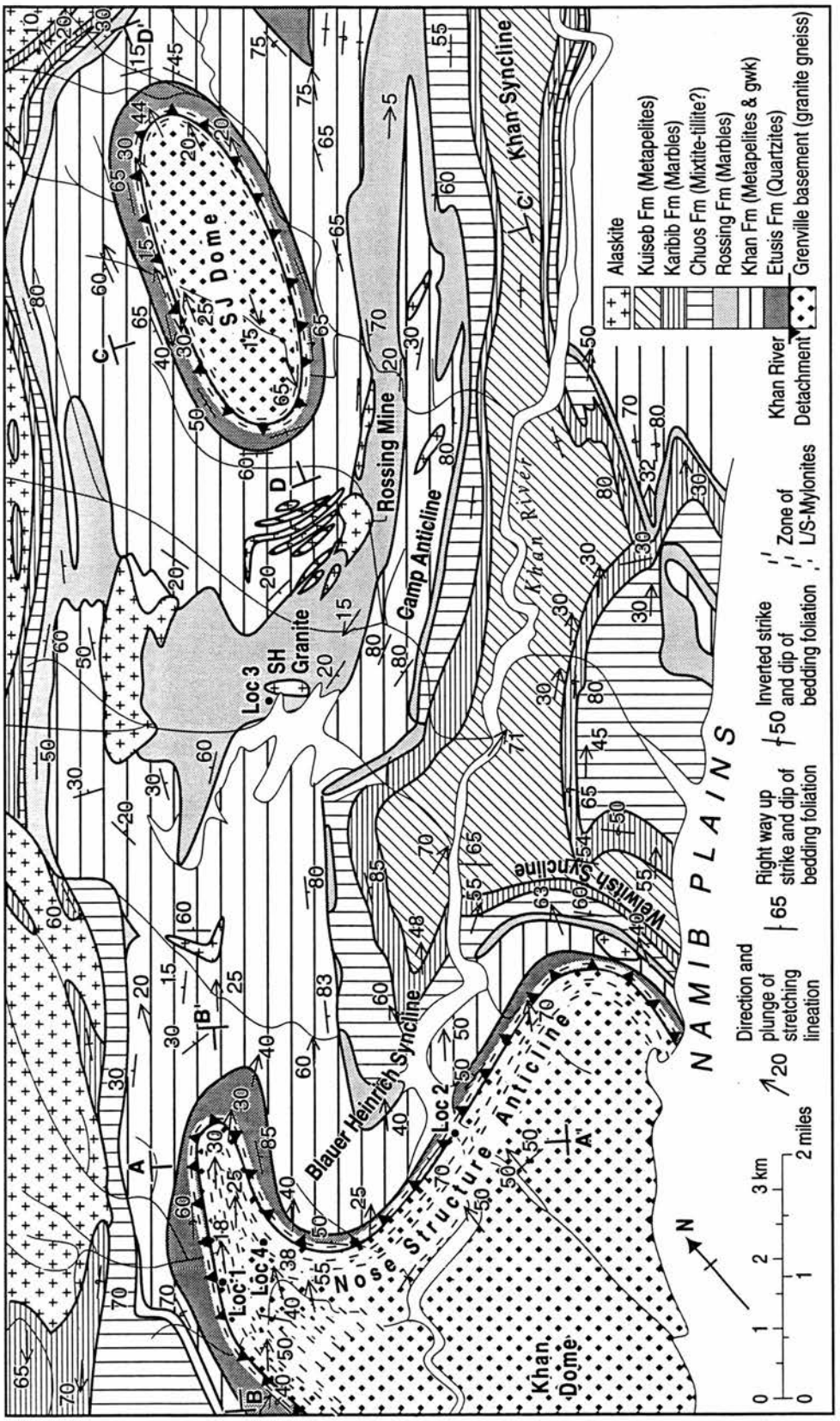

Figure 5.6. Geology map of the test area (after Smith, 1965).

In 1965, Smith published a geological map of part of the Lower Khan Gorge (Figure 5.6). An outline of the area covered by this is shown on the multispectral lithological map (Appendix, Map 5). Contained within this area are a wide range of lithologies, all of which are discernible on false-colour and principal component images of the same area (see plates 5.1 and 5.2). These various lithologies are thus within the rather broad spectral resolution of the Multispectral Scanner. The geology and statigraphy of the test area are discussed in detail in section 7.2. By means of visual analysis, lithological contacts have been extended further afield from the area mapped by Smith. Lithological units have been mapped within these contacts on the basis of a similar spectral response and spatial texture, to cover the whole study area. By these means, a remotely-sensed geological map is produced, containing recognised lithological units, on a regional scale.

Plate 5.1. False-colour composite image of the test area (refer to text on page 72).
Image sub-scene AA (refer to map on page 75).

Plate 5.2. Principal component image of the test area (refer to text on page 72).
Image sub-scene AA (refer to map on page 75).

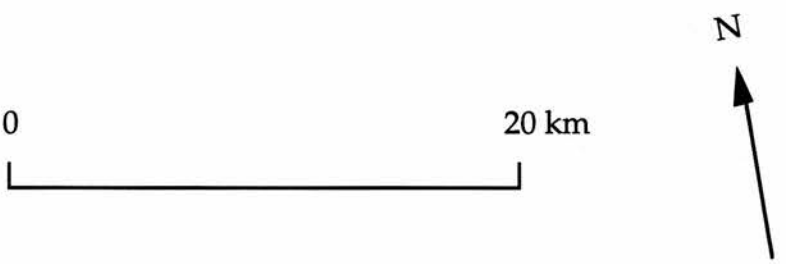

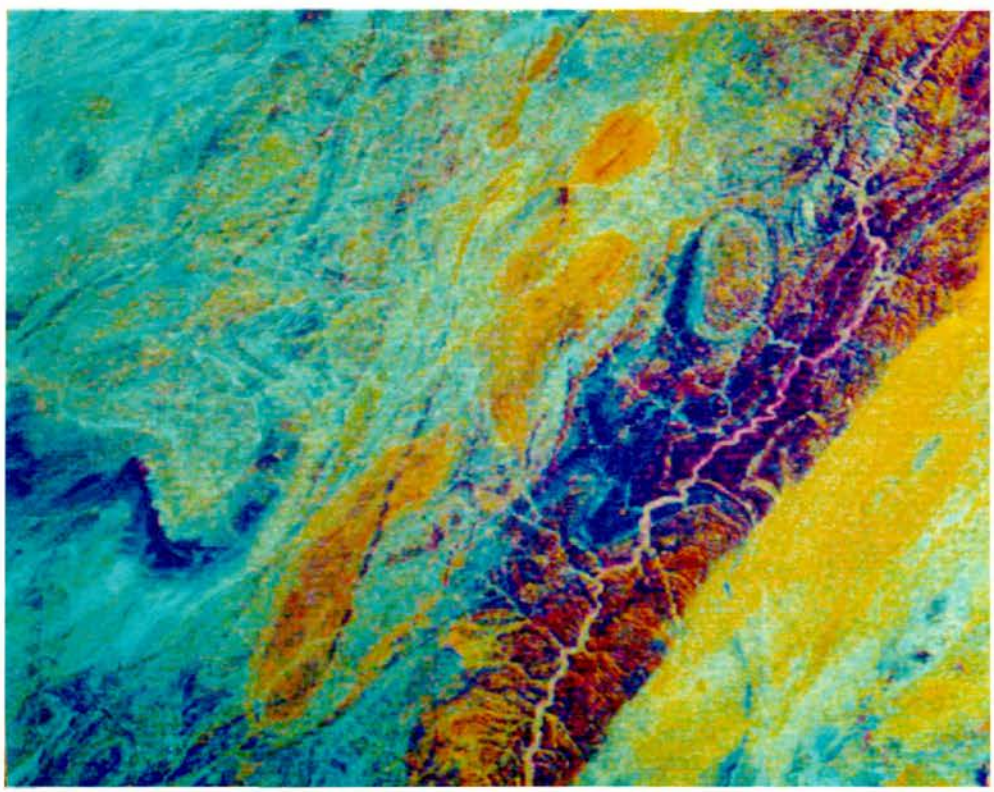

5.4. Digital Image Enhancements.

5.4.1. False-colour composite images.

Multispectral data can be displayed in two basic ways - either one band at a time in black-and-white, or in a combination of three different bands in a colour composite image. Information obtained from black-and-white imagery is often limited because visual perception is restricted to resolving only about 20 - 30 separate grey levels. However, the eye can easily distinguish tens of thousands of different colours.

This colour resolving power can be utilised to display the spectral component of a multi-band image, the simplest way being through the generation of a false-colour composite. This is achieved by displaying a combination of three image bands - one as red, one as green, and the other as blue. These images 'add together', so that the different reflection intensities in each band produce a range of colours in the combined image. This utilises the principle of 'additive primary colours'.

Plate 5.3 demonstrates this principle and shows a range of different colours, in the top left square, produced by combining the three additive primary colours in the proportions shown in the red, green and blue squares. Because the reflection intensities of rocks usually alter between the spectral bands imaged, when data from these bands are displayed in a colour composite, different proportions of blue, green and red add together to produce a range of colours which are representative of a particular lithologies.

MSS data contain four image bands, but only three of these can be displayed in their original form in a colour composite image by using the three colour

Plate 5.3. The 'paintbox' of colours shown in the bottom left square has been produced by mixing the corresponding proportions of red, green and blue (the additive primary colours) shown in the other boxes. Colour composite images are produced by displaying each of three images of the same area, taken in different spectral bands, as different additive primary colours (refer to text on page 73).

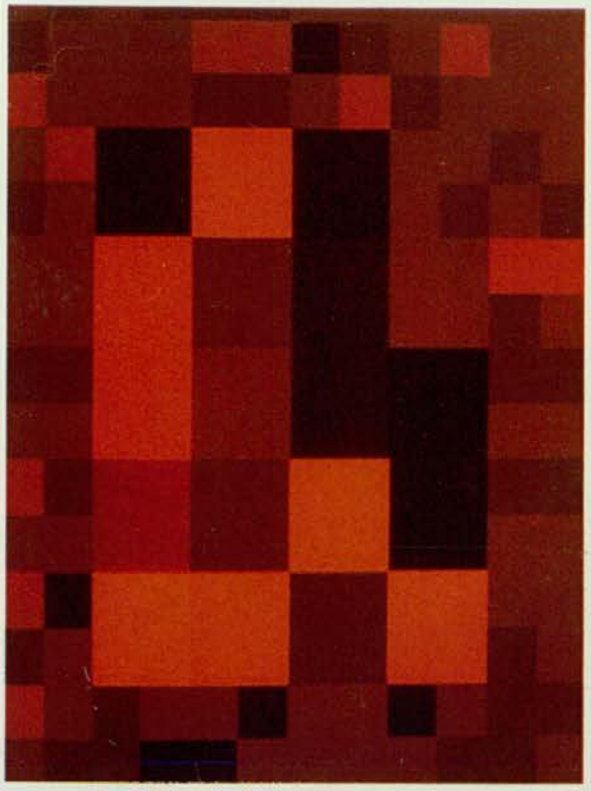

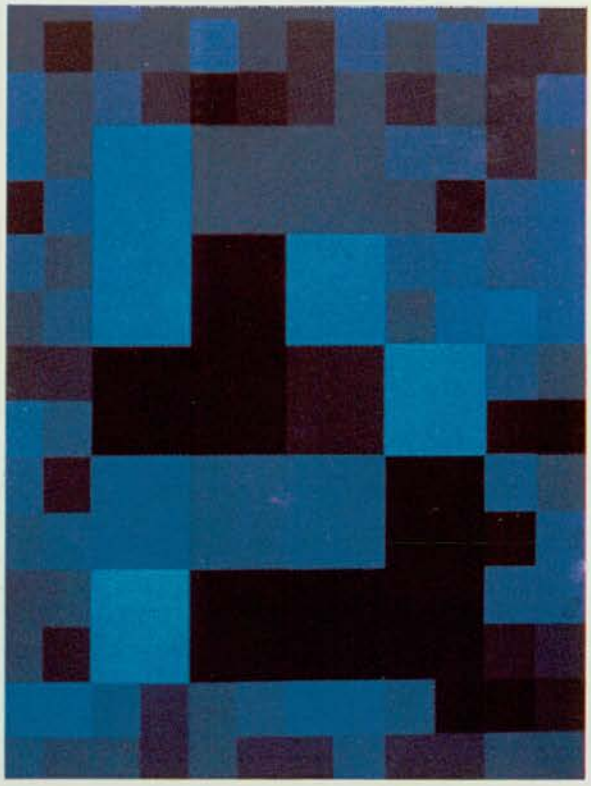

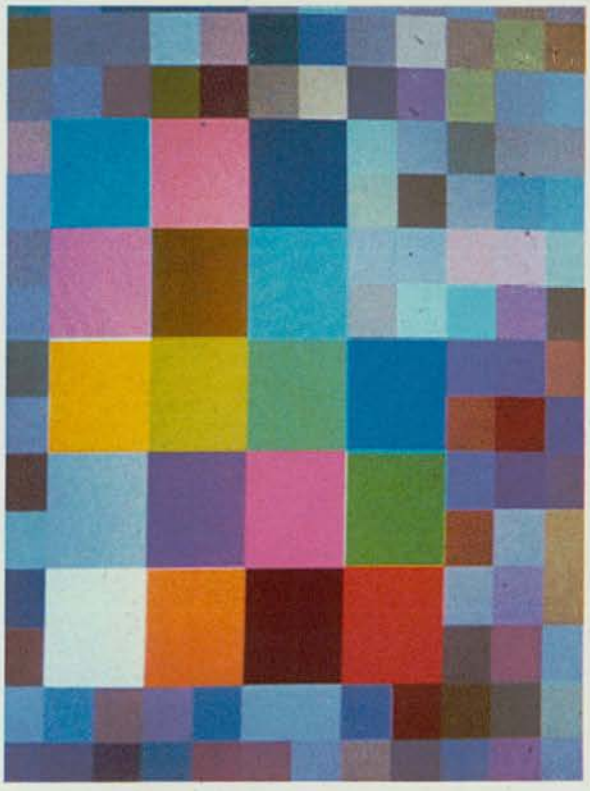

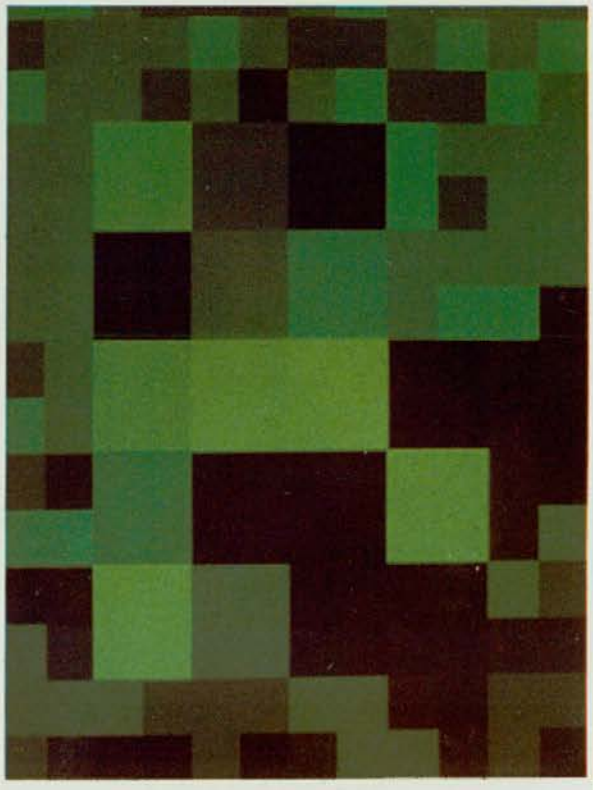

guns of a monitor. A question arises as to which of the four bands to include, and then as to which band should be assigned to which of the three additive primary colours. In theory, any combination of bands can be displayed in any combination of colours, although the usual practise is to display MSS band 7 as red, MSS band 5 as green, and MSS band 4 as blue. MSS bands 6 and 7 are highly correlated so little information is lost by missing out one of these (Canas & Barnett, 1985). Plates 5.4, 5.5 and 5.6 show this arrangement for a representative area; plate 5.7 shows the resulting false-colour-composite image produced when they are 'added together', i.e. displayed simultaneously.

Comparison between plate 5.7 and the test area map (Figure 5.6) shows that the different lithologies mapped by Smith (1965) can generally be discerned on the composite image. Although the spectral resolution of the MSS is low, the rocks are diverse enough in their lithologies so that they appear spectrally distinct from one another. In fact some units can be mapped on single-band black-and-white imagery, so distinct is their appearance - for example the bright marble bands of the Karibib Formation. However, the rocks of the Chuos Formation (Smith, 1965) prove an exception and cannot easily be visually separated from adjacent lithologies.

Working outwards from the study area, lithological contacts have been extended and successive areas mapped, using the stratigraphy established by Smith (1965). The lineament mapping procedure analyses the study area by working systematically, line by line, through a grid of sub-images. However, lithological units have been mapped differently, through a series of slightly overlapping sub-scenes, shown in Figure 5.7. Each scene covers ground further from the study area, but all include some overlap so that information mapped from one area may be extrapolated further afield into another. Spatial information is included in the composite images and aids the visual

Plate 5.4. Band-7 image of the test area, displayed as red (refer to text on page 74).
Image sub-scene AA (refer to map on page 75).

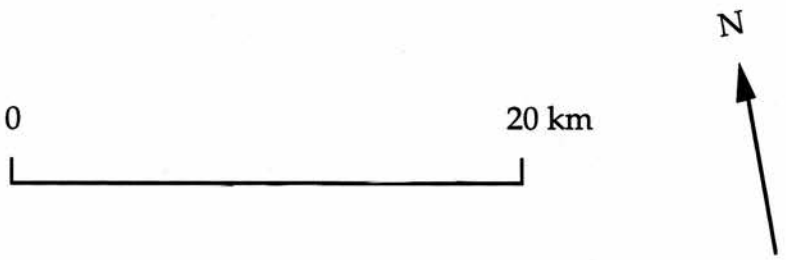

Plate 5.5. Band-5 image of the test area, displayed as green (refer to text on page 74).
Image sub-scene AA (refer to map on page 75).

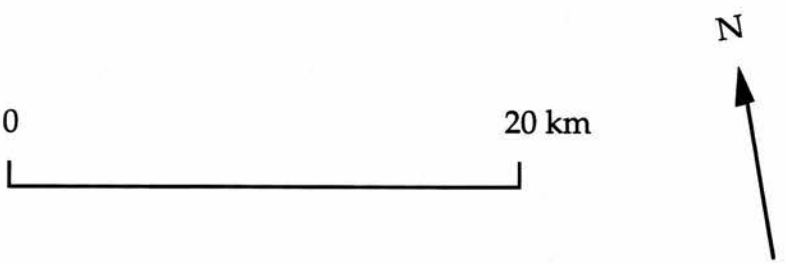

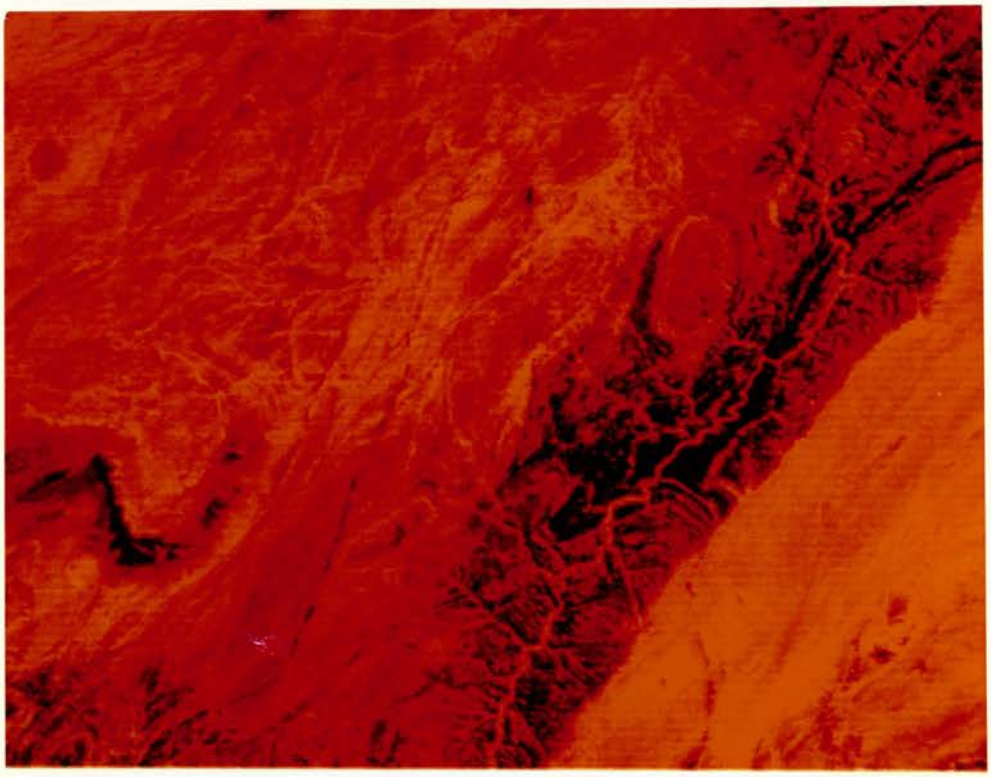

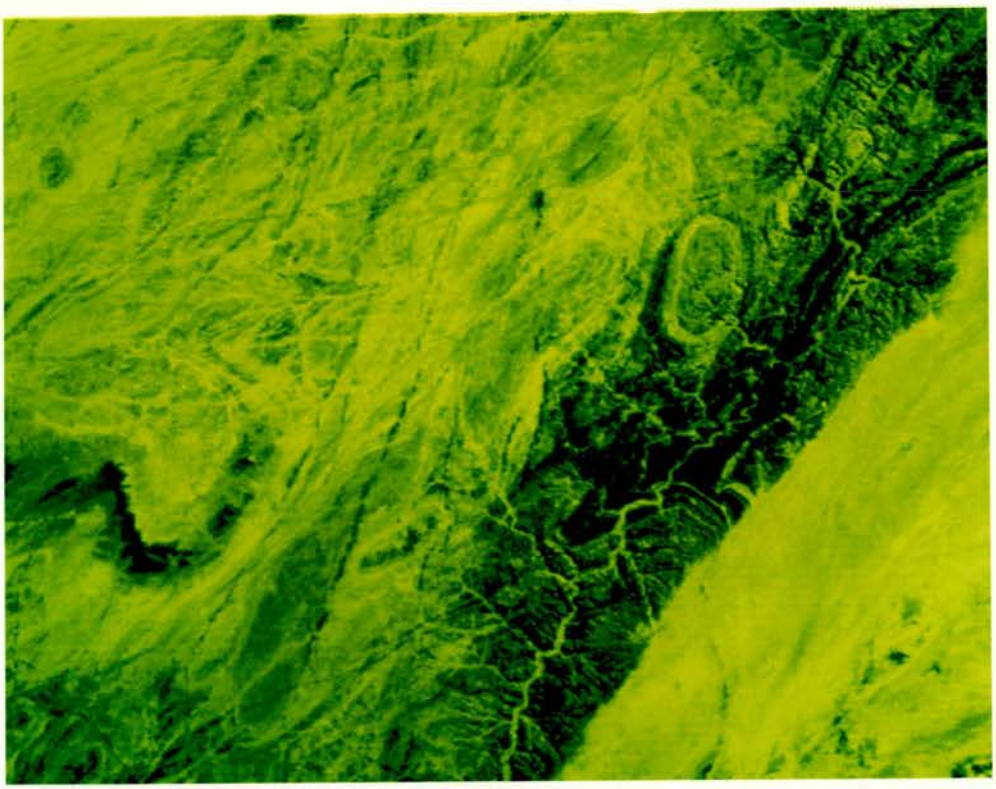

Plate 5.6. Band-4 image of the test area, displayed as blue (refer to text on page 74).
Image sub-scene AA (refer to map on page 75).

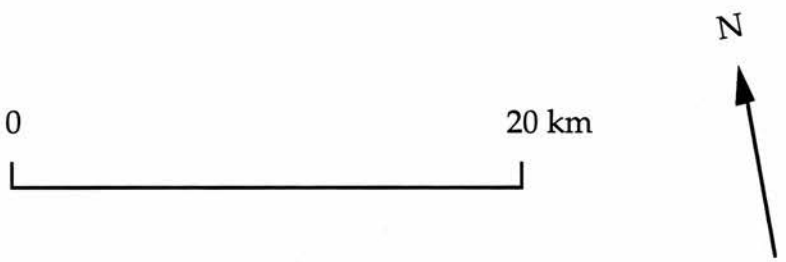

Plate 5.7. False-colour composite image of the test area produced by combining the images shown in plates 5.4, 5.5 and 5.6 (refer to text on page 74).
Image sub-scene AA (refer to map on page 75).

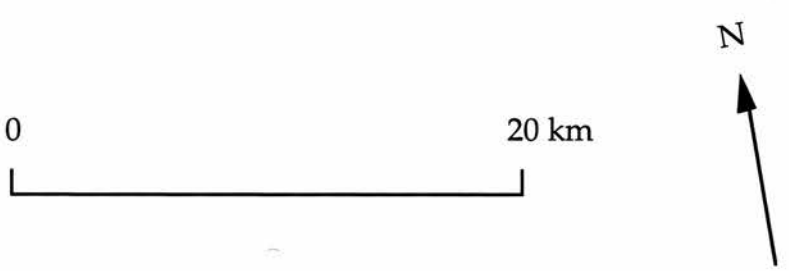

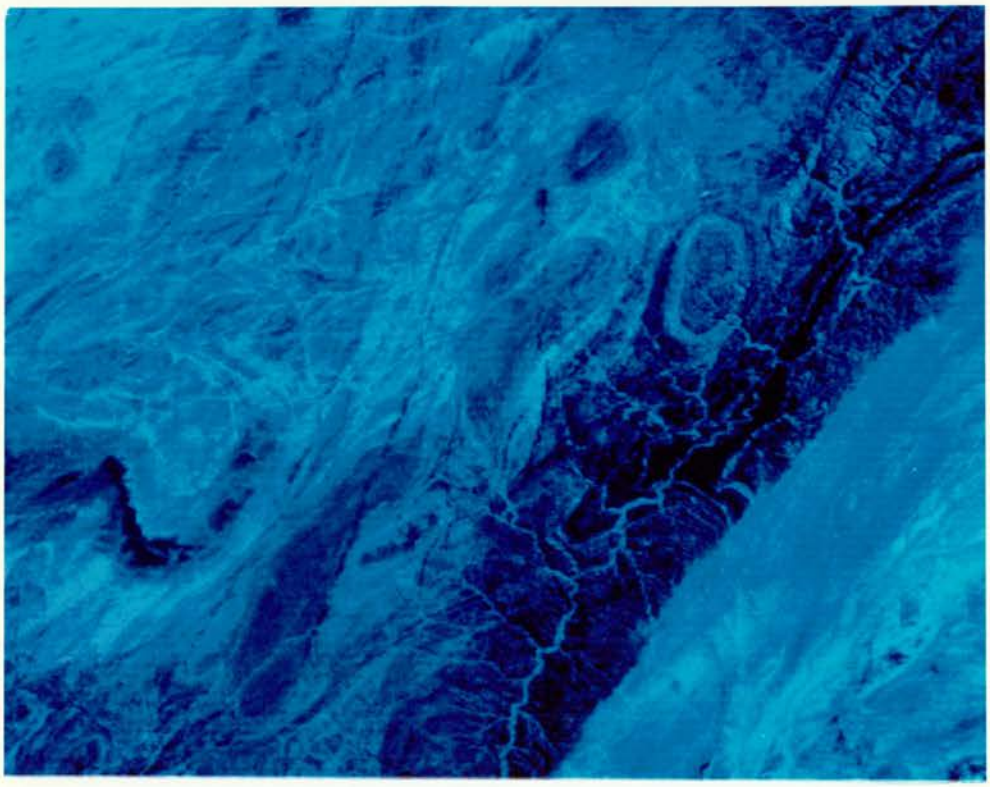

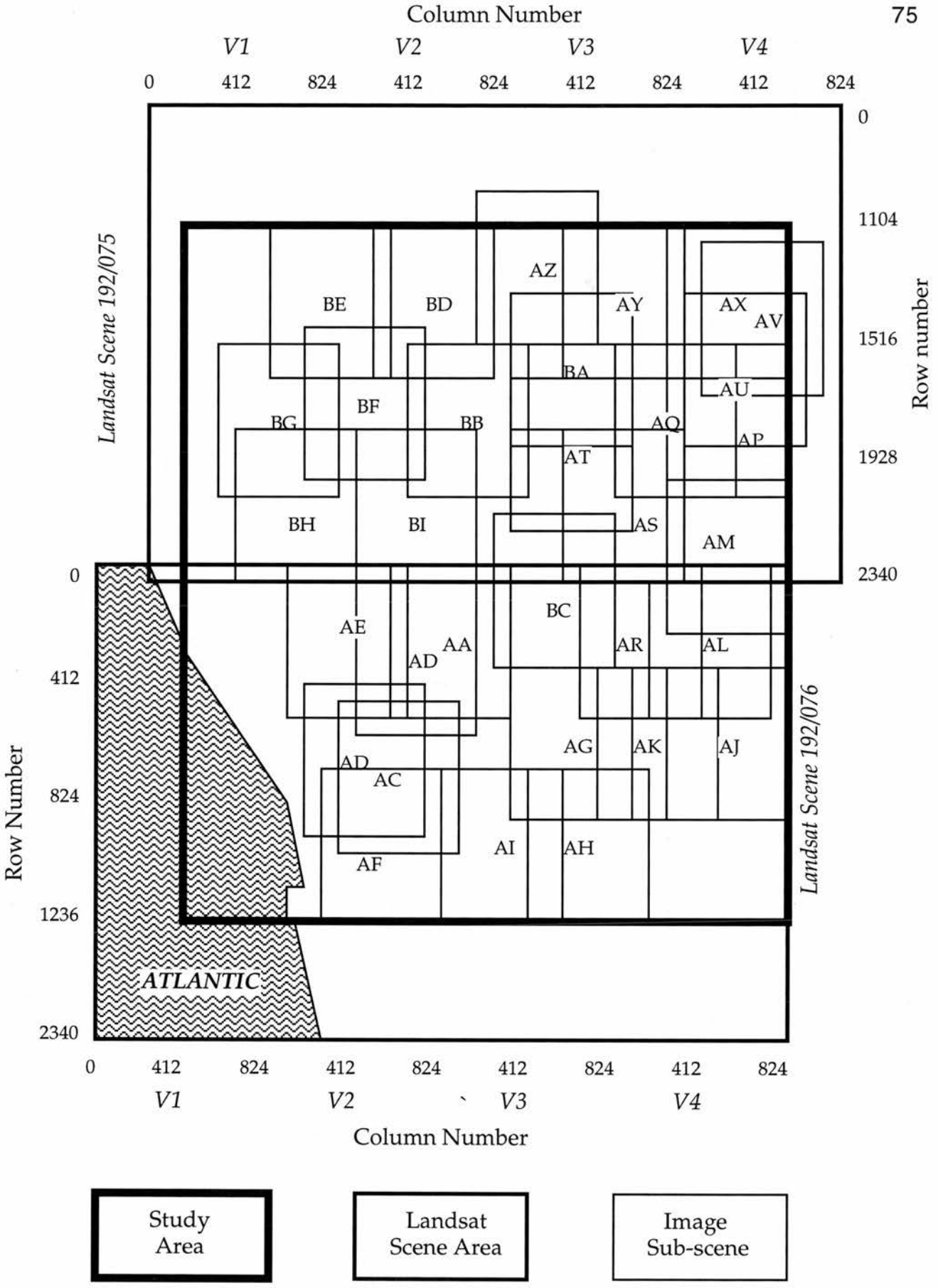

Figure 5.7. False-colour composite and principal component composite sub-scenes.

interpretation. Although different lithologies often have characteristic surface textures, drainage patterns, etc., these features alone cannot be relied upon to map different units. The spectral information revealed by the false-colour-composites provides the extra information necessary to successfully delineate separate ground units. Prior to examination, the colour composite images have been digitally enhanced by 'contrast-stretching' (see section 4.4) to improve their appearance. Because reflected data can be strongly correlated between visible and short-wavelength infrared bands, composite images may not be particularly colourful, only occupying a small proportion of the whole 'colour space' available (Rothery, 1987). Colour space can be thought of as a three-dimensional cube, as shown in Figure 5.8. where each axis represents the intensity of a primary colour. Variations in intensity are used to display the different DN values in each band of a composite image.

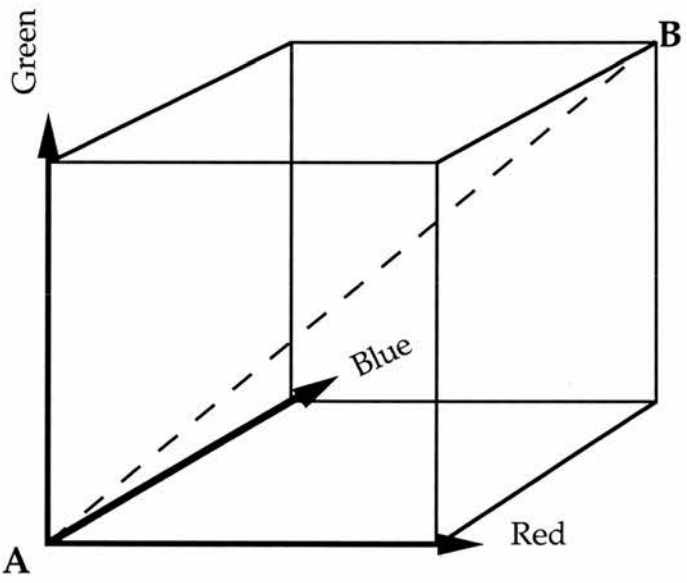

Figure 5.8. Visual representation of RGB colour space. The DN from three different MSS bands can be displayed simultaneously using this system, one band assigned to each colour. Data that plots at A shows as black in a colour-composite, at B as white, and along AB as various shades of grey. Because data is highly correlated between MSS bands, most pixels plot in a narrow, cigar-shaped distribution along AB.

When data between image bands are highly correlated, most pixels plotted in colour space fall into a narrow elipsoid, and so much of the colour space available is not used. Figure 5.9a shows a typical plot of DN for pixels in two bands of the same image. By stretching the DN in each band to cover the full range of the display device (0-255), a greater area of the colour space is filled (Figures 5.9b/c) and the displayed image appears more colourful. The increase in quality accomplished by the 'contrast stretching' (see section 4.4) of each band is shown in plates 5.8 and 5.9.

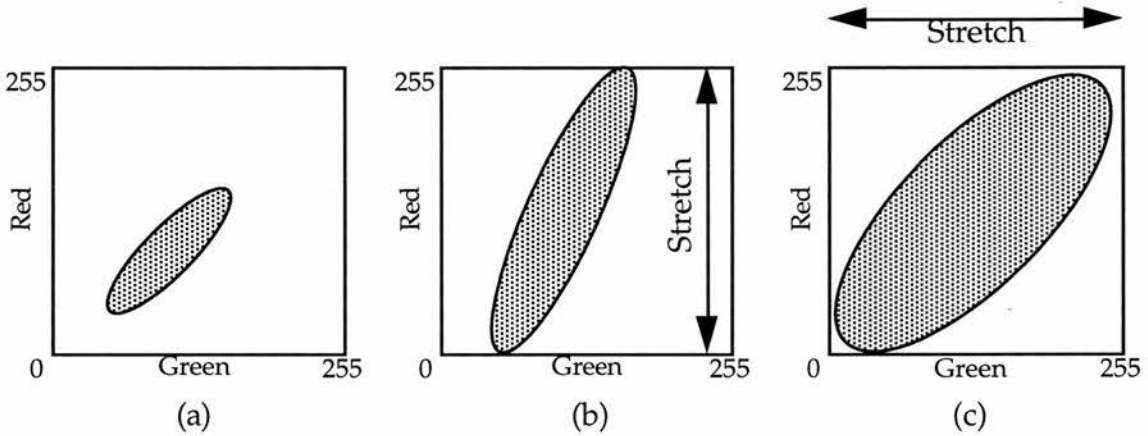

Figure 5.9. The high correlation of reflection intensity between two bands is revealed in a bi-variate plot of DN (a). By stretching the DN in each band to fit the whole range available, more of the colour space is filled (b & c).

5.4.2. Principal Components Transformation.

By contrast stretching the data in each band of a colour-composite image, more of the 'RGB colour space' is filled (see section 5.3) so that the image's appearance, and the spectral information which that represents, is enhanced. However, spectrally similar lithologies may remain inseparable because, even having stretched the data in each band, all of the RGB colour space is not

Plate 5.8. Unstretched false-colour composite of the test area (refer to text on page 77).
Image sub-scene AA (refer to map on page 75).

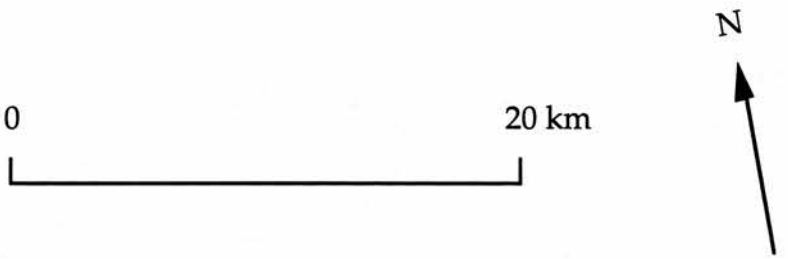

Plate 5.9. Contrast-stretched false colour composite of the test area (refer to text on page 77).
Image sub-scene AA (refer to map on page 75).

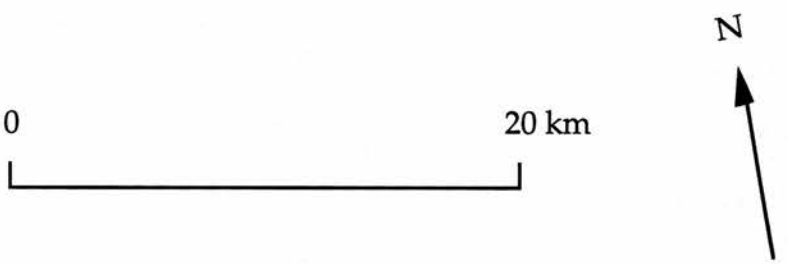

utilised (see Figure 5.9c). The majority of pixels still plot in an elliptical cloud close to the diagonal line AB (Figure 5.8). In three-dimensional colour space the distribution is cigar-shaped.

Any data that fall along the axis AB show up as various shades of grey in a colour-composite image. Those DN which fall in the cigar-shaped data set come out as muted pastel shades that are not always easy to distinguish. Only those pixels that lie far from the diagonal axis AB, towards the corners of RGB colour space, show as bright, easily distinguishable colours, but these are rare. No matter how the data controlling red, green and blue in the image are stretched, the cigar-shaped distribution and muted colours remain (Drury, 1990). If it were possible to expand the data set of a composite image to occupy a larger area of RGB colour space, spectral (lithological) information would be further enhanced.

In section 4.2, principal components analysis was used as a means of data compression. Here, a similar technique is used to analyse the dataset of all four bands of an MSS image. By using a new co-ordinate system, established by the first, second and third principal components of the image dataset, the spread of data can be improved so that more RGB colour space is filled, the image appears more colourful, and even slight variations in reflection between MSS bands are revealed.

It has already been noted that the data between MSS bands are highly correlated. The relationship between two bands (datasets) is a two-dimensional one, and can be displayed geometrically, eg. Figure 5.9a. Because MSS data are composed of four image bands, the dataset is described as being four-dimensional; multispectral datasets are correlated algebraically in n-dimensional space, where n is the number of bands in a multispectral image.

The distribution of DN within an image-band dataset can be described by its variance, which expresses the spread of its values about the mean. A measure of the joint variation of two variables is known as their covariance; this defines the shape of an ellipse enclosing the scatter of points representing DN. Figure 5.10 shows two distributions with the same variance, one with a high positive covariance (**1**), the other with a covaraince of zero (**2**). The mean of each variable gives the location of the centre of the ellipse (or ellipsoid in *n*-dimensional space). The mean vector and the variance-covariance matrix define the location and shape of the scatter of points in *n*- dimensional space of the dataset involved (Mather, 1987)

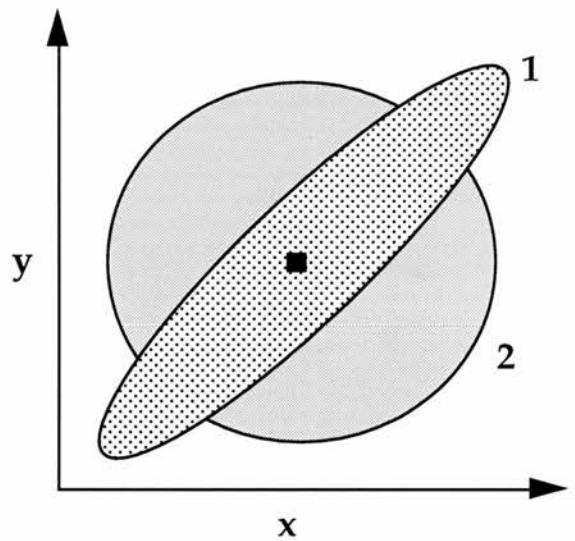

Figure 5.10. The two shaded areas represent two theoretical plots of data. Both have the same variances with respect to variables x and y. Distribution 1 has a positive covariance between measures on x and y whereas the covariance of x and y for distribution 2 is zero. The mean of each variable gives the location of the centre of the ellipse.

The first step in a principal components transformation is to calculate the mean value for each dataset (Figure 5.11a) and then to set those values to zero (Drury, 1987). This is accomplished by shifting the axes to the point that defines the mean of those datasets (Figure 5.11b). At this stage, the axes can be

rotated so that one coincides with the line along which the data have the greatest spread. This vector of maximum variance is referred to as the 'first principal component'. An axis at right angles to this, the second principal component, describes the direction along which the remaining variation is expressed (Figure 5.11c). In space with more than two dimensions, this operation continues to define orthogonal axes which progressively consume all the variation that is not included in the lower-order principal components, giving as many principal components as there were original channels of data (Drury, 1987).

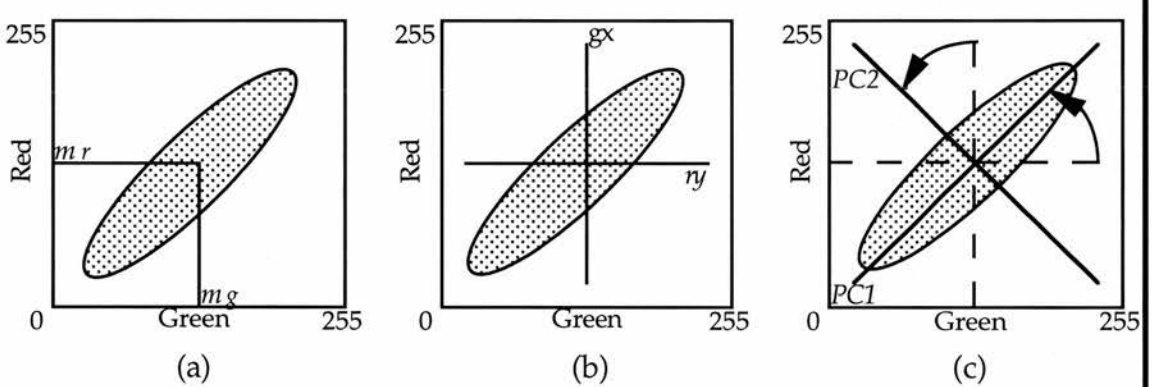

Figure 5.11. (a) shows a typical bivariate plot of DN from two correlated MSS bands. Principal component analysis begins by shifting the origin of the plot to the point defining the means (*mg, mr*) of the two datasets (b). The axes are then rotated so that one is alligned wth the direction of maximum variance through the dataset (c). This becomes the first principal component, another axes at right angles to this, describes the remaining variance - this is the second principal component. In a four-dimensional MSS dataset, four principal components are calculated (Drury, 1987).

Eigenvectors define the directions of the principal components through the original four-dimensional dataset. The variation within that data is recast as variances on the principal components. Eigenvalues measure the variances of the dataset ellipsoid along the new component axes (Canas and Barnett, 1985).

Because these axes are mutually perpendicular, the covariance matrix (shape of the dataset ellipsoid) is also transformed so that the covariances between bands are set to zero. This decorrelation process has the effect of spreading the data to the limits of the new principal component axes (Drury, 1987).

Each successive component accounts for smaller amounts of variance in the dataset (Singh and Harrison, 1985). This is shown in plates 5.10 - 5.13. The first principal component image may contain over 90% of the variance (information) of the dataset and appears the most clear. The information content of higher component images is significantly less, added to which is the contribution of image noise caused by deficiencies in the scanning system. Plate 5.13 shows that the fourth component is composed almost wholly of random noise - this component is rarely included in a composite image.

The data along the first three principal components can be re-scaled to fit the display device (0-255), then combined in a false-colour composite. Because the axes of each component are mutually perpendicular, a great deal more of RGB colour space is filled (see figures 5.12a,b,c). In three-dimensions, the dataset appears spherical, as against the cigar-shaped ellipsoid of an original 3-band composite. Plate 5.14 shows the enhancement of subtle colour differences gained by the principal components transform. Any of the three component images can be assigned to any of the three additive primary colours in a composite image; analysis of the various possibilities reveals that by displaying the second component as red, the first component as green, and the third as blue, the most aesthetic (and easily interpreted) image is produced. The effects of decorrelating the data through the principal components transformation are extremely useful in separating subtly different categories of surface. However, although the colours of a principal component image are vivid, they bear little relationship to the true composition of the surface.

Furthermore, colours in principal component images are scene-dependent - a lithology characterised by a distinctive colour in one image may be represented by a completely different colour in another.

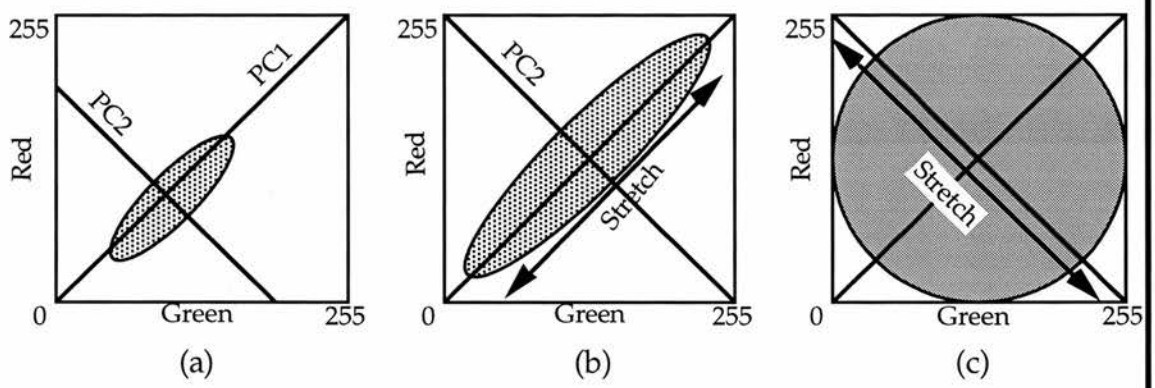

Figure 5.12. The principal components describe the axes of maximum variance within the plot of data from two bands. Because these axes are orthogonal, when stretched, the data is decorrelated and fills much more colour space. Principal component images therefore appear more colourful than their colour-composite counterparts.

Principal component images have been produced for the same sub-scenes as false-colour composites (see Figure 5.7). Because the colours are scene-dependent, mapping is not possible using these component images alone, rather they serve to provide any added resolving power necessary where the colour resolution of a false-colour composite is unable to differentiate between spectrally-similar lithologies.

Plate 5.11. The second principal component image of the test area contains less information, and more noise, than the first principal component image (plate 5.10) (refer to text on page 81).
Image sub-scene AA (refer to map on page 75).

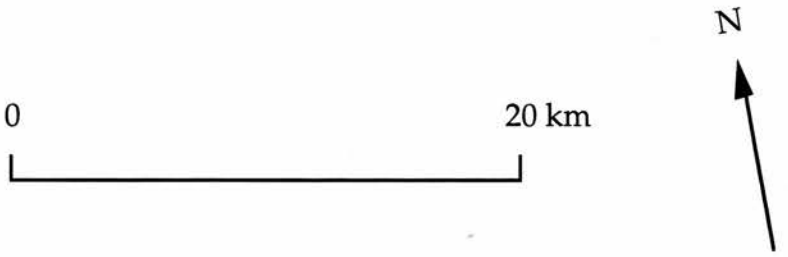

Plate 5.12. The third principal component image of the test area (refer to text on page 81).
Image sub-scene AA (refer to map on page 75).

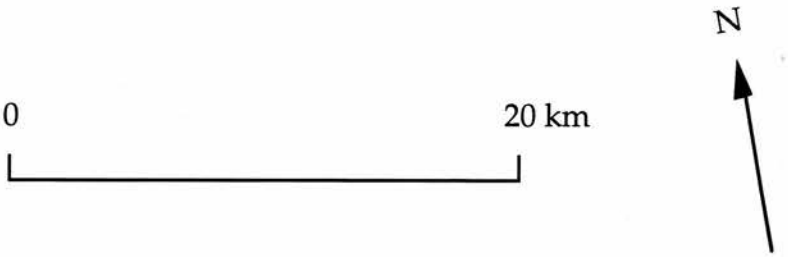

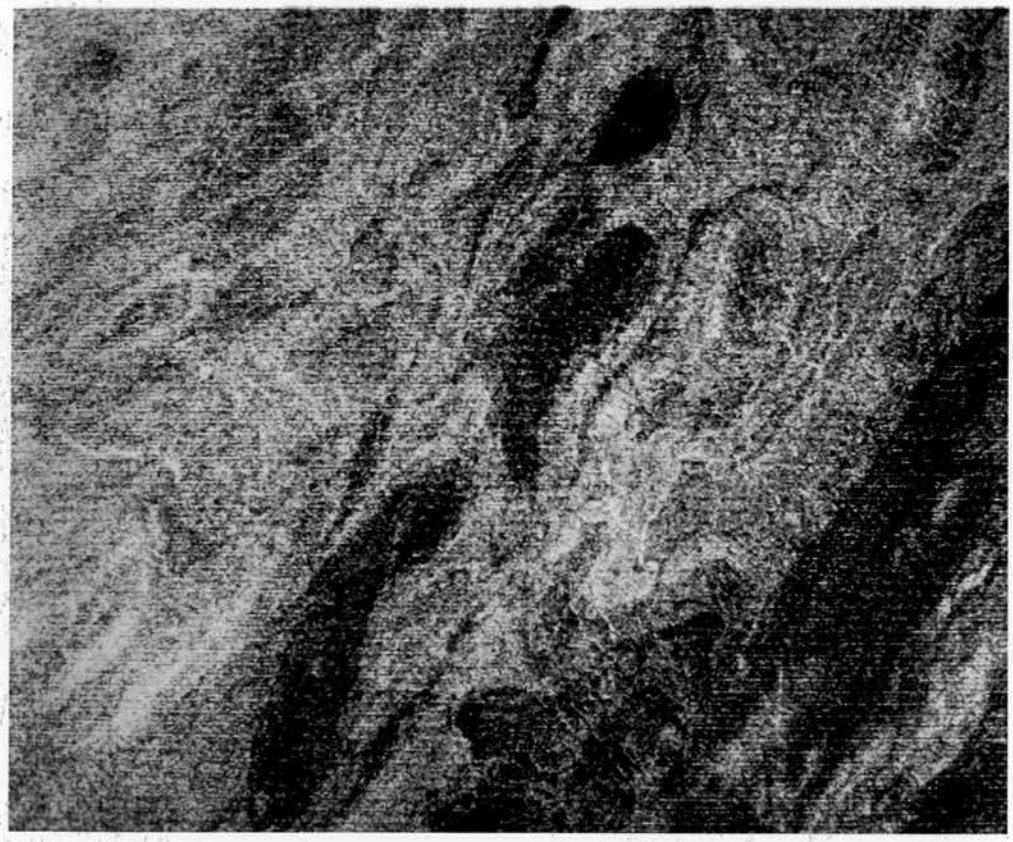

Plate 5.13. The fourth principal component image of the test area contains the least information, and the most noise. The only information available is the path of the Khan River (refer to text on page 81).
Image sub-scene AA (refer to map on page 75).

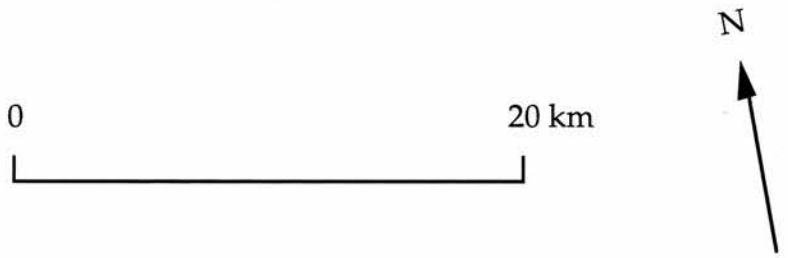

Plate 5.15. Greyscale ratio image of the test area (refer to text on page 84).
Image sub-scene AA (refer to map on page 75).

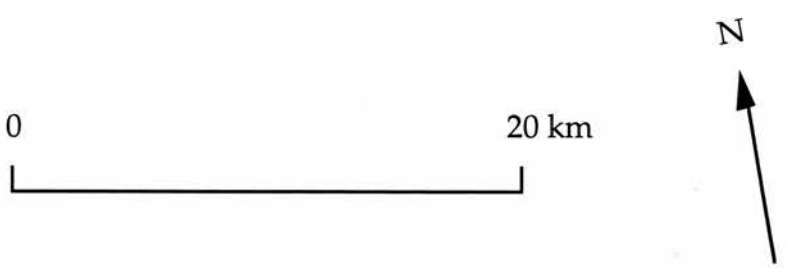

Plate 5.14. Principal component image of the test area (refer to text on page 81).
Image sub-scene AA (refer to text on page 75).

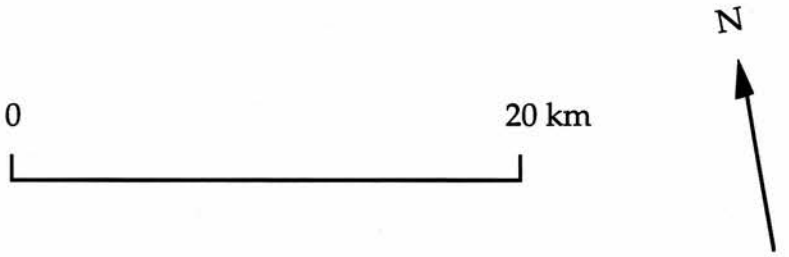

Plate 5.16. Colour band-ratio image of the test area (refer to text on page 84).
Image sub-scene AA (refer to map on page 75).

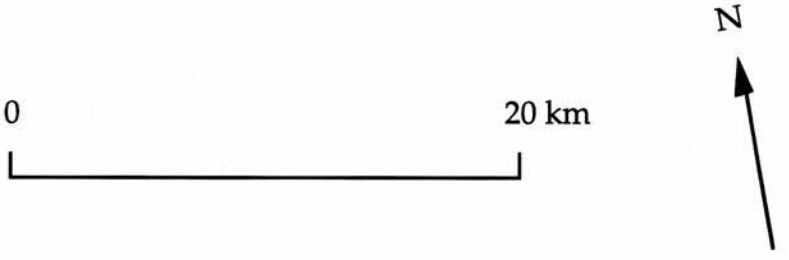

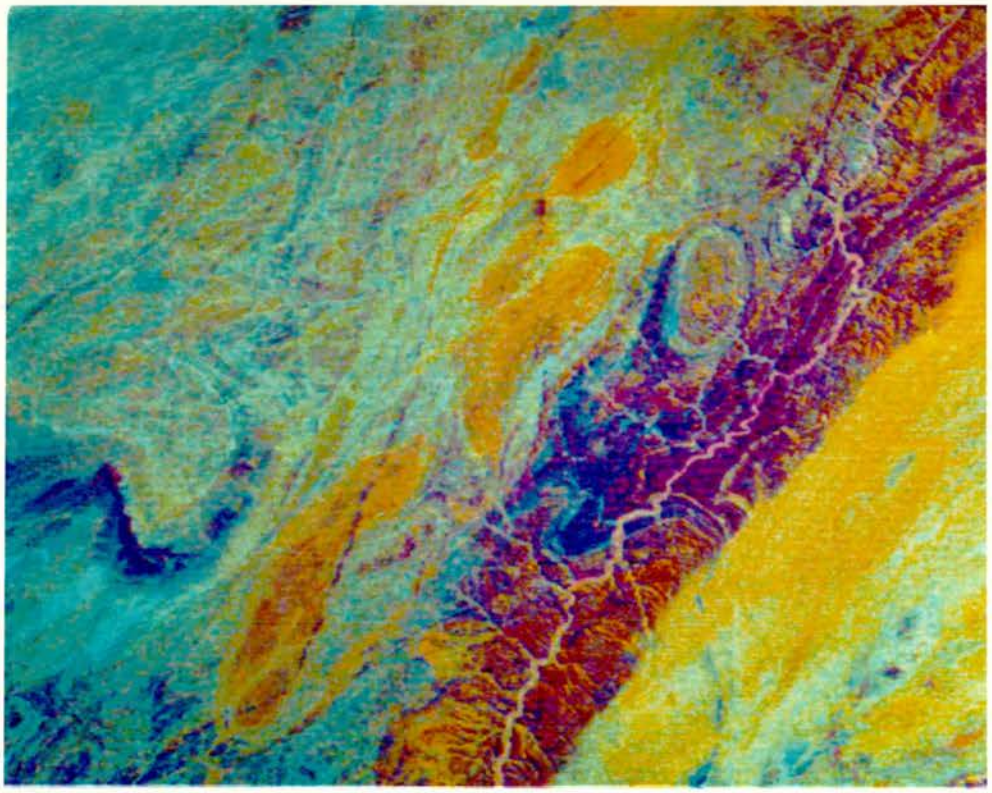

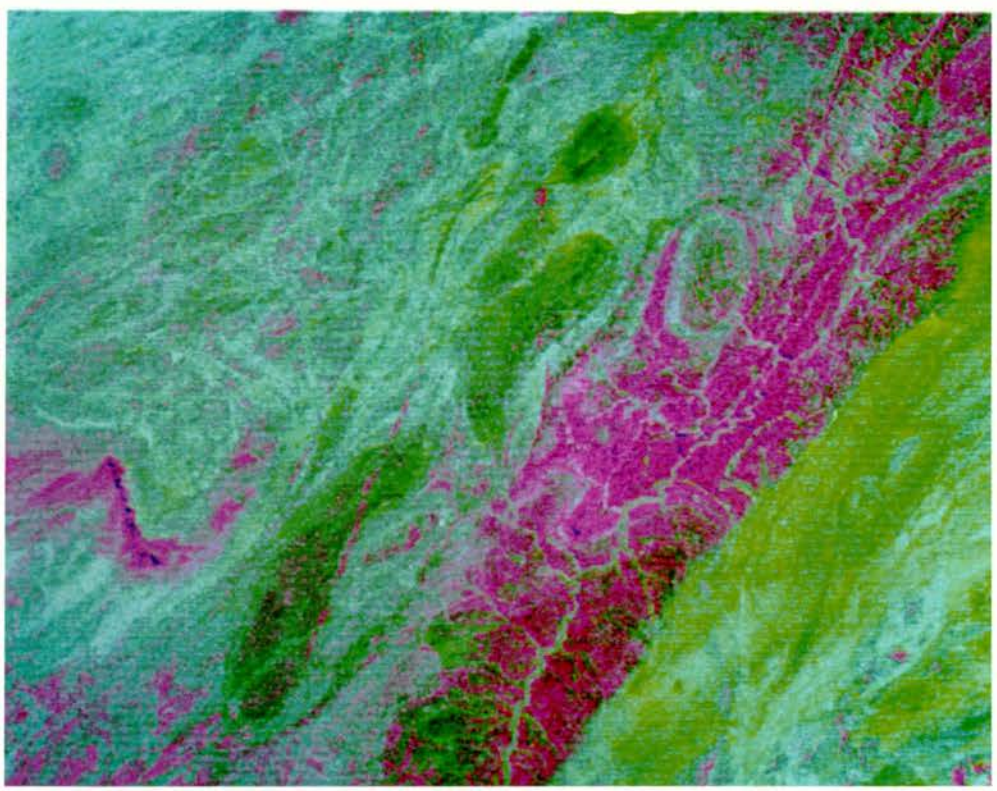

5.4.3. Band-Ratio Images.

Band-ratio images provide yet another means of displaying the spectral component of imagery, which consists of variations in reflection intensity between the different wavebands sensed (see section 3.6). Band-ratio images are created by dividing the DN of pixels in one band by the DN of corresponding pixels in another band of the same image. By rescaling the new pixel values to fit the 0-255 display range, a black-and-white image is produced in which bright areas correspond to those features which are more reflective in the numerator band than in the denominator band.

One of the benefits of band-ratio images is that the effects of shadowing, caused by topography, can be reduced (Mather, 1987). Slopes facing the Sun receive and reflect more radiation than shadowed areas, so DN across the image can often vary over areas which represent the same surface type. Although shadowed areas receive less radiation in absolute terms, they nevertheless reflect the same proportion of any incident radiation as a lit area with the same lithology. The ratio between two bands for pixels containing the same kind of surface should therefore be the same, no matter in which direction the slope faces. A ratio image thus reduces the effects of slope and shadows to a marked degree (Drury, 1987).

Because random noise is often uncorrelated between different bands, the ratios of pixels with spurious DN in either of the two bands produce extreme values. Thus, any noise is enhanced and most ratio images suffer from strong speckling and striping (Drury, 1991). Another problem with ratio images is that ratioing suppresses the ability to discriminate between rocks with

strikingly different albedos, but similar reflectance spectra, for example, between dark basalts and light marls (Gillespie, 1980).

The limited range of wavelengths covered by Landsat MSS data means that only features related to iron compounds and to vegetation can be picked out by ratioing. The presence of iron produces an absorption band in limonite near 0.9 μm (see Figure 5.3) due to an electronic transition (section 5.2). This feature falls within the range of MSS band-7. The ratio of band 6 to 7 therefore shows higher values for limonitic rocks than for other types (Drury, 1987).

Ratio images have been created for test areas, and although lithological differences can be picked out (see plates 5.15 and 5.16) the information content of these images is far less useful than either colour-composite or principal component images.

5.5. Conclusions.

1--In arid and semi-arid regions, rocks are sufficiently well-exposed to allow their spectral response to be used as a means of identification on remotely-sensed imagery. Various digital processing techniques can be employed to enhance this spectral information.

2--Different interactions occur between electromagnetic radiation, provided by the Sun, and different surface lithologies. Electronic and vibrational transitions add to and subtract from the total reflected radiation intensity to produce a unique reflectance curve (the 'spectral signature') over the wavelengths imaged by the MSS.

3--A traditional spectral classification technique proves unsuitable for geological mapping because real lithological contacts are often gradational, and even quite distinct rock types may have very similar spectral responses. Visual analysis of both the spectrally-enhanced and spatial components of the imagery by a trained interpreter yields far better mapping results.

4--Mapping of the Khan Gorge area, by Smith (1965), provides a test area where spectral and spatial image characteristics can be compared to known lithologies. By extending lithological boundaries outwards from this area, units can be mapped across the study region, where sufficiently exposed, to produce a remotely-sensed geology map.

5--Three of the four MSS bands can be displayed simultaneously in a false-colour composite image. The most effective combination is to show MSS

band-7 as red, MSS band-5 as green, and MSS band-4 as blue. By stretching the DN in each band to fit the whole display range, the image appears more colourful because more 'RGB colour space' is utilised. However, the strong correlations between MSS bands mean that image colours may remain muted.

6--The principal components transformation analyses the four band dataset and establishes four new, mutually orthogonal axes which far better describe the variation of that dataset. As the data is effectively decorrelated, when the first principal component image is shown as green, the second as red, and the third as blue in a composite image, a far more colourful image is produced. The fourth component is composed largely of noise and is rarely included in a composite image. One drawback of a component image is that colours are largely scene-dependent; by using overlapping images, results can be extrapolated from one area to another with more certainty.

7--MSS band-ratio images prove to be of limited use; lithological variations are far better expressed in false-colour composite and principal component images.

Chapter 6

Lineament Mapping: Discussion of Results.

Chapter 6. Lineament Analysis: Discussion of Results.

6.1. Lineament trends and their structural significance.

6.1.1. Positive topographic lineaments.

Map 1 shows the results of the analysis of the Landsat imagery for positive topographic lineaments. A total of 413 lineaments were recorded; the histograms produced by digitising those lineaments are shown in Figures 6.1 and 6.2.

A strong directional trend is instantly recognisable from Map 1; both histograms confirm this and show that trend to be orientated between 19 - 45 degrees to the east. Map 1 also shows that the positive topographic lineaments are conspicuously absent from the eastern half of the study area, so that most lineaments of this type are confined to the west, in a zone which appears to get slightly narrower to the north. Visual inspection of Map 1 also shows that the few lineaments which fall outwith the modal classes tend to be situated further to the south of the study area. The histograms just pick out this small subset, which appears orthogonal to the main trend.

Comparison with geological maps of the area show that the majority of the positive topographic features mapped are in fact a group of large dolerite dykes which cut across the region. These dykes belong to the Cretaceous Etendeka Volcanics (Erlank, 1985) which form a later part of the Karoo Volcanics succession. These dykes were erupted between 140 - 120 Ma ago (Duncan *et. al.*, 1990) and are believed to be associated with the splitting of Gondwana and the

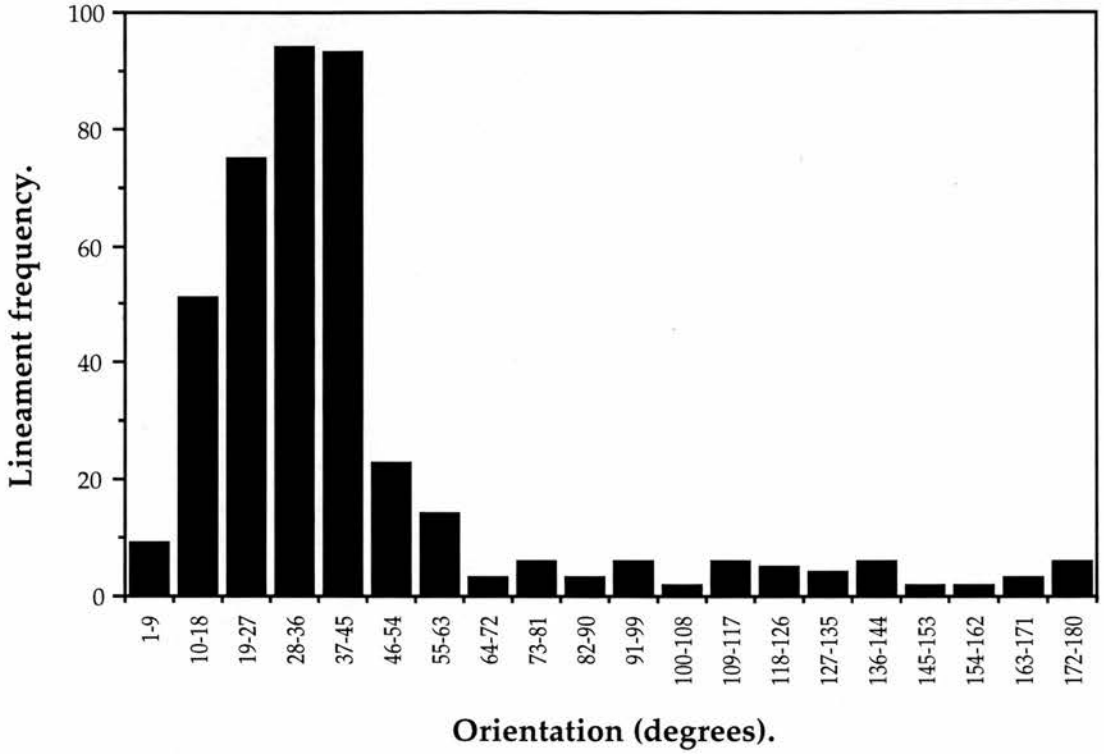

Figure 6.1. Frequency of positive topographic lineaments within each chosen azimuth class.

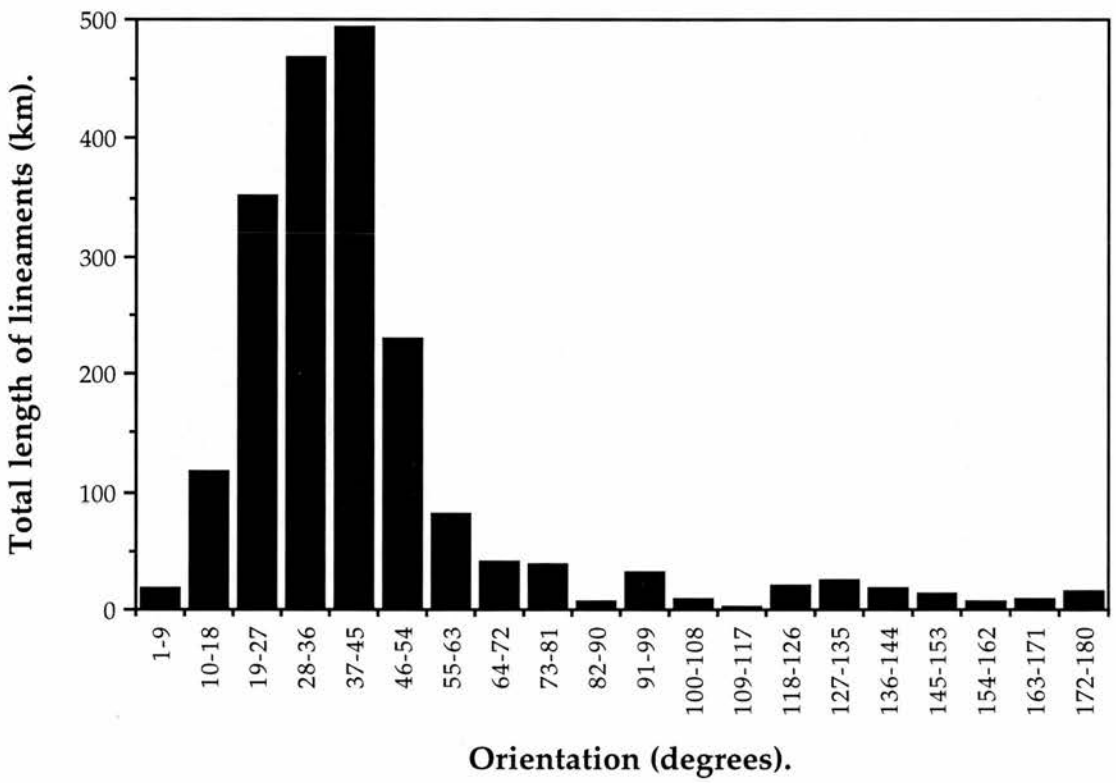

Figure 6.2. The total length of positive topographic lineaments within each chosen azimuth class.

opening of the Southern Atlantic Ocean.

The positive topographic lineaments (dykes) tend to be more easily distinguished in areas of sandy cover, although there are a few picked out that are contained within rocky exposures. Against the highly reflective background of light-coloured sand, the dolerite dykes appear very dark. They also have a pronounced topographic expression, with an associated area of shadowing. Many of these dyke features are well below the spatial resolution of the Multispectral Scanner (79 X 56 m). However, the presence of a dyke within a pixel area will detract from the overall reflection intensity of that pixel. Neighbouring pixels will have a slightly higher DN (the digital number from 0 - 255 used to represent the reflection intensity of a pixel in a digital image); these slight differences can be enhanced through the use of spatial frequency filtering (see section 4.3.2.) enabling the dyke features to be recognised.

Those dykes that outcrop within rocky areas may only be slightly darker than their immediate surroundings. Where the host rocks are similarly resistant to erosion, any topographic expression might be slight, and could even be negative if the host rocks are more resistant to erosion. Therefore, it may be that dykes are under-represented in rocky areas, a consequence of the resolving characteristics of the imaging system and the reduced topographic expression of the dykes themselves.

However, it seems likely that the distribution of positive topographic lineaments in the study area has some sort of control other than the type of cover because, even in the large sandy areas in the eastern half of the study

area, positive topographic features are noticeably absent. If one assumes that the majority of positive topographic lineaments are in fact dykes, the outcrop pattern relates well to the pattern associated with a regional dyke swarm. Similar dyke swarms are associated with divergent plate boundaries (Gudmundsson, 1990), for example the Quaternary and Tertiary dykes that occur in Iceland. Dating from the time of the splitting of Gondwana, the Etendeka dykes are likely to have been emplaced under similar divergent plate-boundary conditions, associated with the opening of the Southern Atlantic Ocean.

An investigation of aeromagnetic data by Corner (1983) identified a number of anomalies and aeromagnetic lineament zones (see Figure 6.3). One of the zones identified, the Welwitschia Lineament Zone, corresponds very well to the outcrop of positive topographic lineaments, although this zone is difficult to reconcile from Corner's own aeromagnetic data. Corner does note that the axes of basement folds deviate from the more usual north-east trend to follow a north-northeasterly trend in the vicinity of the Welwitschia Lineament Zone. Steven (1993) suggests that the Welwitschia zone may represent 'deep-seated (Proterozoic) fractures that were reactivated during the Damaran D_4 deformational phase'. The regional dyke swarm, shown by the positive topographic lineaments, may be the latest activity along this crustal weakness.

Corner (1993) states that, according to the magnetic data, the Welwitchia Lineament Zone is possibly truncated by the Omaruru Lineament (see Figure 6.3). However, the dykes do continue further north across the Omaruru Lineament, on the same trend, into the Northern Central Zone. Since the dyke swarm overprints the Omaruru Lineament, this implies that the

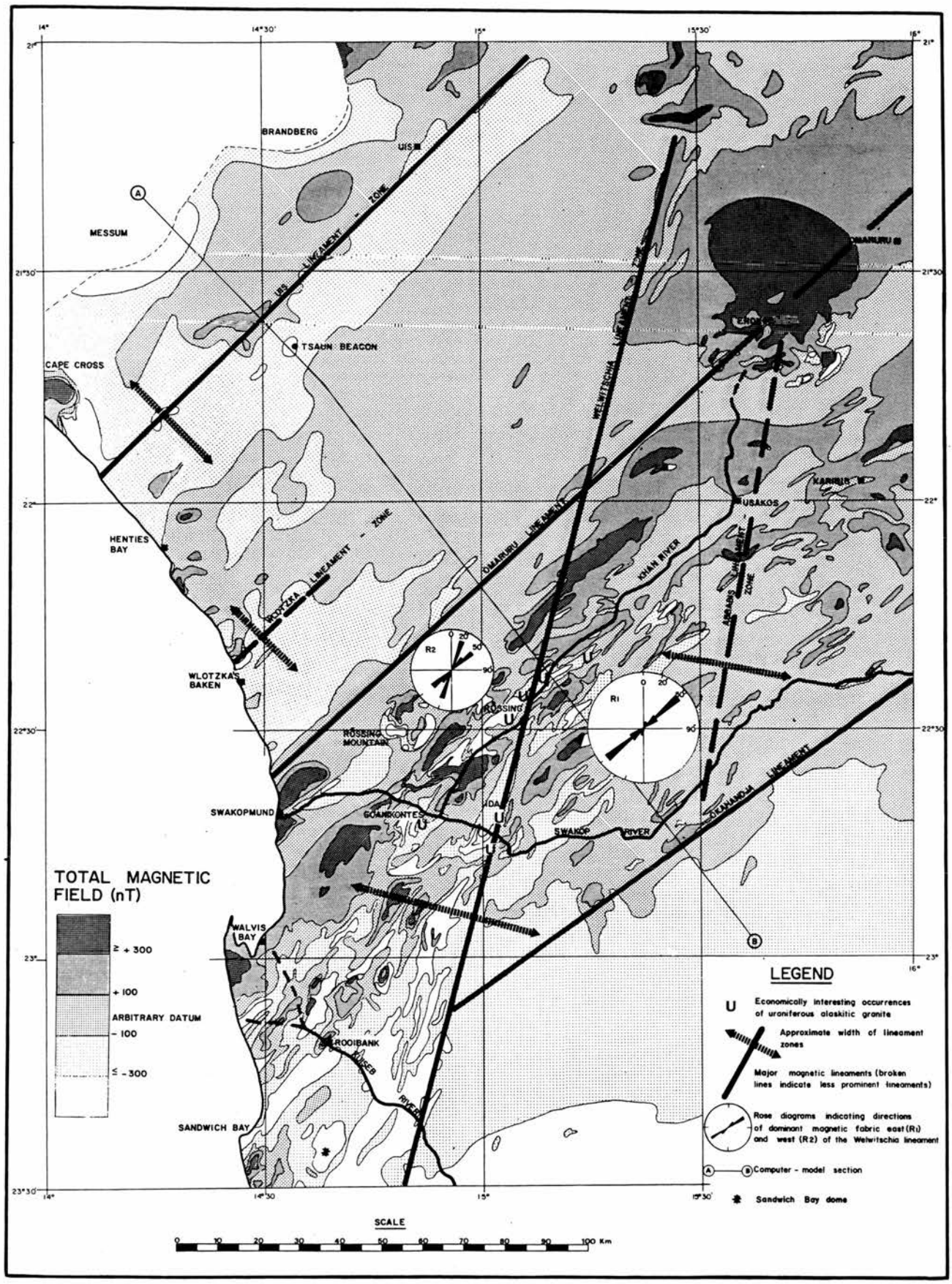

Figure 6.3. Simplified aeromagnetic contour map covering the western portion of the Damara Orogen (from Corner, 1983).

structural control of the Welwitchia Lineament does indeed extend further north. The Omaruru Lineament is considered to represent a monoclinal down-folding of basement rocks caused during the D_3 deformation event (Corner, 1983). Steven (1993) suggests that D_4 deformation was responsible for reactivation of earlier crustal fractures along the Welwitchia Lineament. This would suggest that there has been no lateral displacement along the Omaruru Lineament.

As mentioned earlier, the dykes date from the time immediately before the opening of the Southern Atlantic Ocean. Prior to rifting, basaltic lavas began to spread out on all of the southern continents at almost exactly the same time (Tarling & Tarling, 1982), beginning at about 160 Ma ago. Figure 6.4 shows the distribution of Cretaceous flood basalts, plotted on a map of Gondwana, localized near the separated continental margins (Windley, 1982).

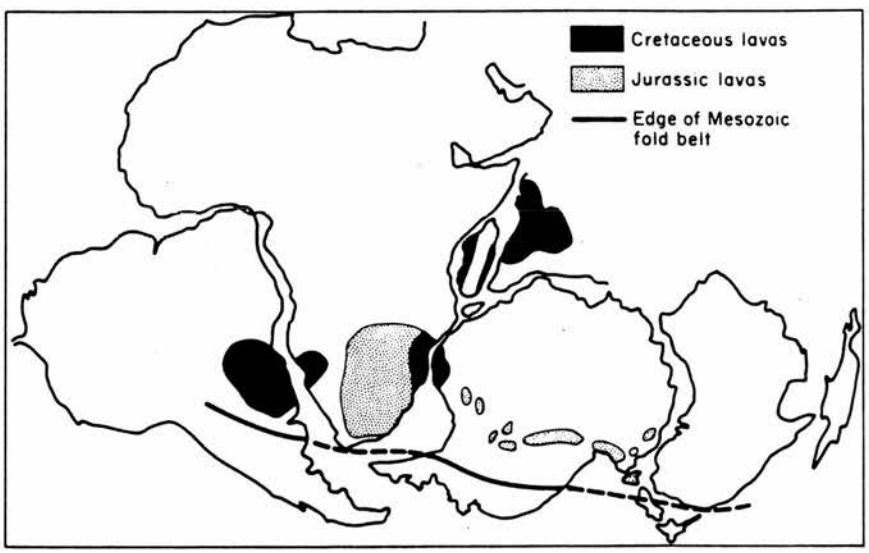

Figure 6.4. The distribution of Mesozoic lavas plotted on a map of Gondwana. The Cretaceous lavas of western Africa and Brazil show a close lithological, geochemical and temporal correlation (Duncan *et. al.*, 1990).

The Etendeka Volcanics, at 140 - 120 Ma, represent the latest series of dyke intrusions before spreading actually began. Marsh *et. al.*, (1991) note that the Etendeka dykes 'exhibit a close lithological, geochemical and temporal correlation with the Serra Garal dykes of the Parana Flood Basalt Province of South America'. Both are immediately adjacent to their continental margins and can be geographically linked in pre-drift reconstruction of Gondwana (Duncan *et. al.*, 1990).

Dykes are one of the key factors in the mechanism of spreading at divergent plate boundaries (Gudmundson, 1990). The dykes of the Etendeka Volcanics, which form the positive topographic lineaments, are clearly related to the rifting environments that ultimately gave rise to sea-floor spreading and the disruption of Gondwana, and occur in areas where substantial lithospheric thinning occured (Duncan *et. al.*, 1990). Figure 6.5 shows that the trend of the Etendeka dyke swarm is parallel to the divergent plate boundary. It is possible that the dykes became emplaced along the area of the Welwitchia Lineament Zone because they exploited a pre-existing crustal weakness that the zone is thought to represent. This crustal weakness exploited by the regional dyke swarm may represent a 'proto-rift'; had there not been a stronger rift to the west, now represented by the mid-Atlantic ridge, Gondwana might theoretically have split further to the east.

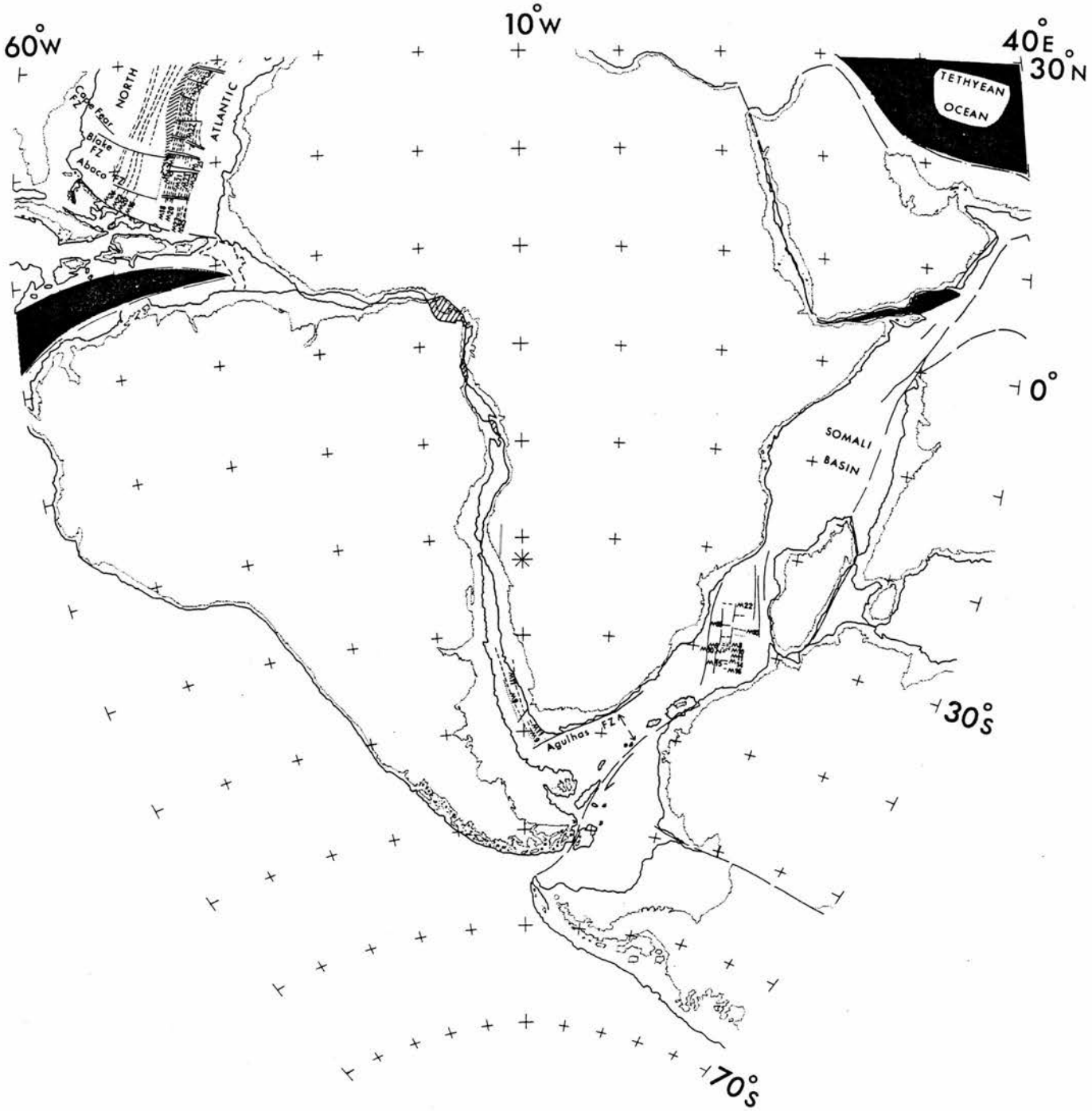

Figure 6.5. The trend of the Etendeka regional dyke swarm and its relationship to the divergent plate margins of the African and South American continents (map from Owen, 1983).

6.1.2. Negative topographic lineaments.

Map 2 shows the results of the analysis of the Landsat imagery for negative topographic lineaments. A total of 527 negative topographic lineaments were recorded; the histograms produced by digitising those featuress are shown in Figures 6.6 and 6.7.

Although different from the trend for positive topographic lineaments, a strong directional trend is again evident; both histograms confirm this and show that trend to average at 145 -153 degrees to the east. However, this trend is orthogonal to the solar azimuth and it may be that other trends are under-represented, especially those parallel to the sun's orientation. Within the study area, the negative topographic lineaments occupy only rocky outcrops and they cannot be distinguished in those areas that are covered by sand. Their occurrence largely corresponds to the paths of the Khan and Swakop Rivers (see Fig 1.2), and their immediate tributaries, and the confluence of these two rivers is picked out well on Map 2 in the southwest portion of the study area.

Some of the larger negative topographic lineaments show up as faults on geological maps of the area. Because the other lineaments mapped have a similar topographic expression, and because they follow a similar prominent trend, it is likely that they too are surface expressions of unmapped faults, which have been created during the same episode of deformation. Some of the smaller features may simply be major joints, although the fact that many cut across adjacent, but different lithologies suggests that faulting is more likely to be the cause of their formation.

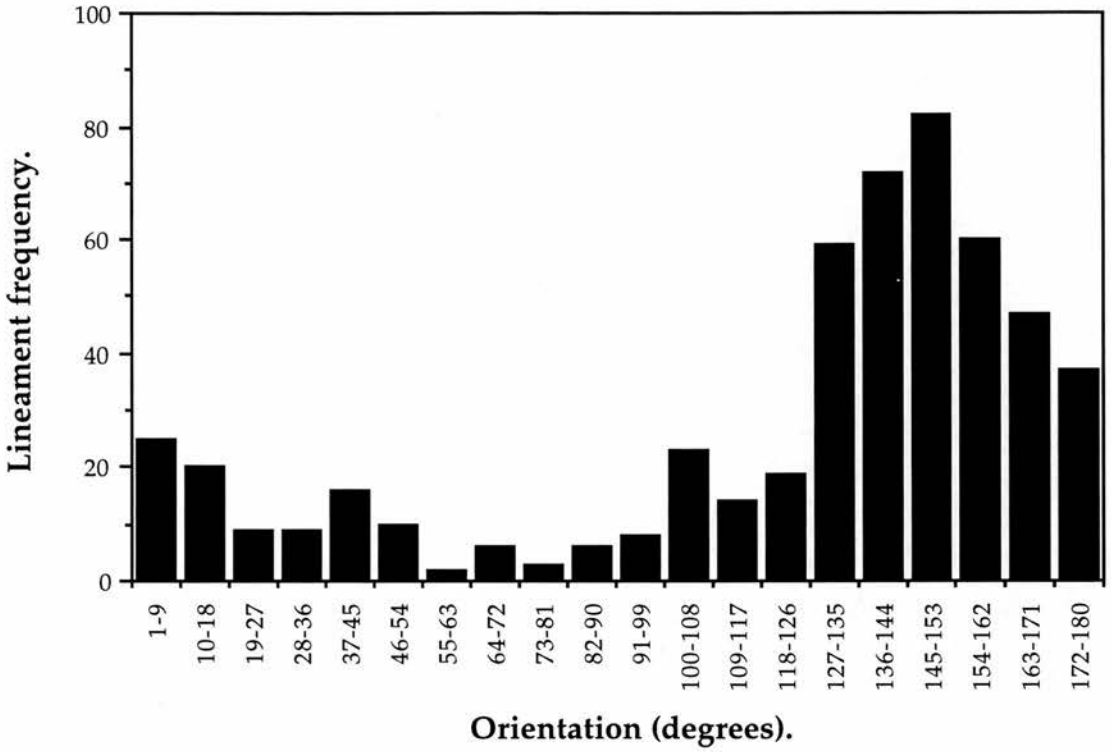

Figure 6.6. The frequency of negative topographic lineaments within each chosen azimuth class

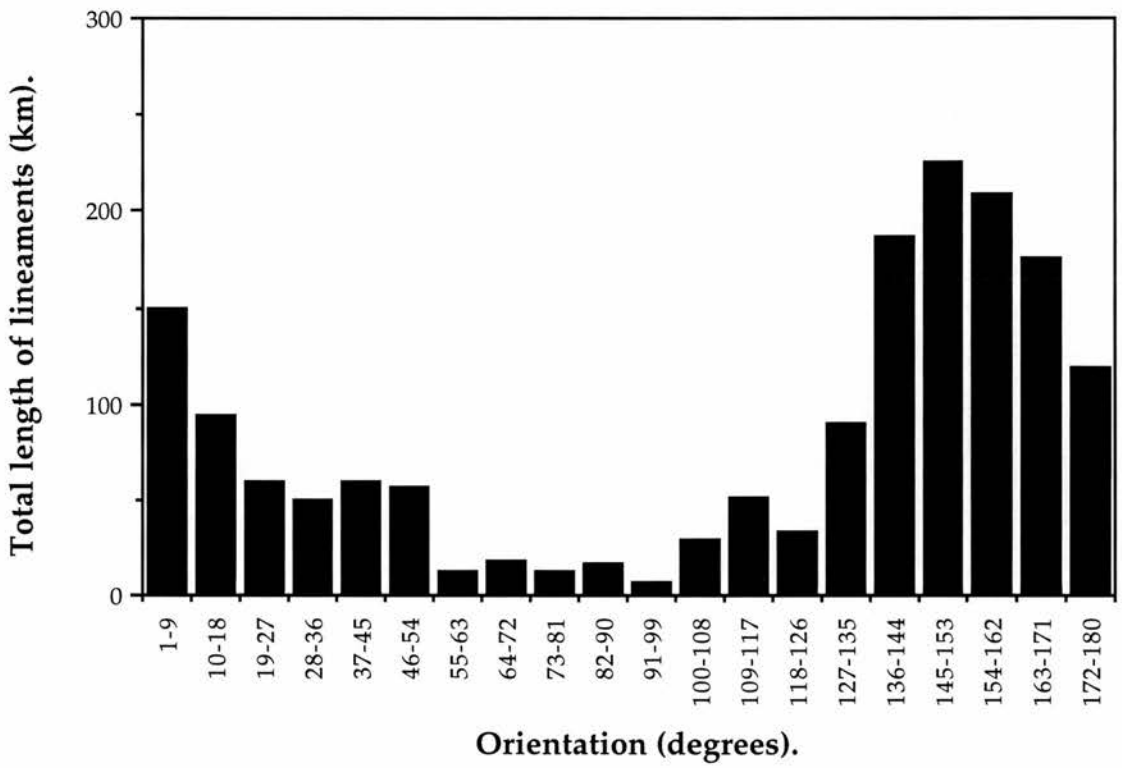

Figure 6.7. Total length of negative topographic lineaments within each chosen azimuth class.

Many of the negative topographic lineaments are seen as straight stream valleys, especially those that are tributaries to the Khan and Swakop Rivers. Again, as these follow a similar trend to known faults, it seems likely that these valleys are fault-controlled. It is because so many of the negative topographic lineaments are tributary valleys that the greatest densities of these lineaments are to be found following the course of the Khan and Swakop Rivers. Periodic fluvial activity along these two rivers, and their tributaries, ensures that sediment is removed from their immediate vicinity; hence the best rock outcrops in the study area closely mirror the paths of these two rivers.

By visual inspection of the faults on the imagery, at least as closely as the resolution of the MSS data will allow, some lateral displacement of units either side of the fault-line can be recognised. Where discernible, all faults show sinistral offsets. For example, in image sub-scenes AK and AM, faults show sinistral offset of the order of 150 - 300 metres (see Plate 6.1). In sub-scene AA the same sense of movement can just be seen on a fault which cuts the north-western limb of the SJ Dome (see Figure 5.6, after Smith, 1965). This has lateral offset in the order of 200 metres.

It is impossible to see whether or not there is any vertical sense of movement along these fractures, although any such movement is likely to be minimal because the same stratigraphic horizons are generally seen on either side of the fault-line. The coarse spatial resolution of the MSS imagery hampers the identification of critical movement relationships along the fault-lines and this inability to resolve simple structural features is a major drawback of the data. The increased spatial resolution of Thematic Mapper (TM) imagery (30 m),

and SPOT panchromatic data (10 m), which also has a stereoscopic image capability, proves more useful in determining such critical structural relationships (Drury, 1993).

The faults will have formed under conditions of brittle deformation and so are unlikely to have formed during the main episode of the Damara Orogen, which occured at depth with associated conditions of plastic deformation. In Smith's (1965) outline of the tectonic history of the Damara, he suggests that two main orthogonal episodes of deformation were responsible for the formation of the characteristic basement dome structures of the Central Zone. The first of these deformation events, D_1, was orientated northeast-southwest, and was responsible for the formation of northwest-trending folds. Smith then suggests that there was a change in the stress field to the northwest-southeast, and that this more powerful stress, D_2 (D_3 of Miller, 1983), led to the formation of the major northeast-trending structures - elongate synforms and antiforms.

These D_1/D_2 events were synchronous with metamorphism, so deformation conditions were plastic rather than brittle. Smith states that when metamorphism declined, the rocks did become brittle and were gently fractured in places. The fractures seen as negative topographic lineaments are aligned at right angles to the northeast-trending fold axes. The axial planes of nearly all the major folds are close to vertical (Steven, 1993) and so both the folds and the faults may have formed under a similar stress field. As such, the small sinistral fault displacements may have been formed by any residual D_2 stresses under more brittle conditions at the close of the Damara Orogen, which also was sinistrally transpressive (Oliver, 1993). Steven (1993) reports of

late orogenic semi-ductile and brittle D_4 deformation, which might also have been responsible for the formation of these faults.

If not late-, then presumably, post-Damaran deformation was responsible for the formation of these negative topographic lineaments (faults). However, the only tectonic event of any real significance in the area was the rifting and splitting of Gondwana to form the Southern Atlantic Ocean, and the orientation of the negative lineaments does not fit well to this event. Were any of the later dykes of the Etendeka regional swarm seen to be offset, one could place the faulting after their intrusion. The MSS imagery does not show any faulted dykes, although this may possibly be a factor of spatial resolution. Field evidence (Nex, *pers. comm.*, 1994) does show that these dykes are faulted in places, but these faults usually trend north-south, and rarely is there any marked displacement. It is likely that two separate deformation events have occurred, and that the negative topographic lineaments pre-date the Etendeka dyke faults.

While negative topographic lineaments tend to be seen in rocky exposures, the dykes tend to be more visible in the lighter-coloured sandy areas. Because of the way in which the two sets of lineaments are identified, they appear almost mutually exclusive. However, some dykes can be seen cutting through areas of exposed bedrock, and undoubtedly there are faults beneath those areas that are covered by sand. Nevertheless, it is not possible to see evidence where the dykes have been affected by faults, so deformation is assumed to have taken place between the end of the Damaran Orogeny (~460 Ma, Miller, 1983) and the intrusion of the Etendeka dolerite dykes (~140-120 Ma, Duncan *et. al.* , 1990).

Plate 6.1. A large fault, expressed as a linear drainage segment, cuts across the southern portion of the Rooikuiseb Anticline. The lithological units on the northwestern flank of the anticline show sinistral displacement across this fault (refer to text on page 98).
Image sub-scene AK (refer to map on page 75).

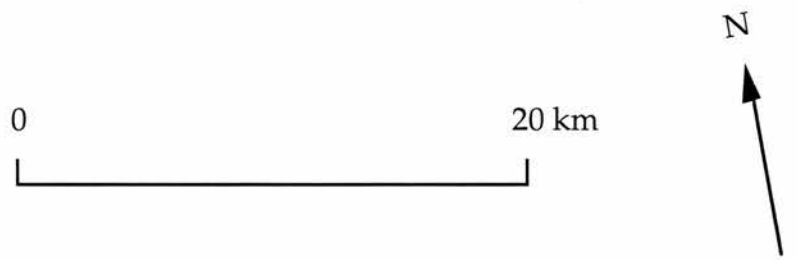

Plate 6.2. Tonal lineaments caused by different lithological horizons on the southeastern flanks of the Chuos Mountains (refer to text on page 101).
Image sub-scene BC (refer to map on page 75).

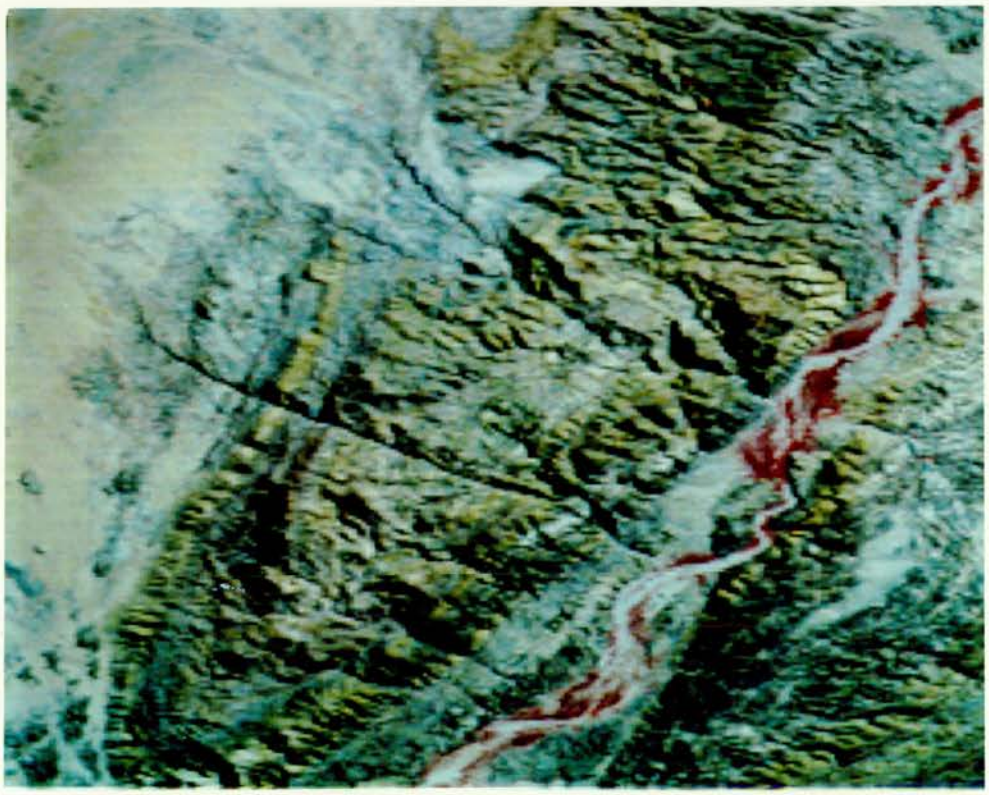

6.1.3. Tonal lineaments and fold axes.

Map 3 shows the results of the analysis of the Landsat imagery for tonal lineaments. Fold axes have also been included on this map, for reasons discussed below. A total of 384 tonal lineaments were recorded; the histograms produced by digitising those lineaments are shown in Figures 6.8 and 6.9. A total of 66 identifiable fold axes were also recorded. The histograms produced by digitising these features are shown in Figures 6.10 and 6.11.

A strong and corresponding trend is recognisable from Map 3 for both the tonal lineaments and the fold axes; all the histograms confirm this and show that the trend is orientated approximately northeast-southwest. The tonal lineaments and fold axes follow the general trend of the pan-African Damara Orogen and they appear orthogonal to the negative topographic lineaments (see Map 4). The tonal lineaments and fold axes have a corresponding orientation because the former tend to be lithological horizons on the limbs of the elongate domes and basins (whose centres are taken to be fold axes) which characterise the Central Zone. An example is shown in Plate 6.2.

Fold axes are mapped as the long axes of the dome and basin features. This assumes that the features are symmetrically folded, which may not necessarily be the case. Nevertheless, although the quantitative positions of the fold axes may not be entirely correct, the directions of the marked fold axes will be fairly accurate. The distribution of tonal lineaments largely mirrors that of the negative topographic lineaments in that they tend to be more readily distinguished along the paths of the Khan and Swakop Rivers, where rock outcrop is better. One feature of note is that while the fold axes (and associated

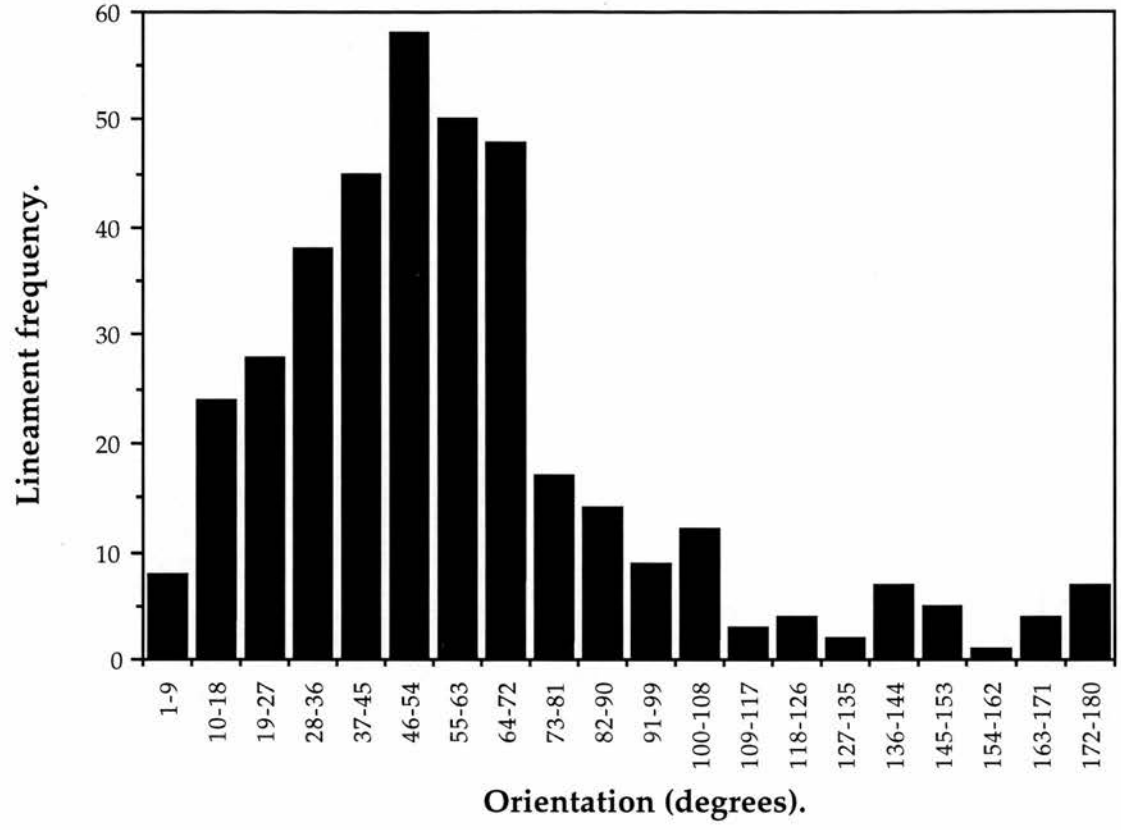

Figure 6.8. The frequency of tonal lineaments within each chosen azimuth class.

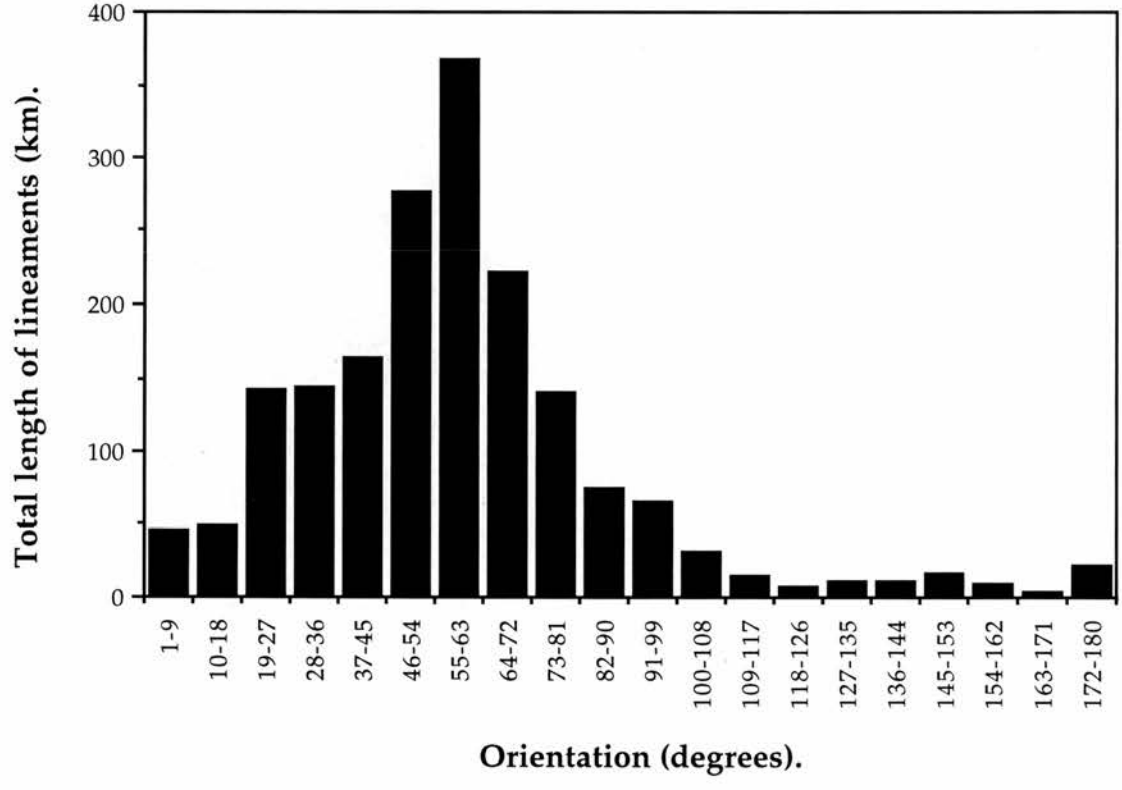

Figure 6.9. The total length of tonal lineaments within each chosen azimuth class.

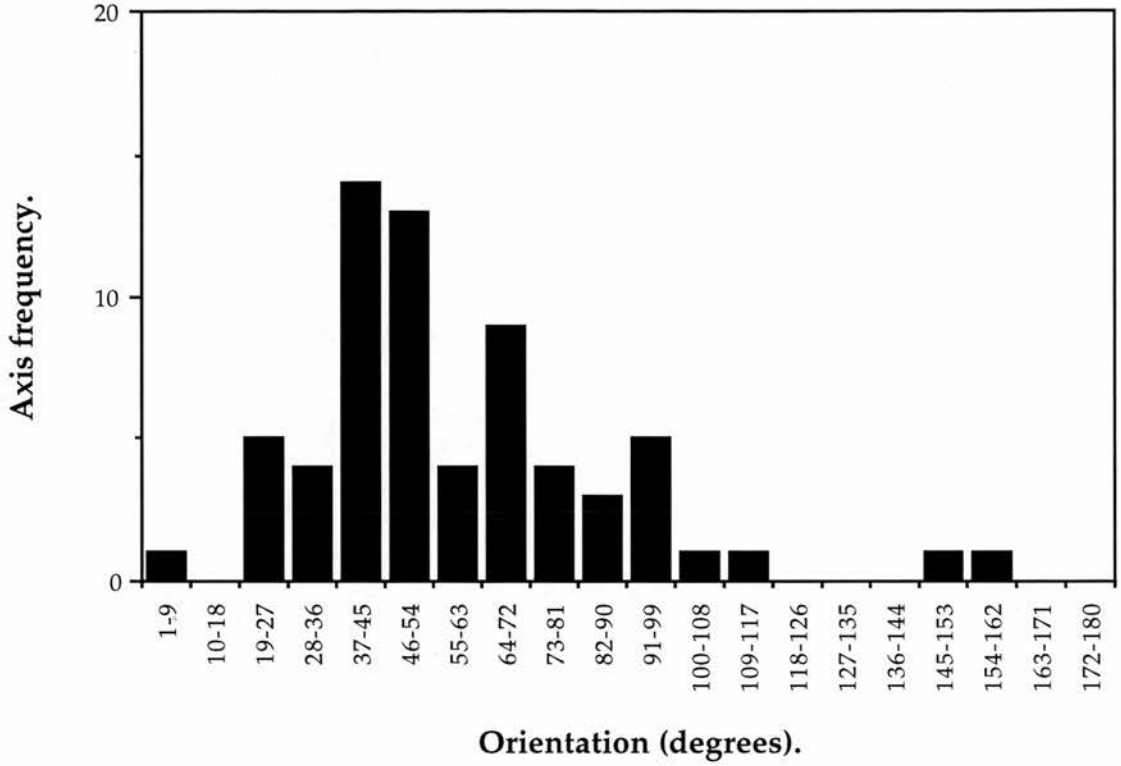

Figure 6.10 The frequency of fold axes within each chosen azimuth class.

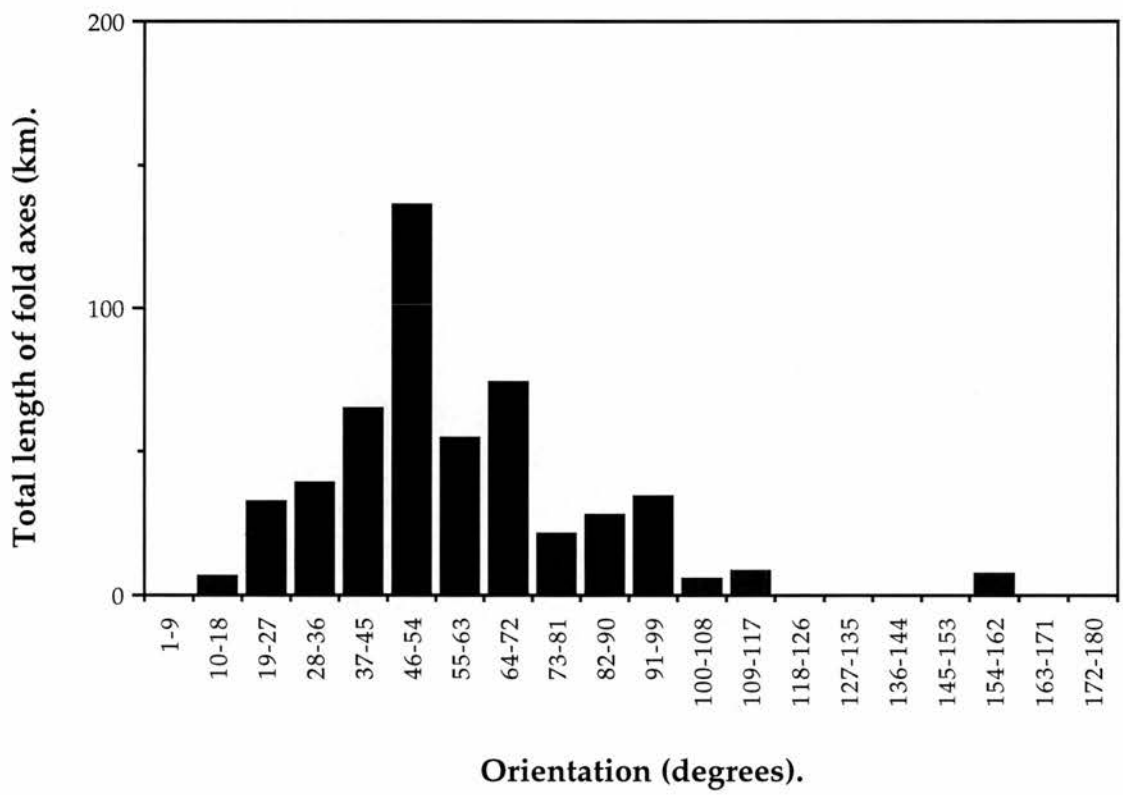

Figure 6.11 The total length of fold axes within each chosen azimuth class.

tonal lineaments) appear to generally trend in the same direction, the kurtosis of the histograms reveals that this trend is rather broad. This is because the trend of the Central Zone seems to bend towards the south in the southwestern part of the study area, and to the east in the northeastern part of the study area, i.e. the trend is not a uniform one. Corner (1983) also notes that in the vicinity of the Welwitchia Lineament Zone (see Figure 6.3) basement domes are aligned more towards a north-northeasterly trend. The trend mirrors the path of the Okahandja Lineament, and probably reflects the oblique nature of continental collision between the Congo and Kalahari cratons.

The tonal lineaments are usually revealed on the flanks of domes of basement rocks, and the inter-lying synclines of younger cover rocks. Although these features are readily apparent from the satellite imagery (see Map 5), the cause of their formation is controversial. As stated in the previous section, Smith (1965) considers the basement domes to have formed as a result of two separate and orthogonal deformation events, the first orientated northeast-southwest, and a second, more severe event, orientated northwest-southeast, responsible for the linear margins of the dome structures. Other proposed methods of formation have included diapirism of granitic basement into denser meta-sedimentary cover (Ramberg, 1972), and the ballooning of basement-derived granites which have intruded pre-existing anticlinal structures of metasedimentary cover (Kroner 1984). However, the granitic gneisses have been dated to the Kibaran Orogeny (1038+/-58 Ma[Rb/Sr]) and are therefore pre-Damaran, so these methods of formation can be excluded. The elongate nature of the domes and basins, which causes the tonal lineaments, suggests structural controls are inherent in the cause of their

formation.

Based on the interpretation of new field evidence, Oliver (1993) has proposed a new method of dome formation in the Central Zone of the Damara Orogen, based on the idea of a single deformation event, rather than Smith's two-stage hypothesis. This interpretation attempts to tie in the presence of a profound ductile shear zone situated between the cover and the basement, previously interpreted by Smith (1965) as a deformed gneiss formation - the Abbabis augen gneiss, and now interpreted by Oliver (1993) to be L/S tectonites. Oliver recognises that extension lineations within the shear zone are consistently orientated northeast-southwest. He suggests that they have formed as a result of combined northwest-southeast compression and southwest-northeast extension when the cover detached itself from the basement and plastically flowed and escaped to the southwest during the collision of the Kalahari and Congo Cratons. This scenario would also help to explain an apparent metamorphic gap of between 4 and 6 kilometres that Oliver recognised between the basement and cover rocks.

The interpretation of either Smith (1965) or Oliver (1993) would explain the tonal lineaments seen on the imagery, although the latter better explains field evidence. Although the imagery in no way resolves the argument, it does provide the benefit of a synoptic regional view which shows the spatial relationship between basement dome outcrop and sedimentary cover. While accepting Oliver's concept of a mid-crustal detatchment, without age constraints it is impossible to say whether or not detachment and dome formation were contemporaneous, or whether the detachment event simply modified a pre-existing folding pattern.

6.1.4. Regional Lineament Patterns.

The lineaments shown in Map 4 are those combined from the three previous maps. The lineament patterns can be broadly correlated with the regional lineaments described by Corner (1983), as shown in Figure 6.12. Map 4 includes 1,390 lineaments in total; the histograms produced by digitising those features are shown in Figures 6.13 and 6.14. The distribution appears bi-modal at first; the smaller right-hand peak represents the negative topographic lineament population, and the larger left-hand peak represents both the positive topographic lineaments (dykes) as well as tonal lineaments. Although the latter two appear to trend in the same direction, Figures 6.1/2 and 6.8/9 show that this is not the case, rather the two populations become blurred together when the data is combined.

Although some of the lineaments mapped are in excess of 20 km, these only represent localised features. When the study area is viewed as a whole, regional-scale lineaments can be observed in the order of hundreds of kilometres. Some of these are apparent on Corner's (1983) simplified aeromagnetic map (Figure 6.3) and on Maps 4 and 5. These larger-scale lineaments generally mirror the trends seen in the smaller-scale features.

One of these regional lineaments is picked out in Map 1, which shows the dykes trending along the Welwitchia Lineament Zone, a feature that Steven (1993) suggested was controlled by deep-seated, Proterozoic fractures. Corner (1983) noted that, in the vicinity of the Welwitchia Lineament Zone, fold axes were aligned along that trend of that zone. Comparison between Maps 1,4 and 5 shows that in the southern part of the study area the trend of the the dykes

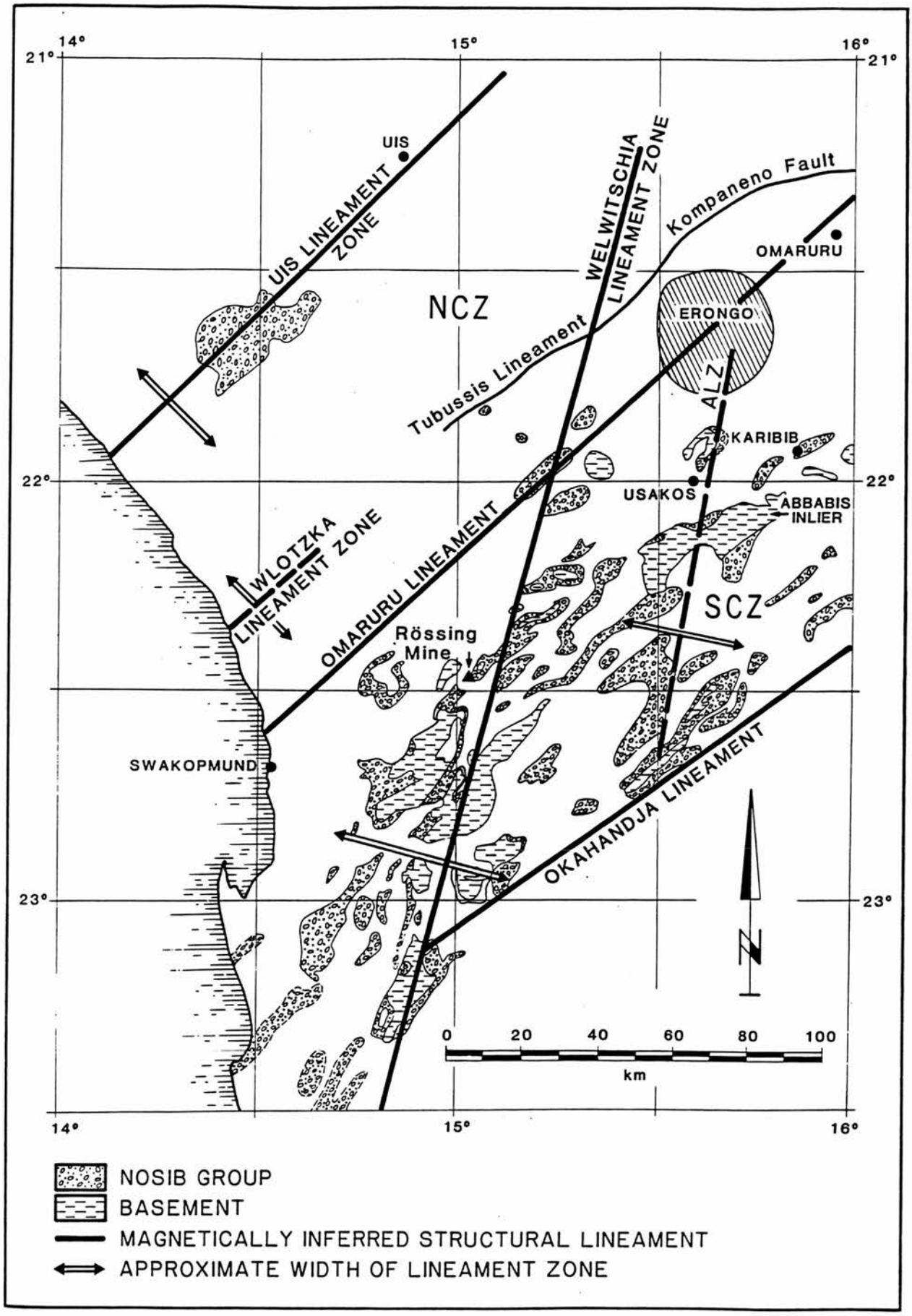

Figure 6.12. Previously recognised regional lineaments (from Stevens, 1993).

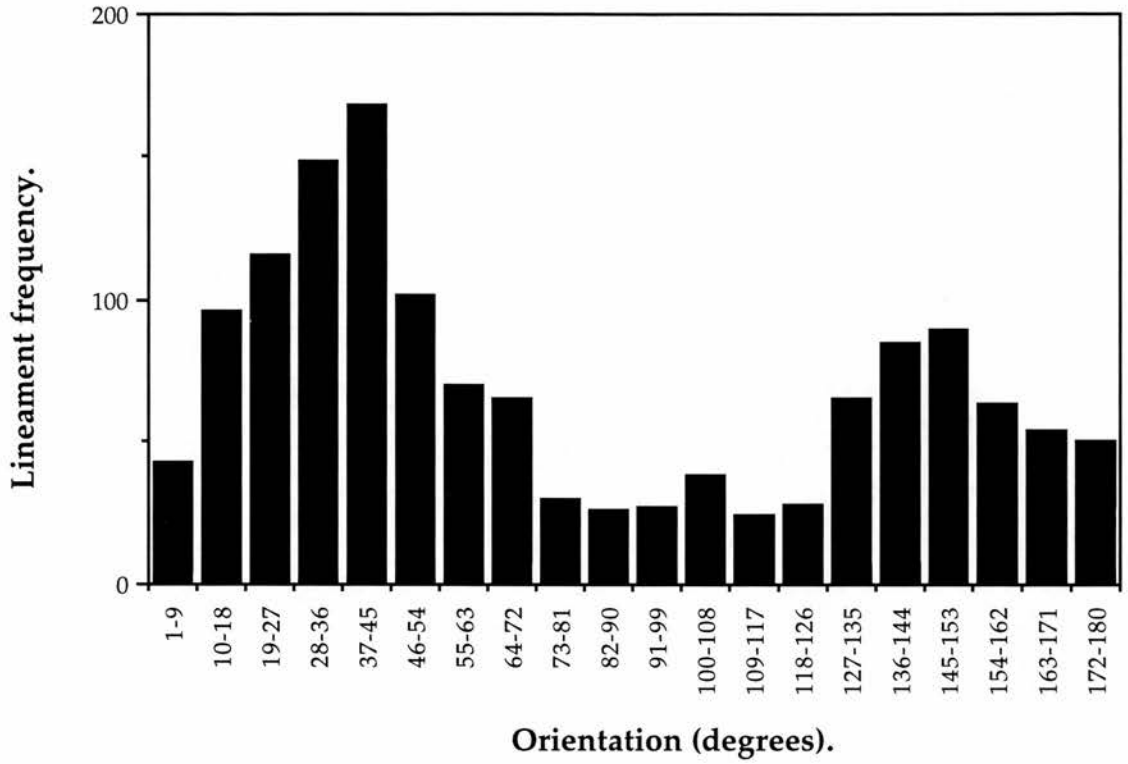

Figure 6.13 The frequency of lineaments within each chosen azimuth class.

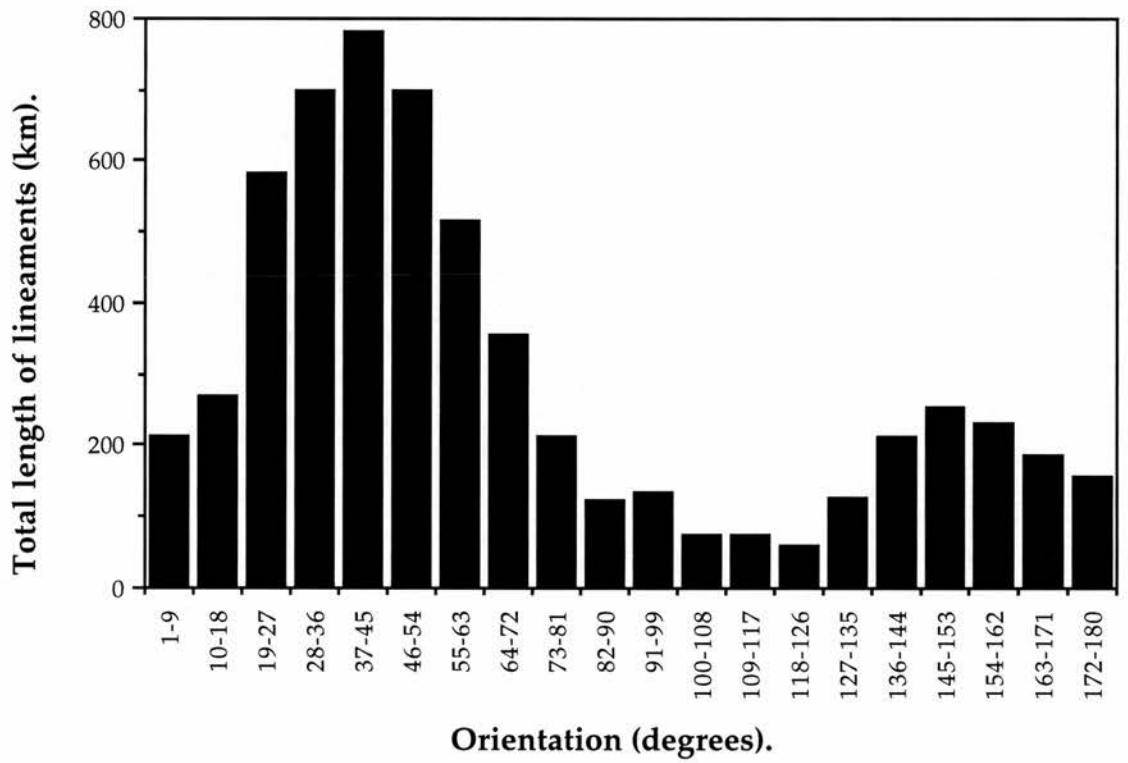

Figure 6.14. The total length of lineaments within each chosen azimuth class.

changes slightly, as does the trend of the tonal lineaments and fold axes, so that the two sets converge and become almost parallel.

The Okahandja lineament is clearly seen on the imagery (see frontispiece, Plate 6.3, and Figure 1.2) separating the Central Zone, to the north, from the Okahandja Lineament Zone to the south. This regional lineament trends for at least 530 km inland from the coast, and separates two zones of contrasting stratigraphy and tectonic style (Miller 1983). The lineament is thought to represent a monoclinal down-folding of the rocks of Damara succession of the Central Zone (Downing, 1983) and Miller (1979) believes that the feature marks the edge of the Congo Craton. He also suggests that uplift of the Central Zone relative to the Okahandja Lineament Zone was of the order of 20 km or more.

The lineament follows the trend of the Damara Orogen and mirrors that of the fold axes and tonal lineaments to the northwest. It is considered to have formed during the same period of deformation that was responsible for the formation of the basement domes. Figure 6.15 shows a computer model section along a northwest - southeast geomagnetic profile across the central part of the Damara Orogen (from Corner, 1983). It shows that basement rocks are near to the surface within the Central Zone, then there is a change across the Okahandja Lineament, to the southeast of which are deposited the flysch sediments of the Kuiseb Formation.

Another regional lineament that is picked out in the northwest portion of the study area, shown well on Map 5, is the boundary between the Central Zone

and the Northern Zone of the Damara Orogen. This feature is known as the Autseib Fault and is located slightly to the southeast of the Corner's (1983) UIS Lineament Zone (Figure 6.12). Miller (1983) suggests that the boundary is formed by southward-dipping reverse faults or thrusts. To the northwest, sandy sediments mantle the surface, while across the fault to the southeast, basement rocks are exposed (see Plate 6.4). The computer model section (Figure 6.15) confirms a similar geological arrangement. The trend of the Autseib Fault is identical to the Okahandja Lineament, and might be contemporaneous with that feature.

Corner's (1983) Omaruru Lineament is not easily distinguishable from the Landsat imagery. Map 5 does show that to the southeast of its supposed position, many more basement domes are exposed, and to the northwest rock outcrop is scarce until one reaches the basement rocks exposed along the Autseib Fault. It is possible that the lineament represents a monoclinal down-folding of the basement rocks that are exposed between the position of the Omaruru and the Okahandja Lineament to the southeast. The computer model cross section 2 of Figure 6.15 would seem to confirm this idea, and the total field intensity curve certainly shows a pronounced positive magnetic anomaly over the Omaruru Lineament area.

The Abbabis Lineament Zone of Corner's (1983) simplified aeromagnetic map is not visible at all from the Landsat imagery. Furthermore, it is even difficult to reconcile from Corner's own data. One feature that is very prominent though on the satellite imagery, yet does not feature on Corner's map, is the photo-lineament that trends to the northeast from the confluence of the Khan and Swakop Rivers (see frontispiece). This identically parallels the trend of the

of the Okahandja Lineament situated approximately 50 km to the east. The photo-lineament is picked out by a sharp change from exposed bedrock, to the northwest, to sandy deposits in the southeast. Like the Omaruru and Okahandja Lineaments, it may represent a slight monoclinal down-folding of the strata.

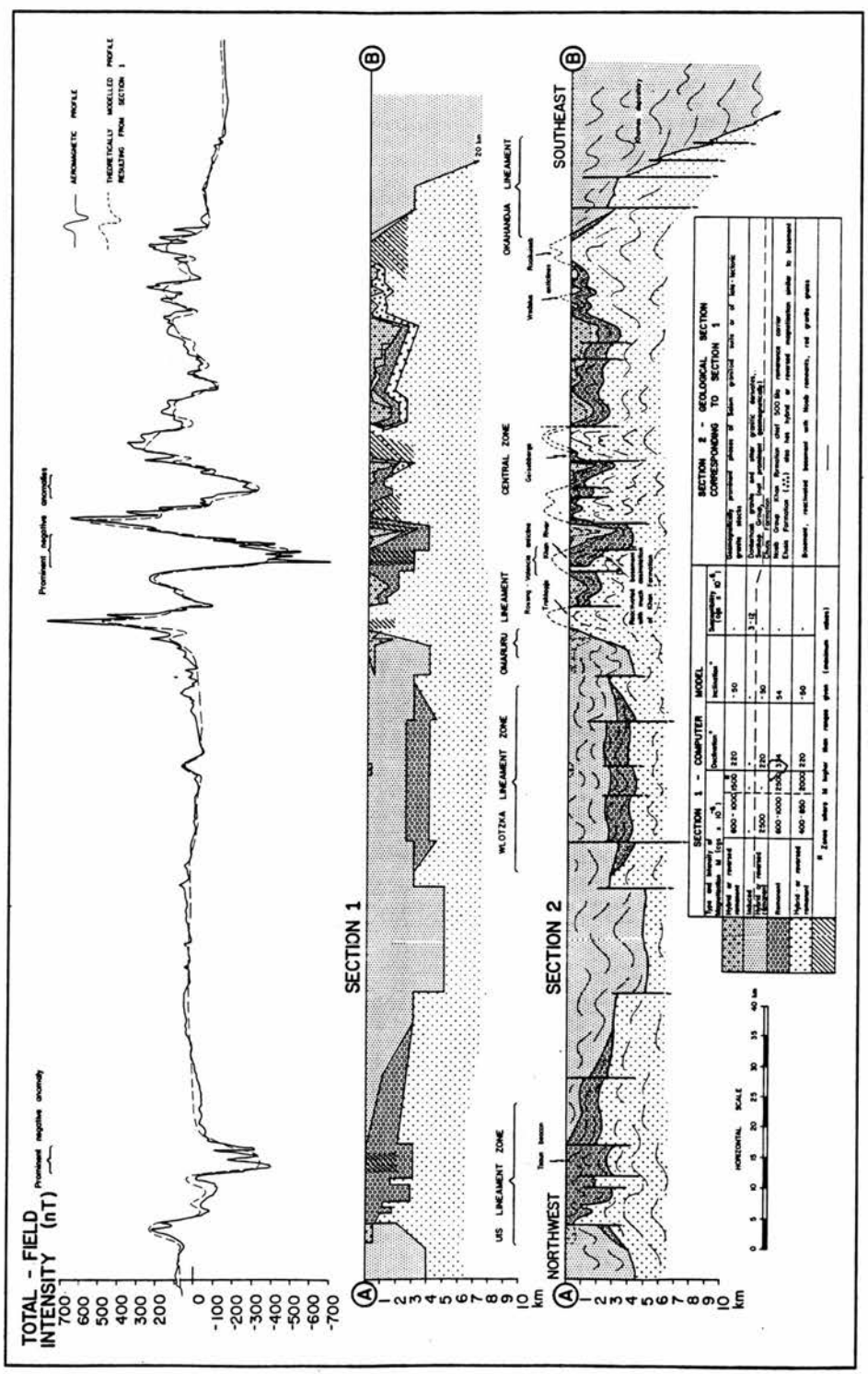

Figure 6.15. Computer cross-section across the Damara Orogen constructed from magnetic profile data (from Corner, 1983).

Plate 6.3. The southeastern boundary of the dark unit running northeast-southwest across this image marks the position of the Okahandja Lineament (refer to text on page 109).
Image sub-scene AK (refer to map on page 75).

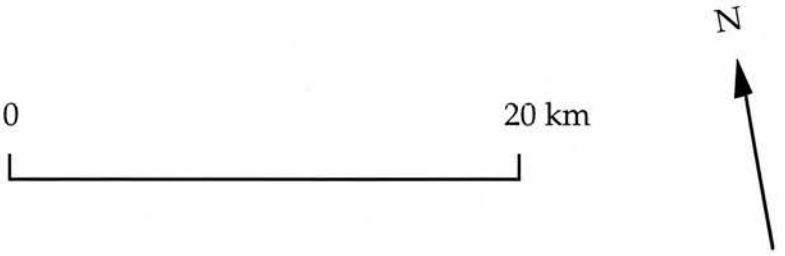

Plate 6.4. The position of the Autseib Fault is shown by the boundary between sandy deposits to the northwest, and rock outcrop to the southeast (refer to text on page 110).
Image sub-scene BE (refer to map on page 75).

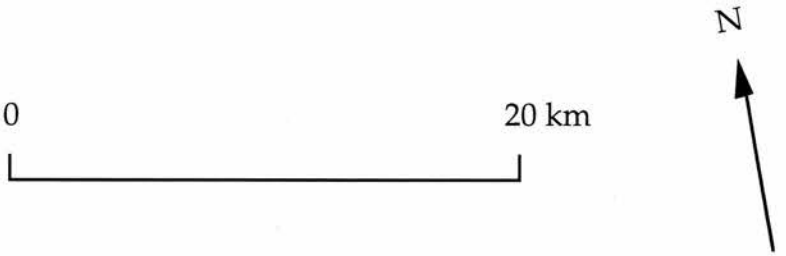

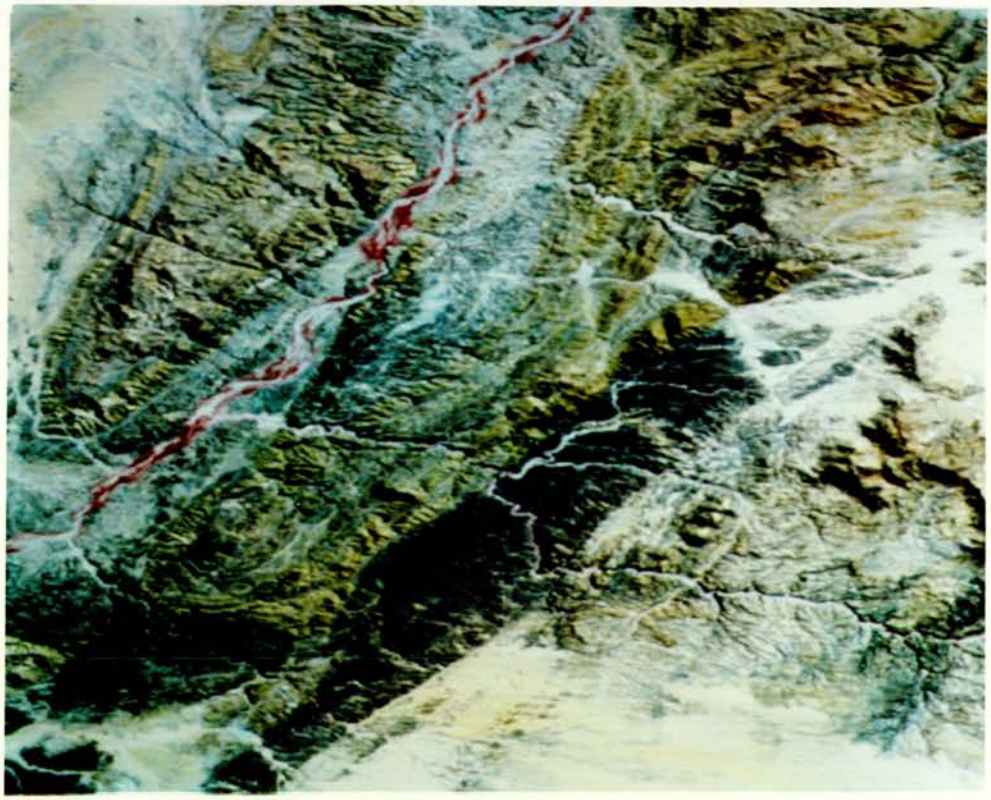

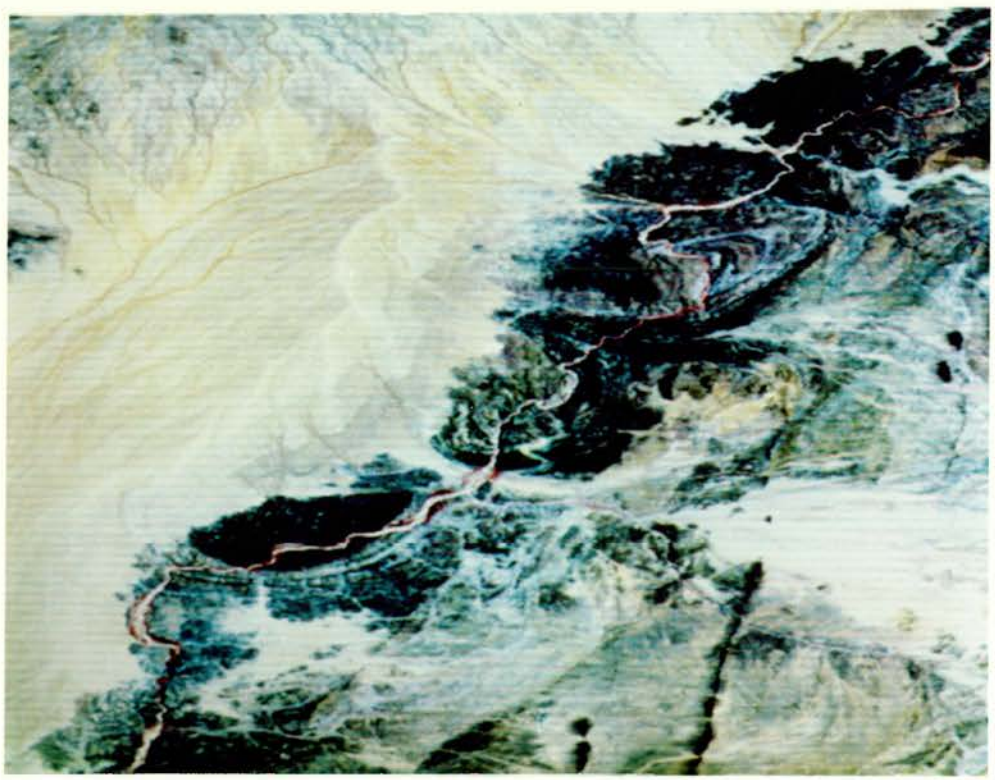

6.2. A Comment on Lineament Density.

Lineament density analysis has been used with variable success by many workers (e.g. Conradsen *et. al.,* 1986, Ananaba and Ajakaiye, 1987, Reddy, 1991) in an attempt to relate known geological phenomena to lineament pattern and distribution. The concept that a higher lineament density might represent a geologically different environment from its surroundings is an acceptable one, but there is a tacit assumption that any lineaments present can be identified with similar ease across the study area. However, rock outcrop may not be similarly exposed across an area, and certain regions may be mantled by vegetation, drift, alluvium, etc.

Map 4 shows the combined lineament data for the study area. Comparison with Map 5 shows that lineament density is largely a function of the exposure of bedrock rather than of any particular geological feature within the rocks. Map 4 also includes many different qualities of lineaments. Many workers do not qualify the nature of the lineaments mapped, yet still try to reconcile different lineament densities to various geological phenomena. Certainly, more heavily fractured rocks might be more open to mineralisation and water storage, but more suitable sites may be present and remain unseen beneath areas of superficial cover. In very arid deserts, radar images (collected in the 8-14 μm region of the electromagnetic spectrum) may give direct information about buried features (Drury, 1993) because they are able to penetrate dry, unconsolidated sediments. The benefits of using radar imagery for geological applications over varied terrain has been demonstrated by Alizai and Ali (1988).

Finally, even where bedrock is uniformly exposed across an area, from work based on studies of the subjectivity involved in lineament mapping by visual

analysis, Parsons and Yearley (1986) state that little value can be placed on lineament density, as any observed density may have as much to do with selective identification from a total population of lineaments as it has to do with geological significance. Because rocks are not uniformly exposed across the study area, and because the total population of lineaments may be subjectively biased, it was decided not to statistically analyse lineament density.

6.3. Water Resources.

Landsat imagery, and the lineament maps compiled from them, have been put to practical use in the field of water resources (Salomonson and Rango, 1980). In many areas, where the existing shallow porous aquifers, regolith and local alluvial deposits have a low water yield, boreholes are sunk into the hard rock in order to tap groundwater stored in fractures (Boeckh, 1992). However, these boreholes often prove unsuccessful. Many lineaments have a water storage potential; the analysis of maps of their distribution could permit more promising locations to be pin-pointed for groundwater abstraction. In addition, Landsat imagery also permits the identification of dry-season active vegetation. This could further delimit areas of possible water resource.

The use of lineament maps for water exploration is particularly suited to areas of crystalline basement rocks. These rocks possess little primary intergranular porosity or permeability and their hydrogeological storage properties are thus mainly determined by secondary effects such as brittle fracturing and weathering (Clark, 1985). The lineaments mapped in the study area from the Landsat imagery have been shown to represent features such as faults, joints and dykes. The fissured rocks associated with these features are more

susceptible to deep weathering and would be a good target for borehole siting (Greenbaum, 1992).

Greenbaum (1992) investigated the location and yields of existing boreholes and their relationship to photolineaments compiled from Landsat MSS imagery of Zimbabwe. It was discovered that the majority of boreholes (more than 90%) were located within 150 metres of a lineament (including dyke lineaments), thus confirming the importance that should be placed on these features in terms of siting boreholes. The work also sought to correlate the yield of productive boreholes to the dominant lineament azimuth frequency. It found that there was a slight positive correlation between the most productive boreholes and the most common lineament azimuth, although successful boreholes could be found associated with lineaments of all orientations.

The negative topographic lineaments mapped in the study area, thought to represent faults and perhaps major joints, are likely to provide open conduits for groundwater. Many of these features are represented at the surface by a drainage line. Evidence for the existence of groundwater in the area is provided by the presence of active, healthy vegetation, even during the summer period, along the dry paths of the Khan and Swakop Rivers, and their associated tributaries. This vegetation is picked out as bright red areas by the Landsat Multispectral Scanner, an instrument which was specifically designed for vegetation studies (see frontispiece). However, Boeckh (1992) notes that the role of dry-season active vegetation as an indicator of groundwater-bearing fractures is not always conclusive. Moisture or groundwater contained in the regolith or local alluvial aquifers independent of major productive fracture zones can also be responsible for stable active vegetation at times.

The data of the negative topographic lineaments, and perhaps of the positive topographic lineaments too, could be usefully incorporated in a reconnaissance exercise for groundwater exploration. Both datasets delimit areas where the mainly crystalline rocks of the Central Zone are likely to be more heavily fractured and therefore have a higher water storage potential. Boreholes sited close to the negative topographic lineaments within the watershed of the Khan and Swakop Rivers are likely to prove most productive. The presence of healthy vegetation, even during the dry season, along the course of these rivers suggests some sort of groundwater recharge; the negative topographic lineaments are likely to be conduits of this groundwater from surrounding rocks. Boreholes sited in close proximity to these lineaments have a greater likelihood of intercepting this groundwater resource.

6.4. Lineament Maps and Mineral Exploration.

As soon as Landsat data became available, Lattman (1973) showed that proven relationships do exist between known mineral deposits in Alaska and certain types and direction of lineaments. A strong correlation between known mineral districts and linear features mapped from Landsat MSS imagery has also been noted in other areas of the United States including Nevada (Rowan, 1975) and Montana, Colorado and New Mexico (Saunders *et. al.,* 1973). In all these areas, a high percentage of the known mining districts occurs within 2-7 km of Landsat linear features (Rowan and Lathram, 1980).

Landsat scenes provide a synoptic coverage of ground areas which might be remote, unmapped and difficult to access. The identification of linear features from Landsat imagery may prove useful in defining target areas for mineral

exploration - local settings in which ore bodies may be concentrated, and which merit more detailed study in the field (Rowan and Lathram, 1980). Just as the fractures within rocks, such as faults and joints, can provide conduits for groundwater, such features can also provide possible routeways for mineralising fluids. Mineralisation may also be associated with the intrusion of dykes. Since lineament maps provide a representation of these features, their integration in a reconnaissance exploration approach is worthwhile, especially where mineralisation is tectonically controlled (Ananaba and Ajakaiye, 1987).

There is much syn- and epigenetic mineralisation in the Central Zone of the Damara Orogen, usually associated with syn- and late-tectonic granitoids and pegmatites (Stevens, 1993). He suggests that mineralisation in the Central Zone is structurally controlled and states that 'major structural breaks or lineaments are believed to have played a role in localising mineralisation in central Namibia'. He adds that in the Central Zone 'D_3 domal structures (in particular the marble horizons) and linear, north-northeast-trending D_4 structures acted as physio-chemical traps for late-tectonic magmas and mineralising fluids such as uraniferous alaskites at Rossing'. The concept of a structural control on alaskite emplacement is also favoured by Berning (1986). He suggests that, at the Rossing Mine, 'the emplacement of the alaskite suggests that granitizing fluids saturated and replaced already migmatised country rock by penetrating shears, fractures, joints, bedding planes, axial planes of folds and foliation planes'.

Much of the mineralisation, such as scheelite and gold skarn mineralisation, is associated with hydrothermal fluids (Steven, 1993). It is likely that pre-existing shear zones, faults, joints and dykes acted as pathways for these hydrothermal fluids. Li- and Be-bearing pegmatite dykes, which form another

important source of mineralisiation in the area, also have a structural control and are believed to have been emplaced along tensional openings (Roering, 1961).

Structural features are considered to be the main controls on the mineral-rich alaskites and pegmatites emplaced in the Central Zone. The combined lineament data shown in Map 4 could be incorporated to delimit possible areas where more detailed exploration might prove more fruitful. Having suggested that lineament density analysis may be flawed, it is interesting to note that the areas of greatest lineament density, where one might argue that the rocks are most fractured, coincide with known occurrences of uraniferous alaskitic granites (see Figure 6.3). Exponents of lineament density analysis would argue that this demonstrates and validates the technique, although it may simply be the case that present-known uraniferous alaskites have only yet been discovered in areas where bedrock is exposed, and where lineament density is coincidentally higher.

6.5. Conclusions.

1--Positive topographic lineaments show a distinct north-northeast trend. The majority of these features are believed to represent dolerite dykes of the Cretaceous Etendeka Volcanics (Erlank, 1985). These date from about 140 - 120 Ma ago (Duncan *et. al.*, 1990) and are closely associated with the Serra Garal dykes of the Parana Flood Basalt Province of South America (Marsh *et. al.*, 1991). They are believed to be associated with the splitting of Gondwana and the opening of the Southern Atlantic Ocean. The regional dyke swarm trends along a recognised aeromagnetic lineament, the Welwitchia Lineament Zone (Corner, 1983), which is thought to represent deep-seated Proterozoic fractures (Steven, 1993). The dykes probably took advantage of this pre-existing crustal weakness and developed a 'proto-rift' along this discontinuity.

2--Negative topographic lineaments show a strong directional trend, orientated northwest-southeast. They can only be picked out in areas of rock outcrop. Some of these features are shown to be faults on geology maps of the area; by inference, other features with a similar topographic expression are considered to be faults also. Where discernible, these faults show a sinistral offset with little apparent vertical displacement. The features are likely to have formed under conditions of brittle deformation, towards the close of the Damara Orogen.

3--Tonal lineaments and fold axes show a similar, dominant trend, orientated northeast-southwest. The tonal lineaments themselves usually represent linear lithological horizons situated along the limbs of the fold axes. The lineaments are orthogonal to the negative topographic lineaments and their

distribution is similar, i.e. they are generally discernible in areas of rock outcrop. They are considered to have formed during the main deformation event of the Damara Orogen (orientated northwest-southeast), although there is controversy as to whether the features were formed under compressional (Smith, 1965) or constrictional (Oliver, 1993) conditions. The trend of the lineaments appears to change slightly along the Central Zone.

4--A number of regional aeromagnetic lineaments, recognised by Corner (1983), are also discernible as photolineaments on the Landsat imagery. These generally follow the same trend as the tonal lineaments (Oklahandja Lineament and Autseib Fault) and the positive topographic lineaments (Welwitchia Lineament Zone). The Omaruru Lineament is not readily distinguishable from the imagery, and a prominent photolineament to the east of the Khan River appears to have little geological significance.

5--Lineament density analysis was considered to be an unsuitable technique for the study area because of the poor exposure of bedrock in those areas mantled by sandy deposits. The technique is also considered questionable, in terms of the subjectivity involved in obtaining the total lineament population (Parsons and Yearley, 1986).

6--The lineaments mapped are likely to indicate areas of fractured rocks which might provide possible conduits for groundwater (Greenbaum, 1992). The lineament data could be used to site boreholes more successfully, in order that any groundwater source could be more successfully intercepted.

7--Mineralisation in the Central Zone of the Damara Orogen is tectonically controlled (Steven, 1993). The lineaments viewed from the Landsat imagery may possibly have acted as routeways for intrusive rocks and hydrothermal fluids. Although lineament density analysis has been questioned, it is interesting to note that the known localities of intrusive, uraniferous alaskites correspond to the areas of highest lineament density on Map 4. The lineament data might prove useful in defining target areas for mineral exploration - local settings in which ore bodies may be concentrated, and which merit more detailed study in the field (Rowan and Lathram, 1980).

Chapter 7

Multispectral Lithological Mapping: Discussion of Results.

Chapter 7. Multispectral Lithological Mapping: Discussion of Results.

7.1. Introduction.

The results of the multispectral lithological mapping are shown on Map 5. Recognisable units established in a test area (outlined on Map 5) have been extrapolated further afield to produce a remotely sensed surface geology map of the Damaran Central Zone. This chapter compares the results of the remotely-sensed map with previously published geology maps of the same area. Two maps have been used as a means of comparison; Smith's (1965) map of The Geology of the Area Around the Khan and Swakop Rivers in South West Africa covers most of the study area, and has been used as the main source of reference. For areas not covered by Smith's map, the 1: 500 000 Geological Map of the Damara Orogen, 1988 (Sheet 2), published by the Geological Survey of Namibia, has been consulted.

Where differences occur between the published geology maps and the remotely-sensed map, the MSS imagery has been re-checked to establish whether or not, on second interpretation, the imagery appears to have been mis-interpreted. New conclusions are mentioned in the text; Map 5 has not been amended and remains the result of the original interpretation.

7.2. Test Area.

Map 5 shows an outline of the test area, which is located in the region around the SJ Dome (see Figure 1.2). This is the area covered by Smith's (1965) map, which is shown in Figure 7.1. The stratigraphy established by Smith is shown

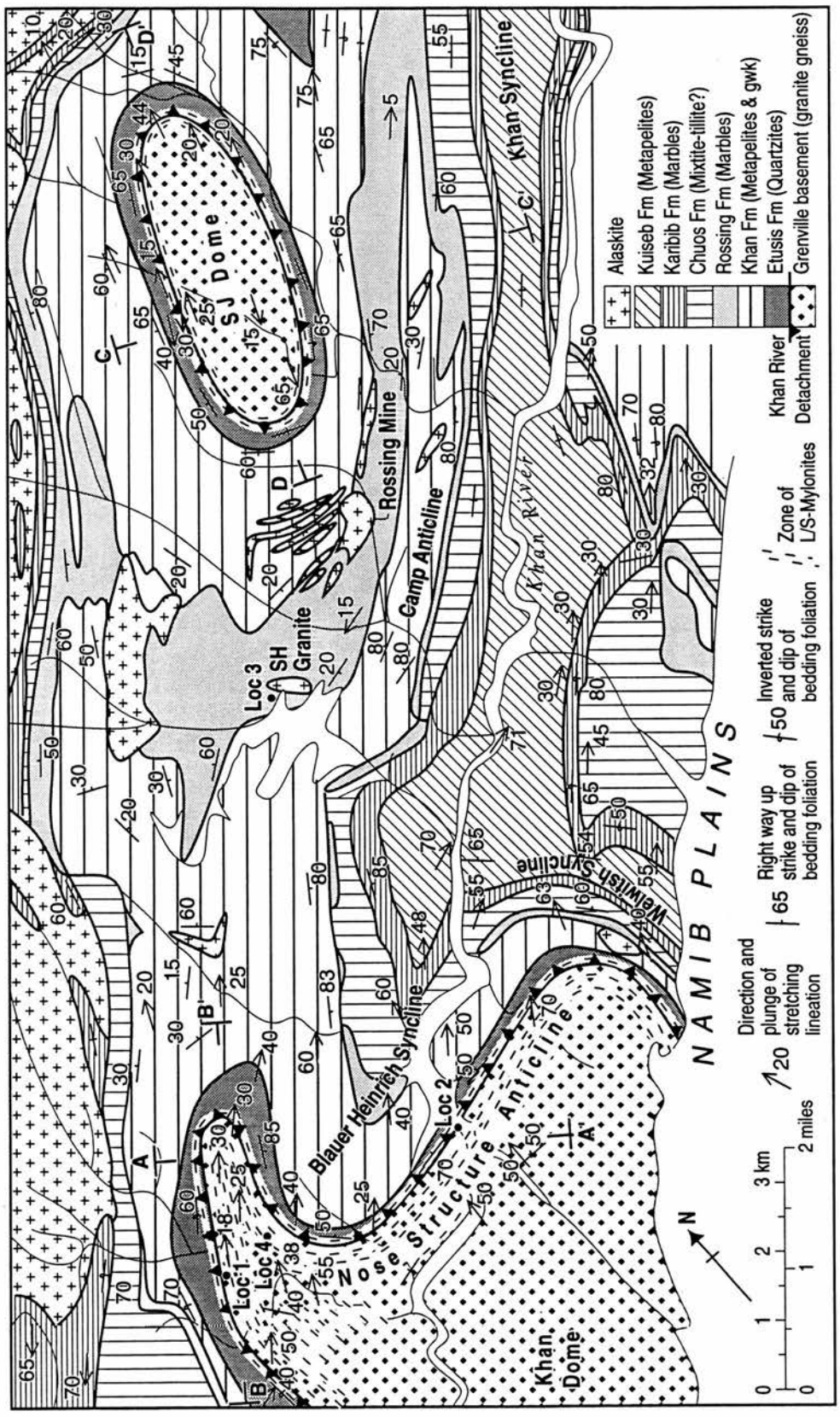

Figure 7.1. Geological map of the test area (after Smith, 1965).

in Figure 7.2. The basement rocks are essentially granitic gneisses, which form flat-topped elongate domes, with steep sides which are separated by keel-shaped periclinal synclinoria of later metasedimentary cover (Oliver, 1993). Smith (1965) mapped the contact between basement and cover rocks as an unconformity, and Oliver (1993) has suggested that this unconformity is in fact a ductile shear zone associated with a regional mid-crustal detachment.

The lowest cover rocks in the metasedimentary stratigraphy are the quartzites of the Etusis Formation. Smith (1965) describes these rocks as felspathic quartzites, generally massively bedded at the base, and becoming thinly bedded towards the top, with narrow, intercalated conglomeratic horizons. Above these, the conformable Khan Formation rocks generally consist of a variable thickness of amphibolite and calc granulite facies, the latter being the most dominant. In the test area, the sediments of the Rossing Formation lie conformably on top of the Khan Formation rocks (Smith, 1965). The former includes white crystalline marble with intercalations of biotite schist, quartzite and local pebble bands; the Formation is generally absent from the east of the study area (Smith, 1965).

The rocks of the Chuos Formation lie conformably above those of the Rossing Formation. The former consists essentially of a glacial conglomerate containing assorted pebbles and boulders in a granulitic or schistose matrix (Smith, 1965). Above the Chuos, the Karibib Formation is also conformable and is widely distributed in the Damara system. It consists of massive blue and white crystalline dolomitic marble, which forms a prominent marker horizon by virtue of its resistance to erosion. It is found throughout the area on limbs of folds and, rarely, in domes and basins. (Smith, 1965). The uppermost unit in

the metasedimentary sequence is the Kuiseb Formation. These rocks, which consist of well-foliated biotite schist alternating with biotite-quartz schist, are widely distributed in synclinoria within the study area (Smith, 1965).

The MSS imagery, corresponding to the test area, was processed, enhanced and analysed in an attempt to establish whether or not the different rock units, established by Smith (1965), were reconcilable, and having established which units were, to then extrapolate those mappable units further afield to cover the Central Zone study area. Plates 7.1 and 7.2 show a false-colour composite and principal component image of the region around the test area (outlined in yellow). The units shown in the test area on Map 5 were established by interactively looking between the display monitor and Smith's map. Basement areas are easily distinguished, showing as fractured green areas on plate 7.1, and as orange/brown areas on the principal component image (plate 7.2). The Etusis Formation (quartzites) above is picked out as a thin milky-white unit. The Khan Formation above is better expressed on the principal component image, as a navy blue unit, and can easily be extrapolated across to Rossing Mountain to the west (see Figure 1.2).

The marbles of the Rossing and Karibib Formations can be distinguished on the imagery only by using Smith's map. In regions outwith the test area, it is impossible to reconcile between the two lithologies from the imagery alone. As such, they have both been mapped simply as the same marble unit. Although the lithologies were differentiated by Smith (1965) in the field, this difference is below the spectral resolution of the Multispectral Scanner, and the two units appear similar on the processed imagery. The Chuos Formation, which separates these two formations, has also been omitted because it is

difficult to differentiate from adjacent lithologies. Effectively, the Rossing, Chuos and Karibib Formations have been mapped as a single unit. Although this is a poor reflection of the limited spectral resolution associated with Landsat MSS imagery, because the three formations are **relatively** minor in terms of outcrop, and because they are adjacent in the statigraphic column, the problem is relatively limited. The Kuiseb Formation, above, is easily differentiated as the dark unit on plate 7.1; this is the uppermost unit in Smith's (1965) map of the test area. The ideal stratigraphy versus the mapped stratigraphy is shown in Figure 7.2.

The mapped stratigraphy (Figure 7.2) shows three other lithological units which appear distinct on the imagery, but which cannot be correlated with known lithologies from the study area. These rocks are discussed in the appropriate locality sections.

Figure 7.2. The stratigraphy of the test area versus the stratigraphy of Map 5.

Test area stratigraphy:	**Map 5 stratigraphy:**
	Alluvium/Eluvium.
	Erongo Granites.
Granites (Alaskites):	Syn-/post-tectonic granites.
	Tsabachias Amphibolite Fm.
	Tinkas Formation (Calc silicate).
Kuiseb Formation (Metapelites):	Kuiseb Formation.
Karibib Formation (Marbles):	
Chuos Fomation (Mixtite-tillite):	Karibib/Chuos/Rossing Formations.
Rossing Formation (Marbles):	
Khan Formation (Metapelites and gwk):	Khan Formation.
Etusis Formation (Quartzites):	Etusis Formation.
Grenville basement (Granite gneiss):	Grenville basement.

Plate 7.1. False-colour composite image of the test area (refer to text on page 125).
Image sub-scene AA (refer to map on page 75).

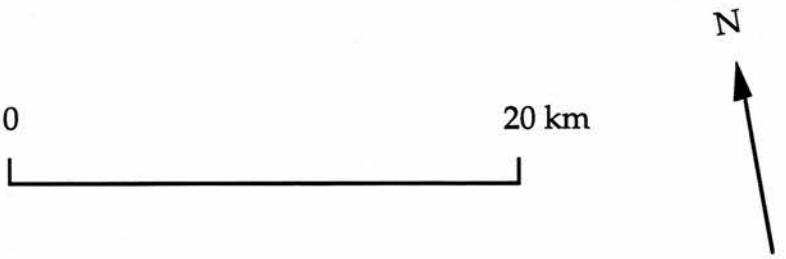

Plate 7.2. Principal component image of the test area (refer to text on page 125).
Image sub-scene AA (refer to map on page 75).

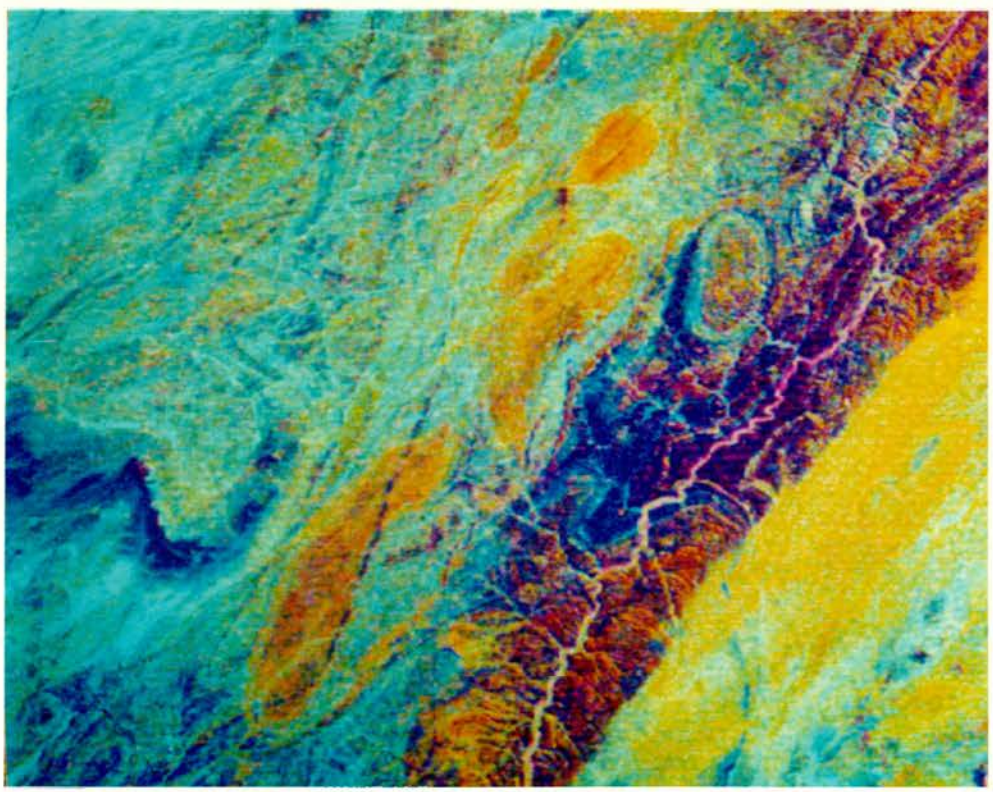

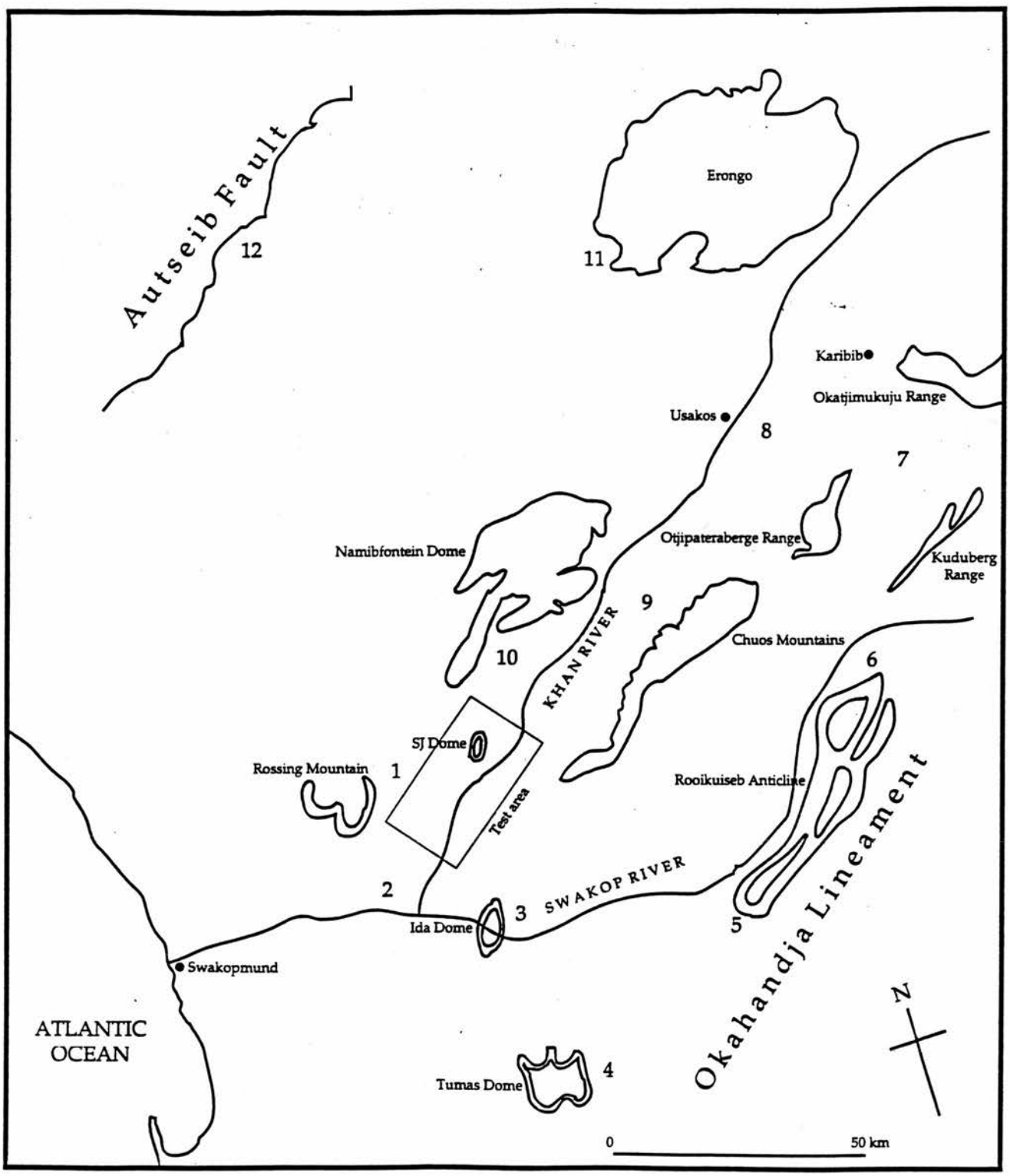

Figure 1.2. Map of the study area.

7.3. Comparison with Published Maps.

7.3.1. Locality 1.

Locality 1 is indicated on Map 5, and covers the area to the west of, and including, the test area. It is the same area that is shown in plates 7.1 and 7.2. Locality 1 on Map 5 relates very well to Smith's (1965) map, which is not particularly surprising since similar spectral and spatial image characteristics can be easily extrapolated from the nearby test area. The outcrop of basement domes is successfully delimited from the Landsat imagery, and nearly all the domes can be seen to be surrounded by marble horizons. Smith links up these marble outcrops between the domes, but this is not readily apparent from the imagery, because recent deposits tend to mantle the surface in the inter-lying synclines.

In the test area, the marbles outcrop between the Khan and Kuiseb Formations, and one would initially expect to find the Etusis quartzites next to basement rocks. However, the contact between the basement and the cover rocks is thought to be tectonic (Oliver, 1993), although it is not possible to ascertain the nature of the unconformity from the Landsat imagery. Oliver (1993) suggests that various units have been tectonically thinned-out so that, in some places, the marbles are in contact with the basement.

On Smith's (1965) map, the Rossing Mountain is a W-shaped outcrop of Khan Formation rocks. The interpretation of the imagery suggests a closure to the north, to form an 'inverted comma-shaped' dome, whose long axis trends in the same direction as neighbouring basement domes to the east.

7.3.2. Locality 2.

This locality covers the area surrounding the confluence between the Khan and Swakop Rivers, and is shown in plate 7.3. The contact between basement rocks and the Khan Formation, downstream of the confluence, coincides with Smith's map, and is again interpreted to be an unconformity between basement and cover rocks. Basement rocks appear to outcrop upstream of the confluence along the Swakop River, until the western flank of the Ida Dome (see Figure 1.2) is reached at locality 3. Here, Etusis quartzites are once again situated adjacent to basement rocks, and these quartzites appear to be overlain by rocks of the Khan Formation.

7.3.3. Locality 3.

The area covered by this locality, shown in plate 7.4, is not covered by Smith's (1965) map, but is covered by the 1: 500 000 regional map. Areas of basement rocks appear orange/brown on the principal component imagery and can be quite easily delineated. These orange areas, shown as basement on Map 5, coincide with the basement rocks shown on the 1: 500 000 map. Plate 7.3 includes the southeast portion of the test area, so one can be reasonably confident that the units mapped in locality 3 are fairly accurate. The Etusis quartzites surround the westernmost dome, the Ida dome, but the easternmost dome appears to be in contact with rocks of the Khan Formation. Once again, an unconformable contact between basement and cover rocks appears to be indicated.

Plate 7.3. The confluence between the Khan and Swakop Rivers (refer to text on page 129).
Image sub-scene AC (refer to map on page 75).

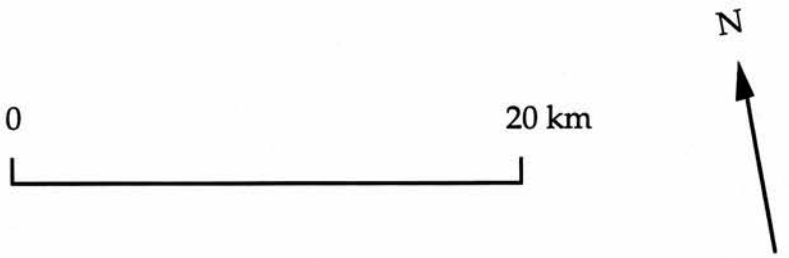

Plate 7.4. The area surrounding the Ida Dome (refer to text on page 129).
Image sub-scene AG (refer to map on page 75).

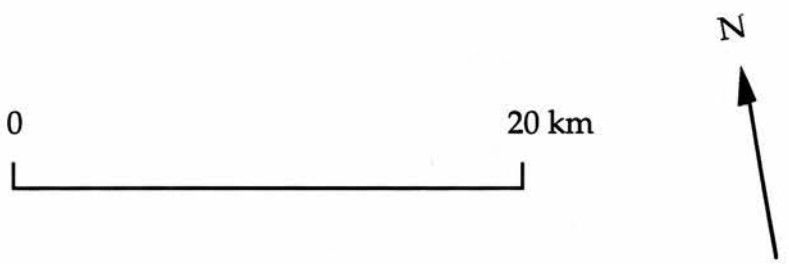

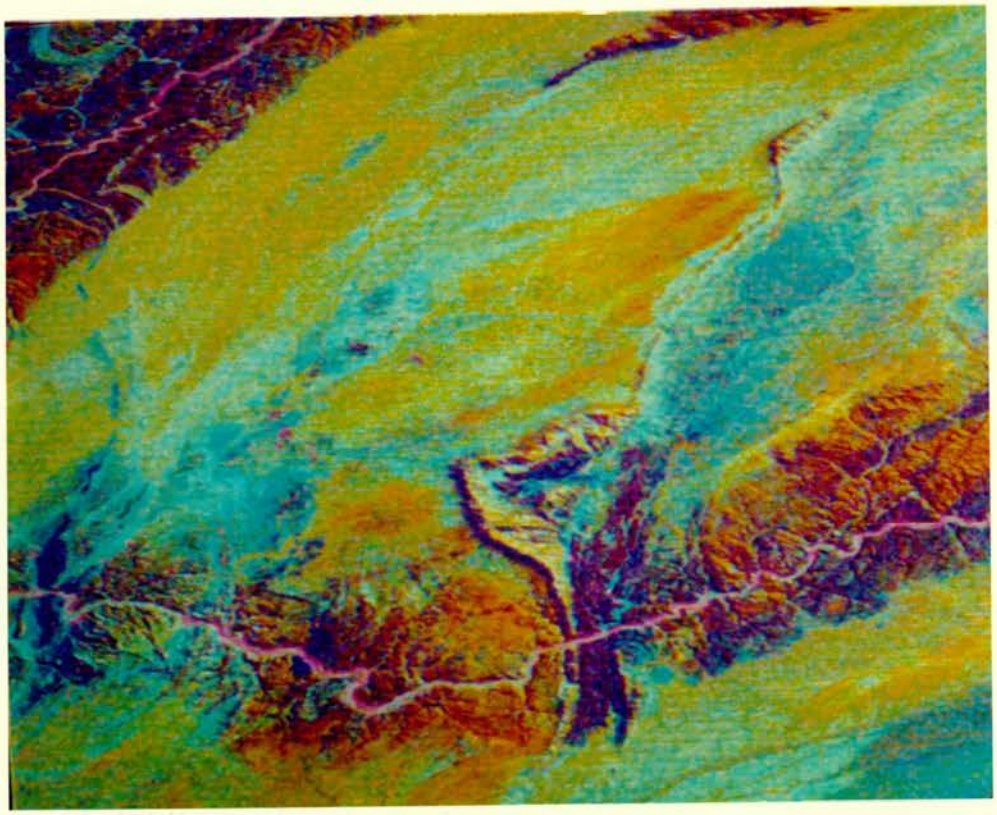

7.3.4. Locality 4.

Locality 4 covers the area surrounding the Tumas Dome (see Figure 1.2) and is shown in plate 7.5. This area is not covered by Smith's (1965) map, so comparison has been made with the 1: 500 000 regional map. The bright marble bands of the Karibib Formation, which surround the Tumas Dome, are easily picked out from the imagery, and are correspondingly shown on the 1: 500 000 regional map. Green rocks, on the false-colour composite imagery, within the core of the dome are taken to represent basement rocks, and Map 5 shows that similar rocks have been identified to the northeast and to the west of the Tumas dome.

To the east of the Tumas Dome, plate 7.5 shows a very dark rock outcrop, which cannot be correlated with any of the rocks within the test area. This is therefore taken to be a new lithology, and has been identified from the 1: 500 000 map as the Tinkas Calc-silicate Formation. Inspection of the imagery shows that this lithology is restricted to the western flank of the Okahandja Lineament, and the dark unit can be easily identified along this feature on the frontispiece. Enclosed within this unit, is an oval area mantled by sandy deposits. This low-relief area is shown on the regional map as a post-tectonic granite, one of a number of such intrusions, of various ages, which outcrop within the Central Zone of the Damara Orogen. It is difficult to distinguish these granites in spectral terms, but because they tend to form characteristically light-coloured areas of low relief, often covered by recent deposits, they can be effectively delineated from a spatial point of view, using the information of texture and tone contained within the image.

Plate 7.5. The area surrounding the Tumas Dome (refer to text on page 130).
Image sub-scene AJ (refer to map on page 75).

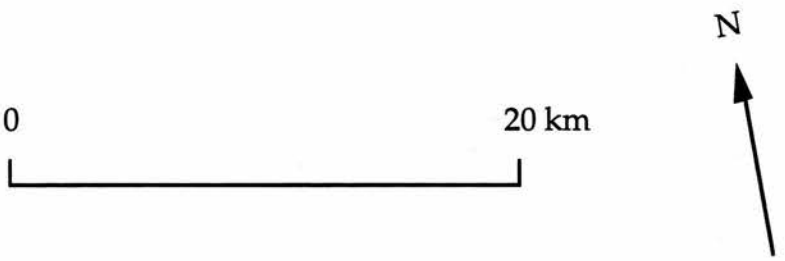

Plate 7.6. The southern portion of the Rooikuiseb Anticline (refer to text on page 131).
Image sub-scene AK (refer to map on page 75).

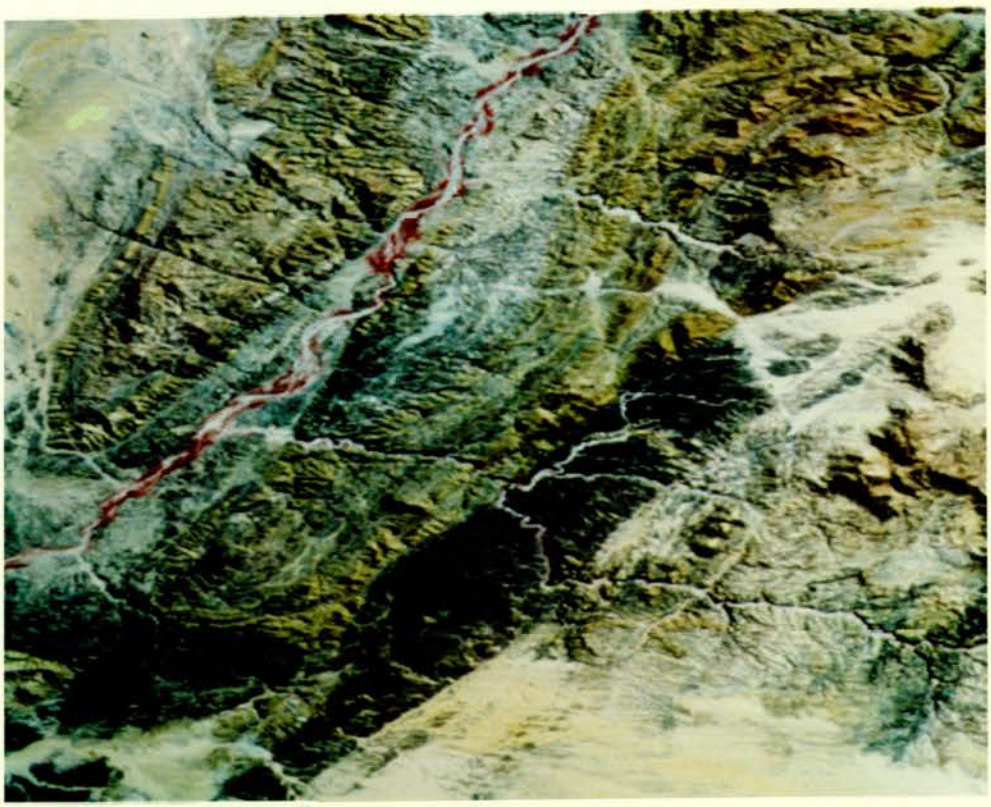

7.3.5. Locality 5.

This locality is situated at the southern end of the Rooikuiseb Anticline (see Figure 1.2) and is not covered by Smith's (1965) map. The area is shown in plate 7.6. From the false-colour composite imagery, it appears that elongate 'green' basement domes outcrop once again in this area, with fold axes which are aligned parallel to the main trend of other basement domes in the Central Zone. The outcrop of basement rocks on Map 5 corresponds to the information on the 1: 500 000 regional geology map. The path of the Swakop River appears from the imagery to be structurally controlled in this area, and its course is restricted to a synclinorium. This synclinorium has been mapped from the imagery as rocks of the Khan Formation, but the regional map indicates that this area is underlain by post-tectonic granites similar to those described at locality 5. However, the imagery shows that the supposedly similar rocks from the two areas are spectrally dissimilar, so identical lithologies seem unlikely, although they may both be granites, but with a different mineralogy. The dark Tinkas Formation can be seen outcropping towards the northeast across the middle of plate 7.6, marking the boundary between the Central Zone and the Okahandja Lineament Zone.

7.3.6. Locality 6.

This locality covers the northern end of the Rooikuiseb Anticline, shown in plate 7.7, and can be compared with Smith's (1965) map of the Central Zone. Map 5 shows that the basement rocks mapped at locality 5, at the southern end of the anticline, have been extended further northwards. In the false-colour

Plate 7.7. The northern portion of the Rooikuiseb Anticline (refer to text on page 131).
Image sub-scene AL (refer to map on page 75).

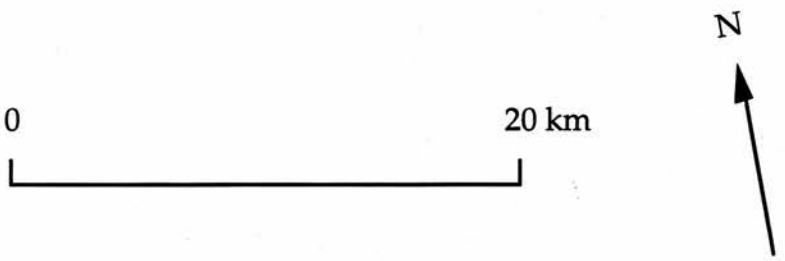

Plate 7.8. The Kuduberg, Otjipateraberge and Okatimukuju Ranges (refer to text on page 132).
Image sub-scene AP (refer to map on page 75).

composite image (plate 7.7) these basement rocks appear as distinct green outcrops, either side of the Swakop River, whose course follows the intermediate synclinorium.

The basement domes identified on Map 5 do not correspond to the units mapped by Smith (1965). He maps the Rooikuiseb Anticline as being cored by Etusis quartzites, surrounded by extensive marble outcrops of the Karibib Formation. Although the lithologies of the Rooikuiseb Anticline have been mapped differently, the shape of outcrops is remarkably identical. It is possible that Smith did not visit this particular locality, but rather interpreted the lithologies using air-photographs (Oliver, *pers. comm.*, 1994). This would explain the identical shapes of the outcrops mapped by Smith and those identified using the Landsat imagery. It would also explain why Smith (1965) has also mapped the rocks of this area incorrectly, for indeed the identification of basement domes from the Landsat imagery is correct (Oliver, *pers. comm.*, 1994). The 1: 500 000 regional map also concurs with the results of Map 5, rather than those of Smith, showing the Rooikuiseb Anticline to be cored by basement rocks.

7.3.7. Locality 7.

This locality covers the area between the prominent Otjipateraberge Range to the southwest, the Kuduberg Range to the southeast, and the Okatjimukuju Range to the north (see Figure 1.2). This area is also shown in plate 7.8. The lithologies mapped from the imagery, shown on Map 5, broadly correspond to Smith's (1965) mapping results. Map 5 shows an area of multiple granitic

intrusions occupying an area of low ground, shown in the southern portion of plate 7.8. The rocks cannot be correlated with any from the test area, but the curved contacts with surrounding host rocks can quite easily be picked out from the imagery.

Map 5 shows that these intrusions are flanked on either side, and to the north, by quartzites. However, Oliver (*pers. comm.*, 1994) states that basement granitic gneisses outcrop within the Kuduberg Range, in the southeastern portion of plate 7.8, and also within the rocks at Okatjimukuju. On re-interpretation of the imagery, this appears possible, and green rocks, characteristic of basement on the false-colour composites, can be seen in these areas. The fact that basement rocks have not originally been picked out from the imagery may have some relevance to the actual size of these outcrops, which only occupy a relatively small area. Furthermore, as one gets further from the test area, it is not surprising that mistakes begin to occur because points of reference become more distant.

7.3.8. Locality 8.

This locality features a prominent elongate synclinal structure situated to the southeast of Usakos (see Figure 1.2). The area is shown in the false-colour composite of plate 7.9. Map 5 broadly corresponds to Smith's (1965) interpretation, but there are some differences. The bright marble bands which flank the feature are well expressed on the imagery, and can be successfully delineated and matched to those mapped by Smith. These marble units pinch tightly inwards at either end of the feature to enclose the core rocks. Plate 7.9

Plate 7.9. The area to the east of Usakos (refer to text on page 133).
Image sub-scene AT (refer to map on page 75).

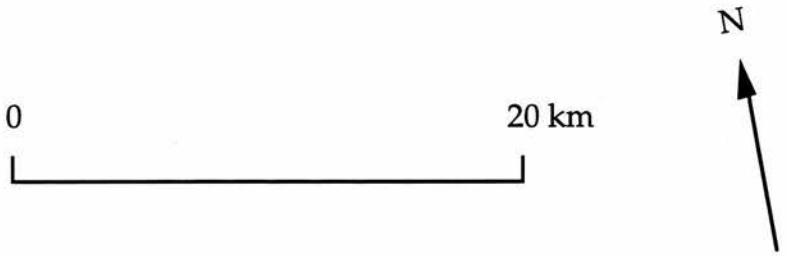

Plate 7.10. The area to the northwest of the Chuos Mountains (refer to text on page 134).
Image sub-scene BC (refer to map on page 75).

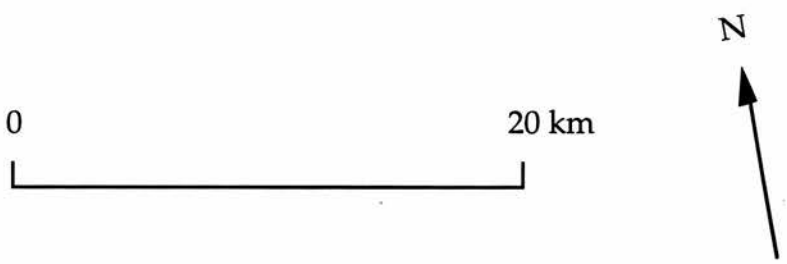

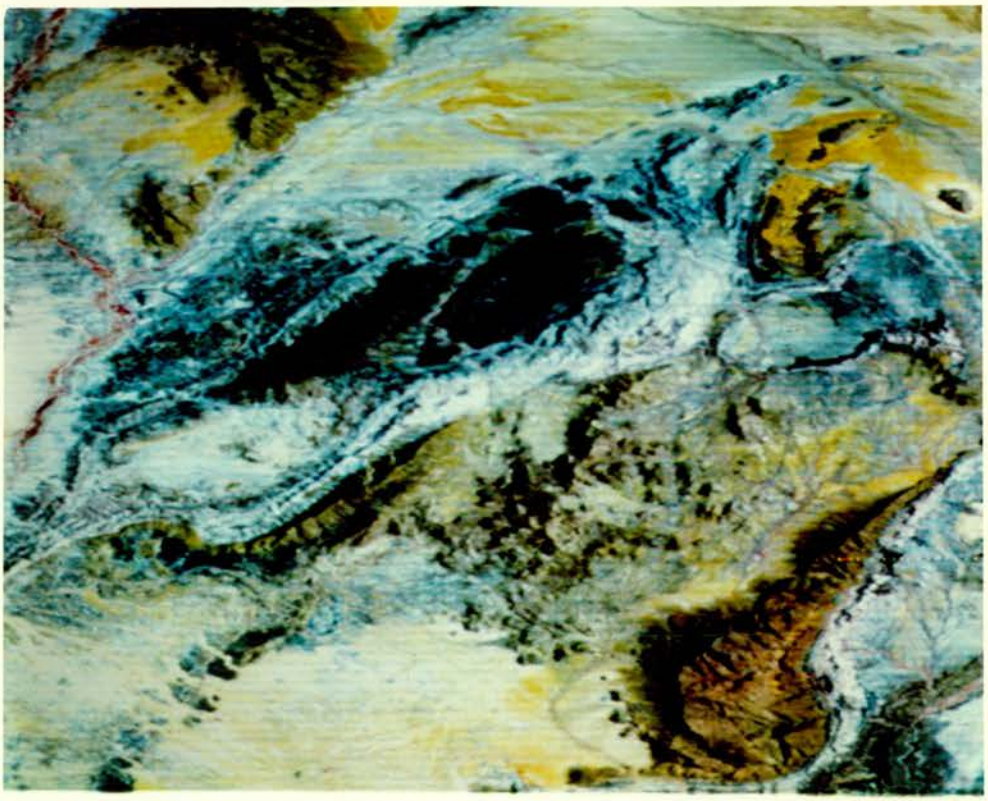

seems to indicate two separate cores, of differing lithologies. The southwesternmost core is expressed as a light-coloured area of low ground, whereas the northeasternmost core appears very different, and forms a very dark area of prominent relief. The former appears physically similar to the other intrusive granites that have been recognised and mapped in the area, and this concurs with Smith's (1965) map. The northeasternmost, keel-shaped outcrop does not appear similar to any of the previously encountered rocks, and reference has been made to the 1: 500 000 regional map, which shows that this rock is, in fact, an amphibolite schist - the Tsabichas Amphibolite Formation.

7.3.9. Locality 9.

This locality covers the area between the Chuos Mountains to the southeast (see Figure 1.2) and, to the west, the eastern flank of the Namibfontein Dome. This area is shown in the false-colour composite of plate 7.10. Much of the area has been mapped from the Landsat imagery as Etusis Formation quartzites, and this concurs with Smith's map. The bright marble bands (of the Karibib Formation) can be easily distinguished from the imagery, running along the linear southeastern flank of the Chuos Mountains, and marbles can also be seen on the western side of the outcrop of Etusis quartzites.

In the eastern part of the locality, a dark, arcuate rock outcrop can be picked out. A similar-looking lithology was noted within the major syncline at locality 9, the western portion of which can be made out in the top-right portion of plate 7.10. There, the rock was ascertained to be an amphibolite

schist. Its close proximity, and similar spectral appearance suggest that the outcrop in this area is of a similar lithology, and indeed Smith's (1965) map marks this area as amphibolite rocks. Low, featureless ground either side of the amphibolite may possibly be underlain by granites, an interpretation which agrees with Smith's map.

In concordance with Smith's (1965) map, further granites are shown on Map 5, to the north of the Khan River, intruded into rocks which appear to be of the Kuiseb Formation. The large, featureless sandy plain to the north has also been mapped as being underlain by granites; Smith's map shows the same area as alluvium, but notes that granites might indeed underlie this area.

Moving eastwards from the core of the Namibfontein Dome, one passes from an anticlinal area of basement rocks, through visible marbles into a synclinal area of rocks of the Kuiseb Formation. The imagery reveals that the syncline appears to control the course of the Khan River. However, the stratigraphy on the other side of this syncline differs, and although marbles are once again present, anticlinal Etusis quartzites outcrop opposite the Namibfontein Dome basement rocks.

The two domes seen either side of the river are clearly identified as being of different lithologies from plate 7.10. Map 5 also shows that an outcrop of Khan Formation rocks apparently ends when it reaches the eastern Etusis dome. These outcrops, once again, reflect the unconformable relationship between basement and cover rocks, and Oliver (1993) suggests is due to tectonic thinning along weaker horizons.

7.3.10. Locality 10.

This area is situated between the Namibfontein Dome to the northeast, and the SJ dome to the southwest (see Figure 1.2). The area is shown in the false-colour composite, plate 7.11. The most important feature of distinction between Smith's (1965) map and Map 5 is the apparent extent of the Namibfontein Dome as revealed by analysis of the Landsat imagery. The basement rocks are revealed as green areas on plate 7.11, and light-coloured marble horizons can be seen surrounding most of these. Smith (1965) maps the majority of the bright marble bands exposed to the west of the Namibfontein Dome, but does not map the underlying rocks which are present within these marble bands, prefering to mark these areas as alluvial and eluvial deposits.

Smith's (1965) map joins the marble bands which run along the northern borders of the Namibfontein Dome, but by tracing the marble units using the Landsat data, one can clearly see that the bands do not join with one another, and the basement rocks of the Namibfontein Dome are linked to an even larger expanse of basement rocks to the north. To the west of the Namibfontein Dome, there is a very large, elongate basement dome, which is an annexe of the same basement exposure. This is surrounded by bright marble horizons and can be seen to trend northeast - southwest along the same trend as adjacent basement domes. Smith marks this area as having poor exposure, but the strong spectral signature of basement outcrop on the Landsat imagery allows this previously unmapped basement exposure to be delineated.

Plate 7.11. The area between the SJ and the Namibfontein Domes (refer to text on page 136).
Image sub-scene AW (refer to map on page 75).

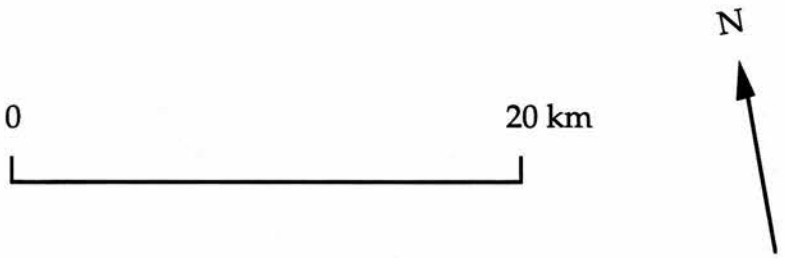

Plate 7.12. The area to the southwest of Erongo (refer to text on page 137).
Image sub-scene BB (refer to map on page 75).

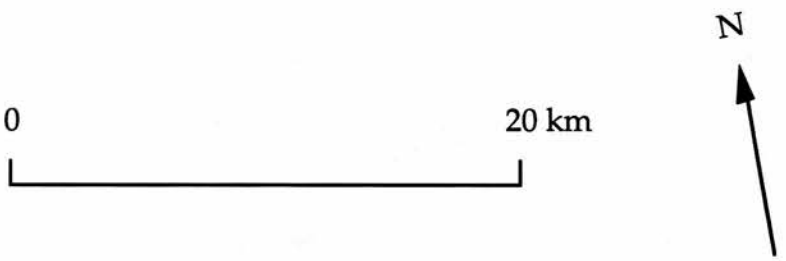

In the central part of plate 7.11, either side of the Khan River, another elongate exposure has been mapped. Map 5 shows that these rocks are considered to belong to the Khan Formation, a result which actually corresponds to Smith's (1965) map interpretation. However, Oliver (*pers. comm.*, 1994) has stated that basement rocks outcrop within this area. The false-colour imagery shows these rocks to be a slightly darker green colour than adjacent basement rocks, but slightly lighter-green areas do appear present at the northeastern end of this structure. On a second interpretation, it does seem likely that basement rocks are indeed present in this area. Although the Landsat imagery has successfully delimited new and extensive areas of basement rocks to the northwest of this area, rocks which are not revealed on Smith's (1965) map, at the same time the interpretation has failed to recognise nearby proven exposures.

7.3.11. Locality 11.

This locality is situated on the southwestern flank of the Karoo Erongo Complex, in the area shown in the false-colour composite, plate 7.12. The Erongo Complex is a post-tectonic (late-Jurassic) intrusive granitic complex which forms a large circular area of pronounced relief. On black-and-white imagery Erongo can easily be picked out from the surrounding rocks, in terms of tone and texture patterns alone. On the false-colour composite imagery, the rocks appear dark green, and they do not appear to be spectrally similar to any of those lithologies recognised within the test area.

To the southwest of Erongo, several light-coloured, oval outcrops can be clearly delineated. Elsewhere, such areas have been found to be underlain by

syn- and post-tectonic granites; these have been accordingly mapped as the same. These elongate igneous bodies seem to follow the trend of the orogen, and may have intruded pre-existing structures formed during the main Damaran deformation. Although this area is outwith that covered by Smith's (1965) map, the 1: 500 000 regional map shows that these bodies are indeed intrusive igneous bodies, and are in fact post-tectonic leucogranites. In the southeastern corner of plate 7.12, Etusis quartzites appear to outcrop. Map 5 shows that they appear to form an anticline which plunges to the northeast. Map 5 also shows that this same unit reappears further to the northeast, to form an anticline which plunges in the opposite direction.

7.3.12. Locality 12.

This locality is situated to the west of the Erongo Complex, where rocks are exposed to the southeast of a pronounced photo-lineament. This is thought to represent the Autseib Fault, considered to be a thrust or low-angle reverse fault (Steven, 1993). A typical exposure is shown in plate 7.13. Thin, bright marble bands can be seen to surround dome structures similar to those which are characteristic of the Southern Central Zone.

These domes appear to be cored by different lithologies, mapped generally as basement granitic gneisses, but also as Kuiseb Formation rocks in one instance. This corresponds to the very dark semi-circular outcrop shown just to the southwest of the centre of plate 7.13. To the northeast, the more typical 'greenish' basement rocks appear to outcrop. This locality is at considerable distance from the test area, but the dome structures can be readily

distinguished. Because there are no nearby known outcrops with which to compare and correlate spectral response, the results for this particular area require field checking. Nevertheless, from the structures seen in the rock outcrops of the Autseib Fault area, it appears that the rocks in this locality have been subjected to similar deformation history as the rocks of the Southern Central Zone.

Plate 7.13. The Autseib Fault (refer to text on page 138).
Image sub-scene BZ (refer to map on page 75).

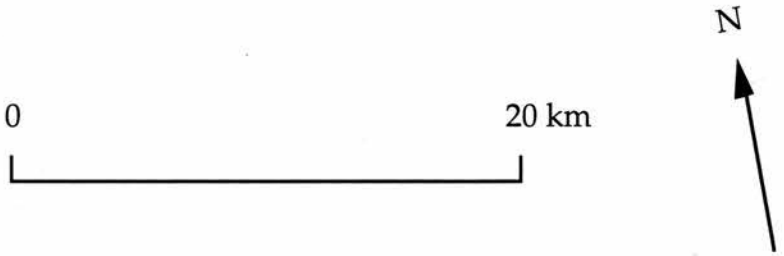

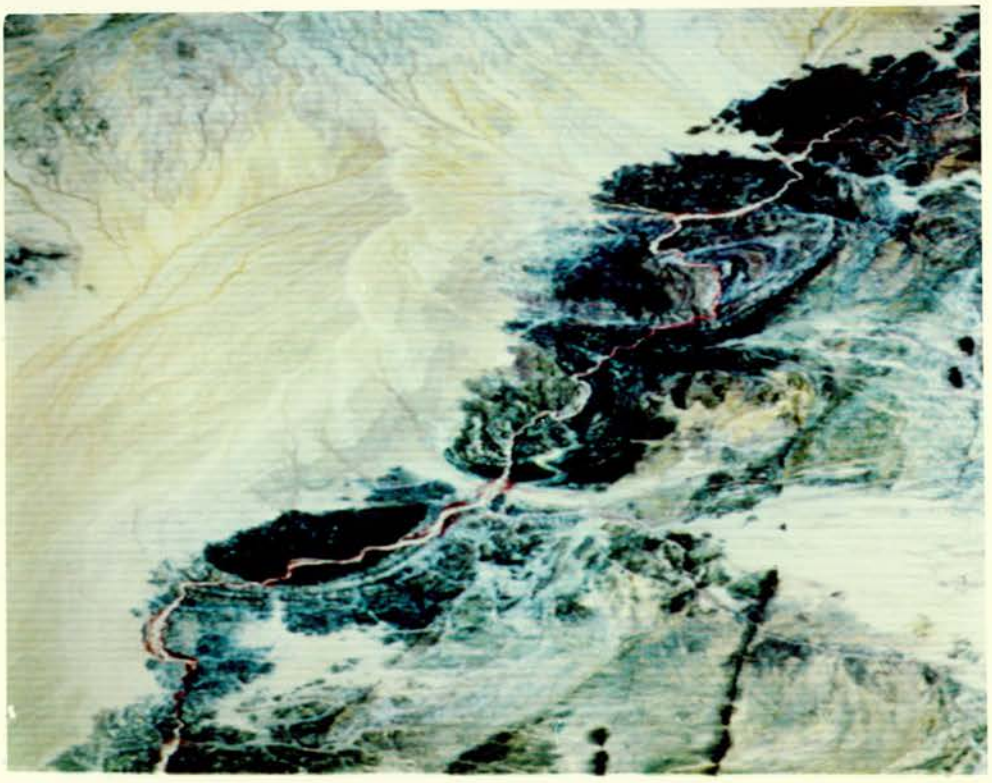

7.4. The effectiveness of reconnaissance mapping using Landsat MSS imagery.

The results of the lithologies mapped from the Landsat imagery have been checked against previously published maps of the same area, and have generally been found to be in accordance with those results. Errors have occurred in places, noted in the previous sections, but mistakes have also been shown to occur in Smith's (1965) map, which was supposedly compiled from field data.

Many advantages are gained by using Landsat data. The imagery provides an extremely useful synoptic view of the Central Zone of the Damara Orogen which reveals the spatial relationship between different lithologies across a wide area. Air-photographs can only provide this facility at a local scale, whereas a single Landsat scene, taken from 913 km above, shows an area equivalent to ~35,000 km^2. Regional geological features can be seen immediately from the Landsat scenes, but similar patterns might only emerge after months or years of mapping in the field. In areas such as the Central Zone, which are remote, and prove difficult to access, the technique is even more valuable, enabling distant locations to be viewed from afar.

The spectral resolution of Landsat MSS imagery is poor by comparison to its Thematic Mapper stablemate. The Multispectral Scanner was originally designed for vegetation studies, but the geological benefits revealed by the early MSS images had great bearing on the introduction of more relevant spectral bands on the TM instrument (Goetz *et. al.*, 1983). The Central Zone of the Damara Orogen, however, has actually proved to be quite well suited to analysis by MSS imagery because most of the rocks exposed in the area are

diverse enough so that they appear spectrally distinct on digitally processed images. A limitation has been revealed by the inability of the data to distinguish between the marbles of the Karibib and Rossing Formations, and to recognise the inter-layered rocks of the Chuos Formation. Nevertheless, the marbles appear very distinct, and their outcrop is associated with the margins of the anticlinal dome features.

The Landsat MSS imagery has proved particularly successful in delimiting the extent of basement domes in the Central Zone, not least because of the very distinct spectral signature that these granitic gneiss rocks show on false-colour composite and principal component images. Areas supposedly mapped by Smith (1965), to the west of the Namibfontein Dome, have successfully been shown to be underlain by basement rocks, but Smith has mapped the same area simply as alluvium. At the Rooikuiseb Anticline, to the southeast, further proven areas of basement rocks have been mapped from the imagery, but Smith, who again supposedly visited this area, mapped the same rocks incorrectly as Etusis quartzites.

Excellent exposure in the area has helped the remote sensing procedure, and most of the exposed bedrock has been identified using the Landsat imagery. Although many of the areas on Map 5 are shown as alluvium/eluvium, there is no greater a percentage area unmapped on Map 5 than on Smith's (1965) map, and if anything, there is slightly more recognised geology on Map 5 for the actual area covered by Smith. In terms of surface geology, the Landsat interpretation has proved to be no less effective than Smith's own efforts on the ground.

It is important to remember though, that without the knowledge of rock types from the test area, the Landsat interpretation would prove far less effective. Although the same lithological units could probably be mapped, without knowledge of the lithology and the stratigraphy of those units, this would prove rather pointless. Nevertheless, while the exercise shows that field interpretation is necessary for lithological mapping using Landsat imagery, it does show that the results from a typical, small locality can be extracted further afield to cover a very wide area. For tracing the contacts between different lithological units, the Landsat imagery proves particularly useful, and it is far quicker to use the imagery than to trace contacts on the ground using conventional field techniques.

Figure 7.3 demonstrates the relative costs and efficiencies of various exploration techniques available. Satellite remote sensing is shown to be far more efficient and cheaper than conventional field mapping techniques (although not necessarily as accurate). A geologist versed in image processing techniques could process, interpret and prepare a map from Landsat imagery for an area similar to this study in a matter of weeks. A similar regional geology map might take months to compile using data collected in the field. With minimal *a priori* knowledge of the Central Zone of the Damara Orogen, a useful, low-cost and fairly accurate regional surface geology map of the area, has been produced, using relatively simple techniques and without ever having visited the area.

Figure 7.3. Approximate costs and average efficiencies of some exploration methods (1988 data). [From Drury, 1993].

Methods	Cost (£ km^{-2})	Efficiency (km^{-1} day^{-1})
Preliminaries		
Satellite remote sensing:	0.01	$>10^6$
interpretation and map:	**0.4**	**10^4**
Airborne remote sensing:	6.3	500
interpretation and map:	3.2	50
Airborne geophysics (magnetic and EM):	16	500
interpretation and map:	6.3	25
Literature search:	158 day^{-1}	--
Field studies		
Geological reconnaissance:	101	10
Detailed geological mapping:	379	1
Geochemical surveying:	9	50
drainage survey:	32	25
soil or biogeochemical survey:	474	2
Geophysical surveying (resistivity)	101 km^{-1}	10
Diamond drill cores:	25 m^{-1}	--
Shaft sinking:	3164 m^{-1}	--

7.5. Conclusions.

1--Although the Landsat Multispectral Scanner was originally designed for vegetation studies, the imagery that covers the Central Zone of the Damara Orogen has actually proved to be well-suited to geological interpretation. This is largely a result of the wide variety of lithologies which outcrop in this region, which appear spectrally distinct from one another on digitally processed MSS imagery.

2--The limited spectral resolution has been highlighted by the inability, from the data, to confidently distinguish between the rocks of the Rossing, Chuos and Karibib Formations. These have been mapped as a single marble unit, which appears to be associated with a break in stratigraphy between anticlinal units, usually of basement rocks, and synclinal cover rocks. This tectonic break is thought to represent a regional, mid-crustal detachment (Oliver, 1993).

3--Although the Landsat imagery allows individual lithological units to be identified, ground checking at typical localities is necessary to establish what those particular units are, and to establish a stratigraphy and the structural relationship between units. Although much of the stratigraphy, established in the Lower Khan Gorge area (as shown in Figure 7.1), could be extrapolated further afield, new and unidentified lithologies were encountered away from the test area. Where maps are not available, these localities would need to be visited in the field to establish their lithologies.

4--The results of Map 5 are generally in agreement with those of Smith's (1965) map. The Landsat imagery has successfully delimited areas of basement rocks

which Smith failed to identify, and overall, there is a similar amount of information concerning surface geology between the two maps. However, the coarse spatial resolution limits the amount of structural information ascertainable from the MSS imagery and does not allow the relationship between the various formations to be recognised.

5--In terms of preliminary reconnaissance geological mapping, satellite remote sensing proves to be a practical, efficient, and low-cost exploration tool. Arid environments, where vegetation is scarce and rock outcrop good, prove particularly well-suited to this technique, as demonstrated in the Central Zone of the Damara Orogen.

Chapter 8

Conclusions.

Chapter 8. Conclusions.

1--Although the Landsat-1 satellite was originally designed for vegetation studies, as soon as the Multispectral Scanner imagery became available, the potential for geological studies was recognised. The success of geological mapping using Landsat MSS imagery had direct bearing on the inclusion of more appropriate spectral bands on the second-generation Landsat satellites, which carried the Thematic Mapper instrument.

2--The information contained within Landsat imagery is present within a spatial and a spectral component. The spatial component consists of variations in texture and tone within single bands, and the spectral component consists of variations in the recorded reflectance between the different wavelengths sensed by the Multispectral Scanner. Lithologies are best discerned using the spectral information component, whereas lineament data is more easily reconciled from the spatial component of the imagery.

3--Landsat MSS data proves to be particularly well-suited to regional lineament mapping studies. However, there is much continued debate as to the subjectivity involved in the visual recognition of linear features from satellite imagery, and different studies tend to use completely different methodologies. Although computer algorithms provide an objective means of enhancing any linear features present, visual interpretation of digitally-enhanced imagery, by the same, experienced interpreter, remains the most suitable means of lineament identification.

It is important to qualify the nature of the lineaments being mapped, since different features may be controlled by completely disparate phenomena. All four bands of MSS data may contain unique lineament information, and the first principal component allows most of this information to be compressed into a single greyscale image. Consideration should be made of solar azimuth where the lineaments mapped have a topographic expression, as these are often identified by areas of shadow.

4--An effective lineament enhancement and mapping procedure has been developed and tested. This includes the objective enhancement of linear features contained with in the imagery by the derivation of the first principal component image, which is then subsequently enhanced through the technique of convolution filtering and contrast stretching. Visual interpretation of a series of image sub-scenes allows near-uniform coverage of the study area, and the digitising of the compiled lineament data allows an objective identification of any orientation trends.

5--Positive topographic lineaments show a distinct north-northeast trend. The majority of these features are believed to represent dolerite dykes of the Cretaceous Etendeka Volcanics (Erlank, 1985). These date from about 135 Ma ago (Duncan *et. al.,* 1990) and are closely associated with the Serra Garal dykes of the Parana Flood Basalt Province of South America (Marsh *et. al.,* 1991). They are believed to be associated with the splitting of Gondwana and the opening of the Atlantic Ocean. The regional dyke swarm trends along a recognised aeromagnetic lineament, the Welwitchia Lineament Zone (Corner, 1983), which is thought to represent deep-seated, early Proterozoic fractures (Steven, 1993). The

emplacement of the dykes probably took advantage of this pre-existing crustal weakness.

6--Negative topographic lineaments show a strong directional trend, orientated northwest-southeast. They can only be picked out in areas of rock outcrop. Some of these features are shown to be faults on geology maps of the area; by inference, other features with a similar topographic expression are thought to be faults too. Where discernible, these faults show a sinistral strike-slip movement with little vertical displacement. The features are likely to have formed under conditions of brittle deformation, towards the close of the Damara Orogen.

7--Tonal lineaments and fold axes show a similar, dominant trend, orientated northeast-southwest. The tonal lineaments themselves usually represent linear lithological horizons situated along the limbs of the fold axes. The lineaments are orthogonal to the negative topographic lineaments and their distribution is similar, i.e. they are generally discernible in areas of rock outcrop. They are thought to have formed during the main deformational event of the Damara Orogen (orientated northwest-southeast), although there is controversy as to whether the features were formed under compressional (Smith, 1965) or extensional (Oliver, 1993) conditions. The trend of the lineaments appears to change slightly along the Central Zone.

8--A number of regional aeromagnetic lineaments, recognised by Corner (1983), are also discernible as photolineaments on the Landsat imagery. These generally follow the same trend as the tonal lineaments (Oklahandja Lineament and Autseib Fault) and the positive topographic lineaments (Welwitchia Lineament Zone). The Omaruru Lineament is not readily distinguishable from the imagery,

and the prominent photolineament to the east of the Khan River appears to have little geological significance.

9--Although the spectral resolution of Landsat MSS imagery is relatively low, this data has nevertheless been successfully used for lithological mapping, particularly in arid areas where lithologies are varied and rock outcrop is good. The availability of imagery in digital form allows the use of various digital image processing techniques to maximise the display of lithological information. The Central Zone of the Damara Orogen has actually proved to be well-suited to geological interpretation. This is largely a result of the wide variety of lithologies which outcrop in this region, which appear spectrally distinct from one another on digitally processed MSS imagery.

10--The limited spectral resolution of MSS imagery has been highlighted by the inability, from the data, to confidently distinguish between the rocks of the Rossing, Chuos and Karibib Formations. These have been mapped as a single marble unit, which appears to be associated with a break in stratigraphy between anticlinal units, usually of basement rocks, and synclinal cover rocks. This tectonic break is thought to represent a regional, mid-crustal detachment (Oliver, 1993).

11--Although the Landsat imagery allows individual lithological units to be identified, ground checking at typical localities is necessary to establish what those particular units are, to establish a stratigraphy, and to establish the structural relationship between units. Although much of the stratigraphy, established in the Lower Khan Gorge area (as shown in Figure 7.1), could be extrapolated further afield, new and unidentified lithologies were encountered away from the test area. Some of these new units could be identified from their

outcrop patterns to be plutonic intrusions, but others appeared to be bedded units with image qualities which could not be matched to the lithologies of the test area. Where maps are not available, these localities would need to be visited in the field to establish their lithologies.

12--The results of Map 5 are generally in agreement with those of Smith's (1965) map. The Landsat imagery has successfully delimited areas of basement rocks which Smith failed to identify, and overall, there is a similar amount of information concerning surface geology between the two maps. However, the coarse spatial resolution limits the amount of structural information ascertainable from the MSS imagery and does not allow the relationship between the various formations to be recognised.

13--In terms of preliminary reconnaissance geological mapping, satellite remote sensing proves to be a practical, efficient, and low-cost exploration tool. Arid environments, where vegetation is scarce and rock outcrop good, prove particularly well-suited to this technique, as demonstrated in the Central Zone of the Damara Orogen.

References.

References.

Abrams, M. J. (1980). Lithologic mapping, *in* Siegal, B. S. & Gillespie, A. R. (eds), *Remote Sensing in Geology*. Wiley, New York, 381-418.

Abrams, M. J., Brown, D., Lepley, L. & Sadowski, R. (1983). Remote sensing for porphyry copper deposits in Southern Arizona. *Economic Geology*, 1983, Vol. 78, No.4, 591-604.

Alizai, S. A. K. & Ali, J. (1988). Comparison of Landsat MSS and SIR-A data for geological applications in Pakistan. *Int. Jn. Remote Sensing*, 1988, Vol. 9, No. 1, 85-94.

Allum, J. A. E. (1978). *Photogeology and regional mapping*.. Pergamon Press, Oxford.

Ananaba, S. E. & Ajakaiye, D. E. (1987). Evidence of tectonic control of mineralization in Nigeria from lineament density analysis: A Landsat study. *Int. J. Remote Sensing*, 1987, Vol. 8, No. 10, 1445-1453.

Auquiere, M., Lavreau, J., Trefois, P. & Volon, C. (1993). Progress in spectral geology of arid and tropical areas. *Mus. Roy. Afr. centr., Tervuren (Belg.), Dept. Geol. Min., Rapp. ann. 1991-1992.*, 1993, 41-63.

Berning, J. (1986). The Rossing uranium deposit, south west Africa/Namibia. *Mineral Deposits of S. Afr.*, 1986, 1819-1832.

Bhan, S. K. & Hegde, V. S. (1985). Targeting areas for mineral exploration - a case study from Orissa, India. *Int. J. Remote Sensing*, 1985, Vol. 6, Nos. 3/4, 473-479.

Boeckh, E. (1992). An exploration strategy for higher-yield boreholes in the West African crystalline basement, *in* Wright, E. P. & Burgess, W. G. (eds), 1992, *Hydrogeology of crystalline basement aquifers in Africa.* Geol. Soc. Spec. Pub., No. 66, 87-100.

Canas, A. D. & Barnett, M. E. (1985). The generation and interpretation of false-colour composite principal component images. *Int. J. Remote Sensing,*

1985, Vol. 6, No. 6, 867-881.

Clark, L. (1985). Groundwater abstraction from basement complex areas of Africa. *Quarterly Jn. of Eng. Geol.*, 1985, No. 18, 25-34.

Corner, B. (1983). An interpretation of the aeromagnetic data covering the western portion of the Damara Orogen in south-west Africa/Namibia, *in* Miller, R. McG. (ed.) *Evolution of the Damara Orogen of South West Africa/Namibia, Spec. Publ. Geol. Soc. Afr.*, No. 11, 339-354.

Conradsen, K., Nilsson, G. & Thyrsted, T. (1986). Statistical lineament analysis in South Greenland based on Landsat imagery. *IEEE Trans. Geoscience & Remote Sensing*, 1986, Vol. GE-24, No. 3, 313-321.

Crain, I. K. (1976). Statistical analysis of geotectonics, *in* Merriam, D. (ed.), *Random processes in geology*. Springer-Verlag, New York, 3-15.

Csillag, F. (1982). Significance of tectonics in linear feature detection and interpretation on satellite images. *Remote Sensing of the Env.*, 1982, Vol. 12, No. 3, 235-245.

Curran, P. J. (1985). *Principles of remote sensing*. Longman, England.

Downing, K. N. (1983). The statigraphy and palaeoenvironment of the Damara sequence in the Okahandja Lineament area,*in* Miller, R. McG. (ed.), *Evolution of the Damara Orogen of South West Africa/Namibia, Spec. Publ. Geol. Soc. Afr.*, No. 11.

Drury, S. A. (1986). Remote sensing of geological structure in temperate agricultural terrains. *Geol. Magazine*, No. 123, 113-121.

Drury, S. A. (1987). *Image Interpretation in Geology*. Allen and Unwin, London.

Drury, S. A. (1990). *A Guide to Remote Sensing: Interpreting Images of the Earth.* Oxford University Press.

Drury, S. A. (1993). *Image Interpretation in Geology.* 2nd ed. Chapman and Hall, London.

Drury, S. A., De Souza, C. R., Denniss, A., Rothery, D. A. & Hunt, G. A. (1993). Geological mapping in arid terrains by remote sensing. *Geoscientist.*,1993, Vol. 3, No. 6, 12-13.

Duncan, A. R., Armstrong, R. A., Erlank, A. J., Marsh, J. S. & Watkins, R. T. (1990). MORB-related dolerites associated with the final phases of Karoo flood basalt volcanism in southern Africa, *in* Parker, Rickwood & Tucker (eds.), *Mafic dykes and emplacement mechanisms.* Balkema, Rotterdam.

Dwivedi, R. S. & Sankar, T. R. (1992). Principal components analysis of Landsat MSS data for delineation of terrain features. *Int. Jn. Remote Sensing*, 1992, Vol. 13, No. 12, 2309-2318.

Erlank, A. J. (1985). The field relationships, age, petrography and geochemistry of the Cretaceous Etendeka Volcanics and their relationship to continental rifting. *Communs. Geol. Surv. S. W. Afr./Namibia,* 1985, Vol.1, 99-102.

Ferrandini, J., Cornee, J. & Simon, B. (1993). Lineament study of Landsat 2 images of the Western High Atlas (Morocco): consequences. *Geodynamica Acta* (Paris), 1993, Vol. 6, No. 3, 161-173.

Gary, M., McAfee Jr., R. & Wolf, C., eds. (1977). *Glossary of Geology.* American Geological Institute, Washington D. C.

Gillespie, A. R. (1980). Digital techniques of image enhancement, *in* Siegal, B. S. & Gillespie, A. R. (eds), *Remote Sensing in Geology*. Wiley, New York, 139-226.

Goetz, A. F. H., Rock, B. N. & Rowan, L. C. (1983). Remote sensing for exploration: an overview. *Economic Geology*, 1983, Vol. 78, No. 4, 573-590.

Gold, D. P., Parizek, R. R. & Alexander, S. S. (1973). Analysis and application of ERTS-1 data for regional geological mapping. *Symposium of significant results obtained from the Earth Resources Technology Satellite-1* : NASA Document SP-327, 231-245.

Gold, D. P. (1980). Structural Geology, *in* Siegal, B. S. & Gillespie, A. R. (eds), *Remote Sensing in Geology*. Wiley, New York, 47-90.

Greenbaum, D. (1992). Structural influences on the occurrence of groundwater in SE Zimbabwe, *in* Wright, E. P. & Burgess, W. G. (eds), *Hydrogeology of crystalline basement aquifers in Africa.* Geol. Soc. Spec. Pub., No. 66, 77-85.

Gudmundsson, A. (1990). Dyke emplacement at divergent plate boundaries, *in* Parker, Rickwood & Tucker (eds.), *Mafic dykes and emplacement mechanisms.* Balkema, Rotterdam.

Harris, R. (1987). *Satellite remote sensing: an introduction.* Routledge & Kegan Paul, New York.

Hobbs, W. H. (1904). Lineaments of the Atlantic border region. *Bull. Geol. Soc. Am.* , 1904, Vol. 15, 483.

Hunt, G. R. (1980). Electromagnetic radiation: the communication link in remote sensing,*in* Siegal, B. S. & Gillespie, A. R. (eds.),*Remote Sensing in Geology*. Wiley, New York, 47-90.

Huntingdon, J. F. & Raiche A. P. (1978). A multi-attribute method for comparing geological lineament interpretations. *Remote Sensing of Env.*,1978, Vol.7, 145-161.

Knepper, D. H. & Raines, G. L. (1985). Determining stretch parameters for lithologic discrimination on Landsat MSS band-ratio images. *Photo. Eng. & Remote Sensing.*,1985, Vol. 51, No. 1, 63-70.

Koopmans, B. N. (1986). A comparative study of lineament analysis from different remote sensing imagery over areas in the Benue Valley and Jos Plateau Nigeria. *Int. Jn. Remote Sensing*, 1986, Vol. 7, No. 12, 1763-1771.

Kroner, A. (1984). Dome structures and basement reactivation in the Pan-African Damara Belt of Namibia, southwestern Africa. *Amer. Jn. Sci.* , Vol. 282, 1471-1507.

Lamb, A. & Lawrence, G. (1993). Remote sensing in oil and mineral exploration. *Geoscientist.*,1993, Vol. 3, No. 6, 2-3.

Lattman, L. H. (1973). Mineral resources, geological mapping and landform surveys. *Symposium on significant results obtained from the Earth Resources Technology Satellite-1,* Vol. 2 (Washington, D. C., NASA), 106-114.

O'Leary, D. W., Friedman, J. D. & Pohn, H. A. (1976). Lineament, linear, lineation: some proposed new standards for old terms. *Geol. Soc. Am. Bull.* 1976, Vol. 87, 1463-1469.

Lowe, D. (1980). Acquisition of remotely sensed data, *in* Siegal, B. S. & Gillespie, A. R. (eds.), *Remote Sensing in Geology*. Wiley, New York, 47-90.

Marsh, J. S., Erlank, A. J. & Duncan, A. R. (1991). Preliminary geochemical data for dolerite dykes and sills of the southern part of the Etendeka Igneous Province. *Communs. Geol. Surv. Namibia,* 1991, Vol.7, 71-73.

Mather, P. M. (1987). *Computer processing of remotely-sensed images: An introduction*..Wiley, New York.

Miller, R. McG. (1979). The Okahandja Lineament, a fundamental tectonic boundary in the Damara Orogen of South West Africa/Namibia. *Trans. Geol. Soc. S. Afr.,* 1979, No. 82, 349-361.

Miller, R. McG. (1983). The pan-African Damara Orogen of South West Africa/ Namibia, *in* Miller, R. McG. (ed.) *Evolution of the Damara Orogen of South West Africa/Namibia, Spec. Publ. Geol. Soc. Afr.,* No.11,

Moore, G. K. & Waltz, F. A. (1983). Objective procedures for lineament enhancement and extraction. *Photo. Eng. & Remote Sensing*, 1983, Vol. 49, No. 5, 641-647.

Norwood, V. T. (1974). Balance between resolution and signal to noise ratio in scanner design for Earth resources systems. *SPIE Proc. Scanners Images Earth Obs.* , 1974, Vol. 51, 37.

Oliver, G. J. H. (1993). Mid-crustal detachment in the Central Zone of the Damaran Orogen, Namibia: An example of regional crustal extension in a transpressive orogen, *in* Seranne, M. & Malavielle, J. (eds.),*Late orogenic mountain belts,* Doc. BRGM Fr. No. 219, 155.

Owen, H. G. (1983). *Atlas of continental displacement, 200 million years to the present.* Cambridge University Press.

Parsons, A. J. & Yearley, R. J. (1986). An analysis of geologic lineaments seen on Landsat MSS imagery. *Int. Jn. Remote Sensing*, 1986, Vol. 7, No. 12, 1773-1782.

Qari, M. Y. H. T. (1989). Lithological mapping and structural analysis of Proterozoic rocks in part of the southern Arabian Shield using Landsat images. *Int. Jn. Remote Sensing*,1989, Vol. 10, No. 3, 499-503.

Rackshit, A. M. & Swaminathan, V. L. (1985). Application of digitally processed and enhanced Landsat imagery for geological mapping and mineral targeting in the Singhbhum Precambrian mineralized belt, Bihar-Orissa. *Int. Jn. Remote Sensing.*, 1985, Vol. 6, Nos. 3/4, 457-471.

Ramberg, H. (1972). Theoretical models of density stratification and diapirism in the Earth. *Jn. Geophys. Res.* , 77, 877-889.

Reddy, R. K. T. (1991). Digital analysis of lineaments - a test study on South India. *Computers & Geosciences*,.1991, Vol. 17, No. 4, 549-559.

Roering, C. (1961). The mode of emplacement of Li- and Be-bearing pegmatites in the Karibib district, south west Africa. *Econ. Researh Unit, Univ. Johannesburg,* Information Circular No. 4.

Rothery, D. A. (1987). Decorrelation stretching and related techniques as an aid to image interpretation in geology. *Proc. 13th Annual Conference of the Remote Sensing Society*, University of Nottingham, September 7-11, 1987.

Rowan, L. C. (1975). Application of satellites to geologic exploration. *Amer. Sci.*, 1975, Vol. 63, 393-403.

Rowan, L. C. & Lathram, E. H. (1980). Mineral exploration, *in* Siegal, B. S. & Gillespie, A. R. (eds), *Remote Sensing in Geology*. Wiley, New York, 553-605.

Sali, E. & Wolfson, H. (1992). Texture classification in aerial photographs and satellite data. *Int. Jn. Remote Sensing*, 1992, Vol. 13, No. 18, 3395-3408.

Salomonson, V. V. & Rango, A. (1980). Water resources, *in* Siegal, B. S. & Gillespie, A. R., (eds.), *Remote Sensing in Geology*. Wiley, New York, 607-633.

Saunders, D. F., Thomas, G. E., Kinsman, F. E. & Beatty, D. F. (1973). ERTS-1 imagery use in reconnaissance prospecting. *Dept. Comm. Natl. Tech. Inf. Service,* N74-20948.

Sheffield, C. (1981). *Earth Watch: A Survey of the World from Space.* . Sidgwick and Jackson, London.

Singh, A. & Harrison, A. (1985). Standardized principal components. *Int. Jn. Remote Sensing,* 1985 Vol. 6, No. 6, 883-896.

Smith, D. A. M. (1965). The geology of the area around the Khan and Swakop Rivers in South West Africa. *Mem. S. African Geol. Survey,* 3, 113pp.

Stefouli, M. & Angelopoulos, A. (1990). Integration of Landsat and aeromagnetic data as aid to the structural analysis of Crete and S.E. Peloponessus. *Int. Jn. Remote Sensing*, 1990, Vol. 11, No. 9, 1625-1644.

Steven, N. M. (1993). A study of the epigenetic mineralisation in the Central Zone of the Damara Orogen, Namibia, with special reference to gold, tungsten, tin and rare earth elements. *Communs. Geol. Surv. Namibia,* 1993, Memoir 16.

Tarling, D. H. & Tarling, M. P. (1982). *Continental Drift.* Penguin, England.

Townsend, T. E. (1987). A comparison of Landsat MSS and TM imagery for interpretation of geologic structure. *Photo. Eng. & Remote Sensing,*, 1987, Vol. 53, No. 9, 1245-1249.

Walsh, S. J. & Mynar, F. (1986). Landsat digital enhancements for lineament detection. *Env. Geol. Water Sci.* , 1986, Vol. 8, No. 3, 123-128.

Whittle, R. A. & Gutmanis, J. C. (1993). Finding lines: a success story for remote sensing. *Geoscientist*, 1993, Vol. 3, No. 6, 8-9.

Wilson, A. K. (1988). The effective resolution of Landsat Thematic Mapper.*Int. Jn. Remote Sensing.*,1988, Vol. 9, No. 8, 1303-1314.

Windley, B. F. (1982). *The evolving continents.* 2nd ed. Wiley, New York.

Zlatopolsky, A. A. (1992). Program LESSA (Lineament Extraction and Stripe Statistical Analysis) automated linear features analysis - experimental results. *Computers & Geosciences*, 1992, Vol. 18, No. 9, 1121-1126.

LANDSAT MSS INTERPRETATION OF THE REGIONAL GEOLOGY COVERING THE WESTERN PORTION OF THE CENTRAL ZONE OF THE DAMARA OROGEN, NAMIBIA.

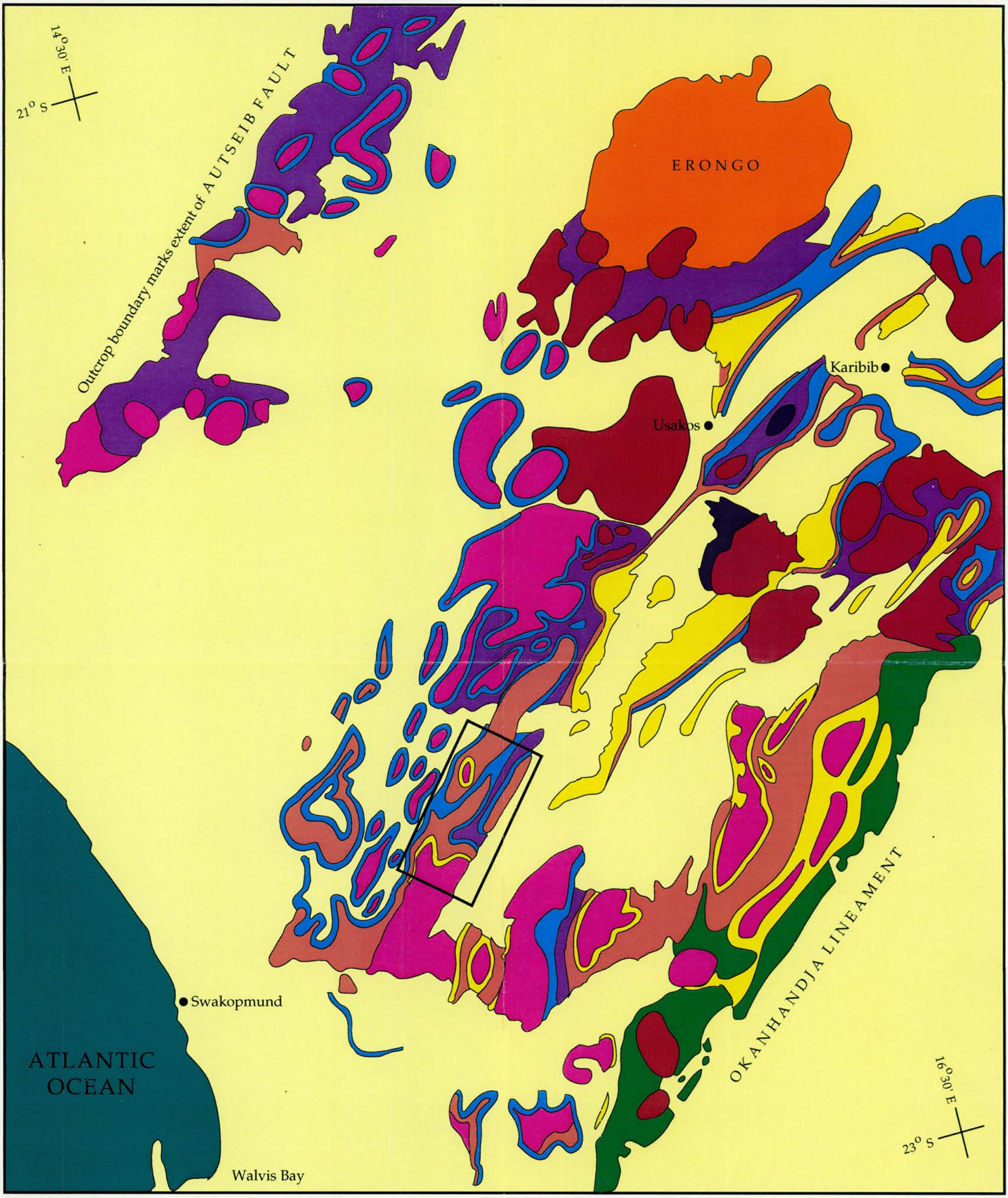

Alluvium / Eluvium.

Erongo Granites.

Syn-/Post-Tectonic Granites.

Tsabachias Fm. (Amphibolite).

Tinkas Formation (Calc silicate).

Kuiseb Formation (Metapelites).

Karibib/Chuos/Rossing Fm.s (Marbles).

Khan Formation (Metapelites).

Etusis Formation (Quartzites).

Grenville Basement (Granite Gneiss).

N

0 50 km

TEST AREA

[Map compiled from the interpretation of Landsat MSS data].